České vysoké učení technické v Praze

Fakulta strojní

Axial Prestretch and Biomechanics of Abdominal Aorta

Lukáš Horný

Habilitační práce 2015

Habilitation thesis

Anotační list (Annotation)

Název (Title): Axiální předpětí a biomechanika břišní aorty (Axial Prestretch and Biomechanics of Abdominal Aorta)

Autor (Author): Ing. Lukáš Horný, Ph.D.

Druh publikace (Kind of publication): Habilitační práce (Habilitation thesis)

Obor habilitace (Branch): Aplikovaná mechanika (Applied mechanics)

Univerzita (University): České vysoké učení technické v Praze (Czech Technical University in Prague)

Fakulta (Faculty): Fakulta strojní (Faculty of Mechanical Engineering)

Ústav (Department): Ústav mechaniky, biomechaniky a mechatroniky 12105 (Department of Mechanics, Biomechanics and Mechatronics)

Rok (Year): 2015

Počet stran (Number of pages): 120

Počet obrázků (Number of figures): 22

Počet tabulek (Number of tables): 2

Anotace: Tato práce přináší výsledky analytických simulací inflačně-extenzního chování lidské břišní aorty modelované jako uzavřené nelineární, anizotropní, předepjaté silnostěnné i tenkostěnné nádoby. Je ukázáno, že podélné předpětí má významný vliv na mechanickou odezvu a to i přes to, že s věkem postupně mizí. Je diskutována fyzikální příčina pozitivního vlivu podélného předpětí na mechaniku lineárních i nelineárních nádob.

Annotation: This study presents the results of an analytical simulation of the inflation-extension behaviour of the human abdominal aorta treated as nonlinear, anisotropic, prestrained thin-walled as well as thick-walled tube with closed ends. Despite significantly decreased longitudinal prestretch with age, the biomechanical response of human abdominal aorta changes substantially depending on the initial axial stretch used. The second part of the thesis is devoted to an explanation of the positive effect of the prestretch on the circumferential distensibility of nonlinear-elastic tubes

List of figures

Figure 5. Inflation-extension behaviour of a 65 year old female donor (F65). The panels are arranged in the same way as in Figure 2. The graphs show two differences when compared with M38 in Figure 2. First, P–λ_{zZ} curve for λ_{zZ}^{ini} = 1 does not exhibit initial shortening. It begins with axial extension. Second, the inflection point does not appear on P–$\lambda_{\theta\Theta}$ curve for λ_{zZ}^{ini} = 1. However, curves for higher axial prestretch do show the inflection. Note that the existence of an inflection point makes P–$\lambda_{\theta\Theta}$ curve S-shaped and results in higher circumferential distensibility $\varepsilon_{\theta\Theta} = \lambda_{\theta\Theta}$(16kPa) – $\lambda_{\theta\Theta}$(10kPa) (in contrast to J-shaped curve without an inflection).

Figure 6. Inflation-extension response of a 61 year old male donor (M61a) – detail. The results of the simulation based on thin-walled approximation. The blue solid curve was computed with expected value λ_{zZ}^{ini} = 1.074; red dashed curve was computed with $\lambda_{zZ,UL}^{ini}$ = 1.153; and black dotted curve was computed with $\lambda_{zZ,LL}^{ini}$ = 1. Shaded rectangle emphasises the region of physiological pressures. Vertical lines aid to identify stretch variation $\varepsilon_{iI} = \lambda_{iI}$(16kPa) – λ_{iI}(10kPa) ($iI = \theta\Theta$ and zZ).

Figure 7. Diastolic-systolic stretch variations. The upper panels show variation of circumferential and axial stretch at r_i and lower panel shows specific values of diastolic (P_{DIA}) and systolic (P_{SYS}) pressure applied in the computations. Due to nonlinear large strain stiffening, ε_{zZ} decreases with increased axial prestretch, which is in contrast to circumferential behaviour ($\varepsilon_{\theta\Theta}$ attained higher values for highly axially prestretched aortas).

Figure 8. Prestretching axial force. Predictions of F_{red} computed with the thin-walled model are depicted: blue solid circles were obtained with expected values of λ_{zZ}^{ini}; red open squares were obtained with the upper limit; and black open circles were obtained when the lower limit of the initial axial stretch was used. The blue solid line is the linear regression model of the dependence of F_{red} (obtained for expected values of the prestretch) on age: $F_{red} = 2.115 - 0.023\cdot Age$ for $Age \in [38;77]$ years. Outside of this domain, one should consider the regression model as an extrapolation which is indicated by the dotted line. The results are compared with experiments adopted from Horny et al. (2013). Note that due to the assumption F_{red} computed with $\lambda_{zZ,LL}^{ini}$ for age > 61 years is 0. The regression model (4) predicts $\lambda_{zZ,LL}^{ini} < 1$ for age > 61 years; however, this is a consequence of the used methodology *expectation* ± *uncertainty*. Since very little is known about initially pre-compressed arteries $\lambda_{zZ,LL}^{ini}$ (Age > 61 years) = 1 was prescribed in our simulation.

Figure 9. Variation of axial stress $\sigma_{zz}(r_i)$ in the course of the pressurisation. The curves are based on the thick-walled model with incorporated residual strain. Circumferential stretch on horizontal axis starts from values smaller than 1 due to simultaneous effect of the initial axial stretch and residual strain. Predictions obtained with the expected value of λ_{zZ}^{ini} are depicted with blue solid curves; red dashed curves were obtained with $\lambda_{zZ,UL}^{ini}$; and $\lambda_{zZ,LL}^{ini}$ was used to create black dotted curves. Solid circles on the curves highlight the positions of diastolic (the left circle) and systolic (right circle) pressure.

Figure 10. Relative change of the axial stress induced by diastolic–systolic pressure increment. The upper panel shows the results computed with the thick-walled model (residual strain incorporated) at the inner radius (small symbols) and at the outer radius (large symbols). The lower panel shows results obtained by thin-walled approximation. The symbols are used in the same way as in Figure 7 and 8. The figure shows that higher initial axial prestretch is accompanied with smaller changes of the axial stress. Correlation coefficients and regression lines correspond to expected initial prestretch.

Figure 11. Components of referential elasticity tensor C for expected axial prestretch. Upper panels show the stiffness in circumferential direction ($\mathsf{C}_{\Theta\Theta\Theta\Theta}$) and lower panels in axial direction (C_{ZZZZ}). The symbols indicate the method and position: red solid boxes – at r_i with thick-walled model; black solid circles – at r_m with thin-walled model; and blue solid diamonds – at r_o with thick-walled model. The regression line indicates significant correlation between age and $\mathsf{C}_{\Theta\Theta\Theta\Theta}$ at r_m for P_{SYS} (R = 0.515 *p–value* = 0.04). Note that logarithmic scale is used on vertical axes.

Figure 12 Stiffness ratio. The figure summarises results obtained for stiffness ratio at inner, middle and outer radius of the aortas. Three important things can be derived from the figure: (1) weakly prestretched aortas give higher stiffness ration; (2) the stiffness ratio varies significantly through the thickness of the wall; and (3) aortas may exhibit different stiffness ratios in different ageing periods.

Figure 13. Relative increment of the stiffness ratio. Highly prestretched aortas gave a higher relative increment in the stiffness ratio during pressure cycle.

Figure 14. Fung-Demiray inflation-extension response. A – initial prestretch and dimensionless force. B – mutual dependence of initial prestretches (λ_{zZ}^{ini} – $\lambda_{\theta\Theta}^{ini}$). C and D – dimensionless pressure vs. stretch. E – traces of inflation-extension responses in the phase space of the deformation (solid curves) and contour curves for dimensionless pressure $P_\mu = k$ (dashed curves). An interpretation is provided in footnote 13. F – stretch difference $\lambda_{\theta\Theta} - \lambda_{\theta\Theta}^{ini}$ achieved by loading a tube with pressure P_μ.

Figure 15. Neo-Hookean and Fung-Demiray incompressible solid in uniaxial extension. The figure demonstrates that only moderate nonlinearity is inherent to the neo-Hooke model in contrast to the Fung-Demiray model which stiffens progressively ($\beta = 1$).

Figure 16. Neo-Hookean inflation-extension response. A – initial prestretches and dimensionless force. B – mutual dependence of initial prestretches (λ_{zZ}^{ini} – $\lambda_{\theta\Theta}^{ini}$). C and D – dimensionless pressure vs. stretch. E – traces of inflation-extension responses in the phase space of the deformation (solid curves) and contour curves for dimensionless pressure $P_\mu = k$ (dashed curves). F – stretch difference $\lambda_{\theta\Theta}$ – $\lambda_{\theta\Theta}^{ini}$ achieved by loading a tube with pressure P_μ. Dotted curves indicate a loss of deformation stability.

Figure 17. Neo-Hookean and linearized inflation-extension response at small strains but large displacements. A – prestrains and dimensionless force. B – mutual dependence of initial prestrains. C and D – dimensionless pressure vs. infinitesimal strain. E – traces of inflation-extension responses. Solid circles and continuous curves correspond to second order linear theory. Dotted curves and empty circles correspond to nonlinear theory applied to neo-Hookean material but results are displayed over infinitesimal strain coordinates according to $\eta_{kk} = \sqrt{(1 + 2E_{KK})} - 1$. The same axial prestretch was applied to both problems which ordinarily leads to different prestretching forces.

Figure 18. Circumferential distensibility of the Neo-Hookean and linearized model in inflation-extension response at small strains but large displacements. A – overall dependences. B – detail.

Figure 19. Inflation-extension responses in the first order linear elasticity. A – circumferential responses. B – longitudinal responses.

Figure 20. Differential increment dW. Infinitesimal contributions of the order higher than the first are neglected.

Figure 21. Internal element of deformed thick-walled circular tube.

Figure 22. Axial equilibrium.

List of tables

Table 1. Age, gender, geometry and constitutive parameters of involved donors; adopted from Labrosse et al. (2013).

Table 2. Initial axial prestretches for donors involved in the simulation estimated with regression model (3) and its prediction intervals (4). The table is ordered in the same way as Table 1. Estimated parameters in (3) a = 2.4016 [1/years]; b = -0.1957 [-]; and in (4) $t_{0.95/2}(363)\cdot S_e$ = 0.0707; $Mean(\mathbf{ln}x_i)$ = 3.8414; and $\Sigma(\mathbf{ln}x_i - Mean(\mathbf{ln}x_i))^2$ = 0.0184.

Shrnutí

Elastické tepny jsou v lidském těle značně axiálně předepnuty. Předpětí minimalizuje podélné deformace během srdečního cyklu (přenosu pulsní vlny). Starobní změny v cévní mechanice vedou mimo jiné k tomu, že podélné předpětí s věkem výrazně klesá. Ačkoliv je toto známý poznatek, pouze malá vědecká pozornost byla doposud věnována důsledkům tohoto poklesu na mechanickou odezvu cév.

Tato práce přináší výsledky analytických simulací inflačně-extenzního chování lidské břišní aorty modelované jako uzavřené nelineární, anizotropní, předepjaté silnostěnné i tenkostěnné nádoby. Konstitutivní parametry a geometrie sedmnácti aort jsou převzaty z literatury a doplněny o statistiku poklesu předpětí v průběhu lidského života. Statistiku poklesu předpětí, založenou na 365 pitevních měřeních, s kolegy publikoval autor habilitační práce.

Inflačně extenzní odezva každé aorty byla vypočtena třikrát a to pro (1) očekávané chování aorty (jako vstupní parametr byly očekáváné střední hodnoty předpovídané regresním modelem závislosti předpětí na věku), (2) simulace inflačně extenzního chování byla provedena s horní a (3) dolní mezí 95%-intervalu spolehlivosti predikce regresního modelu věkové závislosti axiálního předpětí. Tento postup umožnil vyhodnotit meze trendů starobních závislostí s ohledem na variabilitu pozorování a skutečnost, že dochází ke kombinaci literárních dat.

Výsledky simulací ukázaly, že ačkoliv elastické předpětí může být s věkem zcela ztraceno, i malé zbytkové hodnoty významně ovlivňují mechanickou odezvu aorty, a to i přesto, že aorty současně s tím významně tuhnou. Konkrétněji: aorty axiálně předepjaté na horní mezi očekávání vykazují významně vyšší obvodovou průtažnost oproti svým slabě předepjatým protějškům, což pozitivně přispívá k pružníkovému efektu. Tato fyziologická funkce axiálního předpětí doposud v literatuře nebyla popsána. Též byl potvrzen významný vliv axiálního předpětí na proměnlivost axiálního napětí během srdečního cyklu. V simulacích byla také verifikována hypotéza o přibližné konstantnosti poměrů obvodových a axiálních složek tenzoru pružnosti během srdečního cyklu, která byla navržena v nedávné literatuře.

Ve své druhé části se habilitační práce věnuje vysvětlení pozitivního efektu podélného předpětí na obvodovou průtažnost nelineárně-elastických trubic obecně. Je ukázáno, že sama podstata efektu spočívá v nutnosti rozlišovat mezi referenční a zdeformovanou konfigurací, tj. ve velkých posuvech.

Klíčová slova: *břišní aorta, stárnutí, konstitutivní modelování, průtažnost, předpětí, tuhost.*

Summary

Elastic arteries are significantly prestretched in an axial direction. This property minimises axial deformations during pressure cycle. Ageing-induced changes in arterial biomechanics, among others, are manifested via a marked decrease of the prestretch. Although this fact is well known, little attention has been paid to the effect of decreased prestretch on mechanical response. This study presents the results of an analytical simulation of the inflation-extension behaviour of the human abdominal aorta treated as nonlinear, anisotropic, prestrained thin-walled as well as thick-walled tube with closed ends. The constitutive parameters and geometries for 17 aortas adopted from the literature were supplemented with initial axial prestretches obtained from the statistics of 365 autopsy measurements. For each aorta, the inflation-extension response was calculated three-times: with expected value of the initial prestretch and with the upper and lower confidence limit of the initial prestretch derived from the statistics. This approach enabled age-related trends to be evaluated bearing in mind the uncertainty in the prestretch. Despite significantly decreased longitudinal prestretch with age, the biomechanical response of human abdominal aorta changes substantially depending on the initial axial stretch used. In particular, substituting the upper limit of initial prestretch gave mechanical responses which can be characterised by (1) low variation in axial stretch, and (2) high circumferential distensibility during pressurisation, in contrast to the responses obtained for their weakly prestretched counterparts. The simulation also suggested the significant effect of the axial prestretch on the variation of axial stress in the pressure cycle. Finally, the obtained results are in accordance with the hypothesis that circumferential-to-axial stiffness ratio is the quantity relatively constant within this cycle.

The second part of the thesis is devoted to an explanation of the positive effect of the prestretch on the circumferential distensibility of nonlinear-elastic tubes. It is shown that a key point is to distinguish between the reference and deformed configuration that is a problem formulation including large displacements is indispensable to be able to observe the distensibility of tubes enhanced by the axial prestretch.

Keywords: *abdominal aorta; ageing; constitutive modelling; distensibility; prestretch; stiffness.*

Acknowledgement

In the first place the author would like to express his thanks to his wife Vanda who shows incredible patience and endless love although the author is not perfect.

My dear colleagues Tomáš Adámek, Markéta Kulvajtová, Marek Netušil and Tereza Voňvaková kindly helped me in time we collectively investigated the effects of the prestretch and the author would like to express his thanks at this place.

This study has been partially supported by following institutions:

- Czech Technical University in Prague by project SGS13/176/OHK2/3T/12;
- Ministry of Health of the Czech Republic by project NT13302; and
- Faculty of Mathematics and Physics of the Charles University in Prague in project 260098/2014.

Contents

Horný L, Adámek T, Kulvajtová M (2014) Analysis of axial prestretch in the abdominal aorta with reference to post mortem interval and degree of atherosclerosis. *J Mechan Behav Biomed Mater* 33:93-98

Brief biography of the author
List of selected publications

Nomenclature

Typesetting convention

All scalar quantities (and of course components of vectors and tensors) are typed in *italic* font, e.g. r, R, X_K, S_{IK}, C_{IJKL}…
In the symbolic notation, all vectors are in ***bold italic*** font, e.g. $\boldsymbol{x}$, $\boldsymbol{X}$, $\boldsymbol{E}_1$…
In the symbolic notation, all tensors (rank ≥ 2) are in **bold normal** font, e.g. $\mathbf{F}$, $\mathbf{S}$, $\mathbf{C}$… There is one exception from this rule, it is Cauchy stress tensor $\boldsymbol{\sigma}$, which is typed in italic bold as usual.

In what follows, symbols of a theory are typed in Palatino Linotype or Futura Bk BT, contrastingly to meta-language which is in Times New Roman.

Vector and tensor quantities are typed in uppercase letters when they are expressed in the material description, and in lowercase letters when they are expressed in the spatial description.

Unless explicitly stated, preceding rules hold everywhere in the study.

List of symbols

α	[-]	either significance level (statistics), or opening angle (residual strain in thick-walled tube)
a	[year^{-1}]	parameter of regression model (prestretch–age relationship)
β	[-]	material parameter in Fung-Demiray model
b	[-]	parameter of regression model (prestretch–age relationship)
b_{kl}	[-]	components of the left Cauchy-Green strain tensor
$\mathbf{b}$		left Cauchy-Green strain tensor
B		a body
$B(\boldsymbol{x})$		current (spatial) configuration of a body understood as a vector space
$B(\boldsymbol{X})$		reference (spatial) configuration of a body understood as a vector space
c_0	[kPa]	material parameter in strain energy density function
c_1, c_2	[-]	material parameter in strain energy density function
C_{IK}	[-]	components of the right Cauchy-Green strain tensor
$\mathbf{C}$		right Cauchy-Green strain tensor
C_{IJKL}	[-]	components of the material elasticity tensor
C		material elasticity tensor
δ_{ik}, δ_{IK}	[-]	Kronecker's delta
$dB(\boldsymbol{x})$		tangent space at $\boldsymbol{x}$
$dB(\boldsymbol{X})$		tangent space at $\boldsymbol{X}$
$d\boldsymbol{x}$		infinitesimal of a position vector $\boldsymbol{x}$, element in tangent space at $\boldsymbol{x}$
$d\boldsymbol{X}$		infinitesimal of a position vector $\boldsymbol{X}$, element in tangent space at $\boldsymbol{X}$
ε_{iI}	[-]	distensibility; $\varepsilon_{iI} = \lambda_{iI}(P_2) - \lambda_{iI}(P_1)$ for $iI = \theta\Theta$ and zZ and $P_1 < P_2$; in the context of arterial physiology $P_1 = P_{DIA} < P_2 = P_{SYS}$ is used, in general considerations usually $P_1 = 0$ and $P_2 = P$
e_{ik}	[-]	components of the Euler-Almansi strain tensor
E_{IK}	[-]	components of the Green-Lagrange strain tensor
$\mathbf{e}$		Euler-Almansi strain tensor
$\mathbf{E}$		Green-Lagrange strain tensor
F_μ	[-]	normalized prestretching axial force $Fred/(\pi R_m^2 \mu)$

F_{red}	[mN]	prestretching axial force
F_{iK}	[-]	components of the deformation gradient
$\mathbf{F}$		deformation gradient
η_{ik}	[-]	components of infinitesimal strain tensor
$\boldsymbol{\eta}$		infinitesimal strain tensor
h	[mm]	thickness of the deformed tube
H	[mm]	thickness of a tube in the reference configuration
θ		(index) circumferential direction in the deformed state
Θ		(index) circumferential direction in the reference state
$\mathbf{i}$, $\mathbf{I}$		spatial and material unit tensor, respectively
J	[-]	volume ratio
λ_{rR}, $\lambda_{\theta\Theta}$, λ_{zZ}	[-]	radial, circumferential, and axial stretch, respectively
λ_{zZ}^{ini}	[-]	axial prestretch
λ_{zZ}^{ini}	[-]	axial prestretch
$\lambda_{zZ,EXP}^{ini}$	[-]	expected value of the axial prestretch
$\lambda_{zZ,LL}^{ini}$	[-]	lower bound of the prediction interval of the axial prestretch regression model
$\lambda_{zZ,UL}^{ini}$	[-]	upper bound of the prediction interval of the axial prestretch regression model
μ	[kPa]	material parameter corresponding to shear modulus
m	[-]	degree of freedom (statistics)
p	[kPa]	undetermined multiplier accounting for hydrostatic contribution to a stress tensor arising from incompressibility constraint
P, P_k	[kPa]	internal pressure
P_μ	[-]	normalized pressure P/μ
P_{SYS}, P_{DIA}	[kPa]	systolic, diastolic pressure
P_{iK}	[kPa]	components of the nominal stress tensor
$\mathbf{P}$		nominal stress tensor
ρ, ρ_i, ρ_o	[mm]	radius in opened-up configuration of the tube (variable, inner, outer)
r		(index) radial direction in the deformed state
r, r_i, r_o	[mm]	radius in the pressurized configuration of the tube (variable, inner, outer)
r_m	[mm]	middle radius of the pressurized thin-walled tube

R		(index) radial direction in the reference state
R	[-]	coefficient of linear correlation (Pearson)
R, R_i, R_o	[mm]	radius of the closed but not pressurized tube (variable, inner, outer)
R_m	[mm]	middle radius of the thin-walled tube in the reference state
σ_{ik}	[kPa]	components of the Cauchy stress tensor
$\boldsymbol{\sigma}$		Cauchy (true) stress tensor
S_{IK}	[kPa]	components of the second Piola-Kirchhoff stress tensor
$\mathbf{S}$		second Piola-Kirchhoff stress tensor
v	[mm^3]	current volume
V	[mm^3]	referential volume
W	[kPa]	strain energy density function (per unit reference volume)
$\hat{W}$	[kPa]	strain energy density function (after $\lambda_{rR} = 1/(\lambda_{\theta\Theta} \cdot \lambda_{zZ})$ substitution)
χ		a motion considered as a mapping from the reference to current configuration
x_i	[mm]	components of the spatial position vector
$\boldsymbol{x}$		position vector in the deformed configuration
X_K	[mm]	components of the material position vector
$\boldsymbol{X}$		position vector in the reference configuration
z	[mm; -]	axial coordinate or (as index) axial direction in the deformed configuration
Z	[mm; -]	axial coordinate or (as index) axial direction in the reference configuration

Introduction

Author’s interest in axial prestretch has been initiated at the end of 2009 in a discussion with his colleague Tomáš Adámek. Tomáš is a forensic pathologist affiliated with the Third Faculty of Medicine of Charles University in Prague and Fakultní nemocnice Na Královských Vinohradech and he has autopsied almost ten thousands of cadavers in his career. Since 1980s an excision of the aorta and a measurement of aortic circumference has been a routine part of the necropsy procedure at the forensic medicine department he has been employed at. Very large statistics of the measurements gave a confident method to estimate age of a cadaver at the time of death based on aortic circumferences (Štefan and Josífko 1984).[1] Tomáš observed that aortas, when excised, differ not only in the diameter but also in their retraction after the excision. The retraction of an artery is a consequence of a removed loading which holds the artery in its *in situ* length. The ratio of the *in situ* to *ex situ* length is referred to as (axial) prestretch. The first question we posed was whether the prestretch does correlate with age.

State of the Art. A detailed study of the axial prestretch in abdominal aorta resulted in several scientific papers reporting age-related changes in longitudinal prestretch and its correlation with anatomical quantities like heart weight, thickness of left ventricle, circumference of the aorta (Horný et al., 2011; 2012a). It was shown that an inverse relationship (regression model of the dependence of age on the prestretch) is a suitable instrument to obtain the estimate of age with reliability comparable to other forensic methods based on e.g. osteological and odontological observation (Horný et al., 2012a, 2012b). But in contrast to them, the prestretch is determined just in the autopsy room and at the time of autopsy, and with minimal costs. One only has to have a rule and marker. A discovery of a fact that the ratio of aortic diameter to axial prestretch depends linearly on age motivated the combined arteriosclerotic index to be defined – it roughly gives predictions of age ±12.7 years at confidence level 95% in male population (Horný et al., 2012b).[2] Another interesting conclusion of the previous research is that axial prestretch in aorta is not significantly affected by atherosclerosis (Horný et al., 2014) which may be considered somewhat surprising at the first look.[3] Final, more methodological, conclusion was that post-mortal changes (in the range from 0 to approximately 120 hours) do not significantly affect the determined axial prestretch (Horný et al., 2014).

---

[1] It is a reality in the forensic practice that from time to time cadavers of unknown identity are examined.

[2] It has to be noted that usual population variance of anatomical quantities is really high in comparison with variances which engineers know from their practice.

[3] Remind that atherosclerosis is a focal disease present on inner layer of an artery wall where it appears as a formation of lipid riche and calcified plaques prone to a rupture. A boundedness of atherosclerotic plaque explains the conclusion. On the other hand there is arteriosclerosis which manifests as a calcification and subsequent disruption of elastin membranes inside the artery wall and it is likely that arteriosclerosis is a mechanistic cause of the decreasing prestretch during ageing. However, quantitative correlation between elastin disruptions and decreased prestretch remains to be described.

In Horný et al. (2013), axial prestress was investigated. Uniaxial tensile tests with tubular samples of human aortas suggested that age-related decrease is not only the case of the prestretch but axial prestress also declines in ageing. This is not a self-evident result derivable from mechanical laws due to well-known stiffening of human arteries in age (arteriosclerosis). Human aorta generally stiffens with age, diameter and thickness increase, but the prestretch and prestress decrease. The results in Horný et al. (2013) showed that age-related stiffening does not take place in a neighbourhood of the prestretch determined in autopsies.[4] Moreover, it was found that prestretching force also decreases with age. Altogether led to the hypothesis that the decrease of the axial prestretch is induced by a damage of internal structure of aorta. This damage is likely to be a consequence of arteriosclerosis but clear experimental evidence is still lacking (Horný et al., 2013).

In the time spent with the axial prestretch (2010–2014) the author of the thesis found that there are many gaps in our knowledge of the prestretch. It is actually surprising when one becomes conscious of the fact that an existence of the prestretch had already been reported by Fuchs (1900) as Bergel (1961) mentioned. There are papers of Bergel (1961), and Dobrin and Doyle (1970) who worked with animal models to show that arterial physiology is strongly affected by the prestretch. They however did not investigate how it changes in ageing. The evidence that ageing significantly affects the prestretch was provided by Learoy and Taylor (1966; with human arteries) but their sample was too small to obtain quantitative relationship between age and prestretch. Lagewouters et al. (1984) reported measurement of 20 abdominal and 45 thoracic aortas in autopsies but their successors focused rather on impact of ageing on material properties (constitutive equation) than on the prestretch which, in comparison with material properties, should be interpreted as a boundary condition (Wuyts et al., 1995; Zulliger and Stergiopulos 2007).

Our knowledge of the axial prestretch was improved when Han and Fung (1995) published their study where dependence of the prestretch on anatomical location in aortic tree was quantified (canine, porcine models; the prestretch increases with increasing distance from the heart). Human data of the determined prestretch is frequently dispersed in papers which aim at other objectives (e.g. constitutive models obtained in inflation-extension test post-processing; see e.g. Schulze-Bauer et al., 2003; Humphrey et al., 2009; Sommer et al., 2010, 2012). The systematic study of the prestretch has been lacking in the literature.

Besides recent studies published by the author and his colleagues, one must not miss out the results obtained by Jessica Wagenseil and her co-workers who have put a role of elastin in

[4] The word neighbourhood is here used in the sense of the Calculus. It expresses an existence of a subset in the space of deformations which covers points close to the deformation attained when an artery is stretched to *in situ* length. It should be remarked that artery stretched *in situ* in autopsy room, that is *post mortem*, is in 3D strain state but (neglecting residual stresses) in uniaxial stress state which is significantly different from *in vivo* conditions where the artery is loaded by internal pressure and hence in 3D stress state.

the axial prestretch into a clear light.[5] They use genetically modified animal models to elucidate a role of extracellular matrix insufficiency in development of diseases like hypertension, supravalvular aortic stenosis and others. It has been found that mice unable to synthesise normal elastin have elastic arteries which do not retract upon excision (or shorten significantly lesser in comparison with wild-type mice depending on genotype). Instead of the retraction, arteries become tortuous and curved (Wagenseil et al., 2005, 2009; Cheng and Wagenseil 2012; Carta et al., 2009). The finding that elastin is responsible for bearing the prestretch of artery wall is in accordance with previously mentioned results of Han and Fung (1995). The magnitude of the prestretch increases with the distance from the heart because the amount of elastin membranes inside the wall decreases and, as is assumed, a load per membrane increases.

The axial prestretch, from mathematical point of view, expresses initial boundary condition in initial-boundary value problem describing an inflation-extension behaviour of an artery (in case that inertial forces are considered we should say pressure pulse wave propagation). There is significant difference between hard tissue (bones) and soft tissue (e.g. arteries) biomechanics from engineering point of view. In bone biomechanics, patient-specific models progressed to a state when computational biomechanics can, by their predictions, directly assist surgeons in a development of individual implants and replacements. This is not the case in arterial biomechanics although first attempts have occurred. High population variability in constitutive equations for soft tissues, which moreover are nonlinear and have to be formulated at finite strains, is one of the most important reasons.

It motivates many scientists worldwide to investigate material properties of the arteries. Additional difficulty is that the mechanical response of soft tissues *in vivo* is different from the response *ex vivo* and in a lab (which resembles a term *in vitro* although mechanical engineers do not use test tubes). Nowadays it is clear that arterial biomechanics, if it aims to be not only a basic, say, physiological science but also a key applied discipline in hands of engineers developing instruments and procedures with individual strengths for individual demands, needs a reliable and confident method to obtain constitutive models *in vivo*.

In the new millennium there is an increasing interest in procedures capable to estimate constitutive equations of arteries in living beings and the author considers it to be a strong motivation for his work (Schulze-Bauer and Holzapfel 2003; Stålhand and Klarbring 2005; Stålhand 2009; Masson et al., 2008, 2011; Åstrand et al., 2011; Wittek et al., 2013; Karatolios et al., 2013; MacTaggart et al., 2014; Kamenskiy et al., 2014). However at present, he does not focus on these techniques as such, but would like to deliver to colleagues aimed to *in vivo* constitutive model determination what they cannot measure – the axial prestretch and its role

[5] Elastin is a component of extracellular matrix, biopolymer and protein, responsible for elastic properties of tissues. It can be found for instance in arterial walls, lungs, and skin. A body is normally able to synthesise it only in pre-natal and early post-natal period. It is believed that restricted capability to synthesise elastin in advanced age is one of the most important causes of hypertension because damaged elastin is in arterial remodelling and during adaptation replaced by collagen which is, in comparison with elastin, very stiff.

in arterial mechanical response.[6] It is clear that experimental measurement of the prestretch is impossible in the living beings because it necessitates the excision of arterial segment from a body.

Arrangement of the thesis, objectives and results. The study is divided into two main chapters and three appendices.

The first chapter, **Axial prestretch and biomechanics of abdominal aorta**, is a slightly extended version of the paper published by Lukáš Horný, Marek Netušil and Tereza Voňavková in *Biomechanics and Modeling in Mechanobiology* in 2014.[7] The chapter describes how axial prestretch affects mechanical response of human abdominal aorta in the inflation-extension test modelled by thick-walled and thin-wall incompressible anisotropic hyperelastic tube. It is shown that arterial physiology benefits from the prestretch by increased circumferential distensibility, decreased variation of the axial stress and strain in the pressure cycle and it is also hypothesised that the ratio of the circumferential and axial component of the elasticity tensor is a suitable candidate to be used as a constraint in *in vivo* constitutive model determination because of its approximate constancy. The results however suggested that the minimal pressure-induced variation of the axial stress in the artery wall may be lost in ageing which could be a source of undesirable remodelling of the artery and could be a trigger of a development of pathologies like aneurysm formation.

Enhanced circumferential distensibility of the pressurized tube by applying axial prestretch had seemed to the author that brings somewhat contra-intuitive results and motivated him to add another chapter: **Analysis of effect of axial prestretch in different computational models**. The second chapter, in contrast to the first which focuses on the biomechanics, investigates the effect of the prestretch from general point of view of solid mechanics of deformable bodies. In this section, an effect of isotropy, effect of nonlinear constitutive model (material nonlinearity), effect of finite strains (geometrical nonlinearity), and large displacements with infinitesimal strain formulation, are discussed. It was found that it is crucial to distinguish between the reference and deformed configuration – nonlinearity arising from difference between a nominal and true stress tensor. In other words, second order linear elasticity has shown tubes which are

[6] From mechanical point of view we can say that *in vivo* constitutive model determination does not only consist in an estimation of the model and its parameters from known sequence of deformed configurations as is usual for engineers in a lab, but also in the determination of an unknown reference configuration of a body.

[7] Full bibliographical record:
Horný L, Netušil M, Voňavková T (2014) Axial prestretch and circumferential distensibility in biomechanics of abdominal aorta. Biomech Model Mechanobiol 13(4):783-99. DOI: 10.1007/s10237-013-0534-8.
Biomechanics and Modeling in Mechanobiology has received impact factor 3.251 from the Journal of Citation Reports 2013.

more distensible when axially prestretched. But of course, full nonlinear formulation led to strengthening of the effect. This results have not been published yet.

Appendix A is entitled **Equilibrium equations for incompressible thick-walled tube and in-wall stress distribution**, and is purely supporting and does not deliver new results. It consists in the derivation of the used equations and is placed here for the convenience of readers who otherwise would have to spend time searching through scientific literature. Appendix A can also be helpful for students because the derivation, particularly of the axial equilibrium equation, contains steps (e.g. rearrangement of an integration by part) which, when omitted during a lecture, can make final formulas somewhat mysterious because it is not clear at first look how they were obtained.

Appendix B and C consist of two scientific papers published by the author and his colleagues and document that results obtained in the research managed by the author have international publicity in the scientific community.

Appendix B – **Horný L, Netušil M, Voňavková T (2014) Axial prestretch and circumferential distensibility in biomechanics of abdominal aorta. *Biomech Model Mechanobiol* 13(4):783-99;**

and Appendix C – **Horný L, Adámek T, Kulvajtová M (2014) Analysis of axial prestretch in the abdominal aorta with reference to post mortem interval and degree of atherosclerosis. *J Mechan Behav Biomed Mater* 33:93-98.**

I. Axial prestretch and biomechanics of abdominal aorta

Slightly extended version of **Horný L, Netušil M, Voňavková T (2014) Axial prestretch and circumferential distensibility in biomechanics of abdominal aorta.** ***Biomech Model Mechanobiol*** **13(4):783-99.**

I.1. Motivation

There is extensive literature dealing with the circumferential behaviour of elastic arteries, e.g. aorta, carotids, iliacs (Dobrin 1978; Humphrey 2002; Shadwick 1999; Kalita and Schaefer 2008). This literature includes results of both *ex vivo* and *in vivo* approaches showing the unique *Windkessel function* of these arteries. The manner of how elastic arteries transmit pressure pulse wave has been linked to mortality (McEniery et al. 2007; Greeenwald 2007). Arteriosclerotic changes, which are responsible for age-related loss of elasticity (a key factor for pulse wave transmission), have subsequently been suggested as a potential target for cardiovascular therapy (O'Rourke and Hashimoto 2007). It was well established that circumferential distensibility declines with age. In contrast to the circumferential mechanical response, the axial behaviour of arteries in their natural (tubular) geometry has been studied less extensively, especially for human data which can only be found in a limited number of reports (Horny et al. 2013).

Elastic arteries *in situ* are significantly prestretched in an axial direction (Dobrin and Doyle 1970; Han and Fung 1995; Learoyd and Taylor 1967). They retract upon excision and the difference between the *in situ* and *ex situ* length rapidly decreases in middle age and only small changes follow after the age of 60 (Horny et al. 2011, 2012a,b). For instance, a regression model adopted in this study from Horny et al. (2014) respectively gives axial prestretch 1.33, 1.23, 1.08, and 1.05 at age 20, 30, 60 and 70, which implies a decrease of approx. 30% and 9.5% per decade with reference to 20 years of age (the supposed maximum prestretch due to the end of the growth period).

Axial prestress, induced by the prestretch, has an important physiological function. In an idealised case, it enables the artery to carry the pulse pressure with minimal variation in its length (Schulze-Bauer et al. 2003; Sommer et al. 2010; Van Loon et al. 1977). It is, however, unknown how ageing-induced changes in prestress and stiffness are inter-related together. In other words, how the stress state of an artery is affected by a simultaneous decrease in the prestretch and an increase in the stiffness (at strains corresponding to *in vivo* loading). The interrelation is significantly complicated by the nonlinearity and anisotropy of arterial constitutive behaviour (Holzapfel et al. 2000; Holzapfel and Ogden 2010a).

This study attempts to contribute to this topic with an analytical simulation of the inflation and extension behaviour of human abdominal aorta treated as a homogenous, nonlinear and anisotropic continuum. The constitutive model and its parameters are adopted from Labrosse et al. (2013) who have recently published the results of 17 inflation–extension tests with human abdominal aortas. Data describing the axial prestretch of aortas are adopted from Horny et al. (2014). They systematically conducted autopsy measurements of the prestretch and their sample has reached a total of 365 observations which is suitable to be used as a representative of a population.

I.2. Methods

I.2.1 Brief continuum mechanics introduction

Kinematics. Let $\boldsymbol{X}$ and $\boldsymbol{x}$ respectively denote position vectors of a material particle in the reference and deformed configuration of a body B. Let χ is a homeomorphism from $B(\boldsymbol{X})$ to $B(\boldsymbol{x})$, $\chi : B(\boldsymbol{X}) \rightarrow B(\boldsymbol{x})$.[8] In other words $\boldsymbol{x} = \chi(\boldsymbol{X})$. It is also possible to write an inverse mapping $\boldsymbol{X} = \chi^{-1}(\boldsymbol{x})$. When χ is used in a formulation of equations of continuum mechanics, the approach is referred to as the *material description*. In case of χ^{-1} is used, it is the *spatial description*.

The deformation gradient $\mathbf{F}$, basic measure of a deformation, is defined as $\mathbf{F} = d\boldsymbol{x}/d\boldsymbol{X}$. $\mathbf{F}$ is a two-point second order tensor from which other deformation measures are derived.[9] The basic measures used in the material description are right Cauchy-Green strain tensor $\mathbf{C}$, and Green-Lagrange strain tensor $\mathbf{E}$. They are defined as $\mathbf{C} = \mathbf{F}^{\mathrm{T}}\mathbf{F}$, and $\mathbf{E} = ½(\mathbf{C} - \mathbf{I})$. Here $\mathbf{I}$ denotes second order unit material tensor. Examples of strain measures in the spatial description are left Cauchy-Green strain tensor $\mathbf{b}$, and Euler-Almansi tensor $\mathbf{e}$; $\mathbf{b} = \mathbf{F}\mathbf{F}^{\mathrm{T}}$, and $\mathbf{e} = ½(\mathbf{i} - \mathbf{b}^{-1})$.[10]

Internal forces. Areal intensity of internal forces in a material is measured by stress tensors. Similarly to the deformation, we can define mixed (two-point), material and spatial stress tensors. The most frequently used measures are nominal stress tensor $\mathbf{P}$ (in case of uniaxial

---

[8] Homeomorphism χ is a mapping between two sets which is mutually unique (bijective), and mutually continuous. As a consequence, continuous inverse χ^{-1} does exist. $B(\boldsymbol{X})$ and $B(\boldsymbol{x})$ respectively denote a vector space defined above the reference and deformed configuration of the body B. $B(\boldsymbol{X})$ and $B(\boldsymbol{x})$ are also understood as metric spaces with Euclidean metric. Choosing some orthonormal bases, the position vectors can be written using their components as: $\boldsymbol{X} = X_1\boldsymbol{E}_1 + X_2\boldsymbol{E}_2 + X_3\boldsymbol{E}_3 = (X_1,X_2,X_3)$, and $\boldsymbol{x} = x_1\boldsymbol{e}_1 + x_2\boldsymbol{e}_2 + x_3\boldsymbol{e}_3 = (x_1,x_2,x_3)$. In what follows, vectors and tensors components will always be expressed with reference to some orthonormal basis. Thus covariant and contravariant components will not be distinguished, since they mutually equal. Similarly, all tensors are considered in their physical components.

[9] Two-point tensor means that it creates a (linear) map between two different spaces. In our specific case $\mathbf{F}$ creates the map between $dB(\boldsymbol{X})$ and $dB(\boldsymbol{x})$ where operator "d" denotes tangent space to B at a given point ($\boldsymbol{X}$ or $\boldsymbol{x}$); $\mathbf{F} : dB(\boldsymbol{X}) \rightarrow dB(\boldsymbol{x})$. The word tangent means that instead of position vectors their differentials are elements of the space. In the component notation, $\mathbf{F}$ is written as F_{iK} where the first index refers to the deformed configuration and the second to the reference configuration. Thus components of $\mathbf{F}$ are obtained as $F_{iK} = \partial x_i/\partial X_k$, which has clear geometrical interpretation – deformation gradient measures rate of change of the current coordinate $x_i(X_1,X_2,X_3)$ with respect to an increment of the reference coordinate X_K (where i and K = 1, 2, 3).

[10] In the component notation, the above mentioned tensors are written as C_{IK} ($C_{IK} = F_{jI}F_{jK}$), E_{IK} ($2E_{IK} = F_{jI}F_{jK} - \delta_{IK}$), b_{ik} ($b_{ik} = F_{jL}F_{kL}$), e_{ik} ($2e_{ik} = \delta_{ik} - F_{jL}F_{kL}$). Here δ is understood as Kronecker's delta.

stress state defined as current force per reference area), true or Cauchy stress tensor $\boldsymbol{\sigma}$ (in uniaxial stress state defined as current force per current area), and second Piola-Kirchhoff stress tensor $\mathbf{S}$ (in uniaxial state of stress defined as a force transformed by $\mathbf{F}^{-1}$ to the reference configuration per reference area).

Clearly $\mathbf{P}$ is expressed in mixed description, $\boldsymbol{\sigma}$ in spatial and $\mathbf{S}$ in material description.[11] It should be noted that a choice of the description (material, spatial, mixed) is immaterial from physical point of view. Continuum equations still express the same physical reality (usually balance of mass, momentum or energy). But in specific case, some of the descriptions may lead to easier solution from mathematical viewpoint than others.

Constitutive equations. A material is referred to be hyperelastic (or Green elastic) when and only when the elastic potential W exists and components of the stress tensor are derived from W via a differentiation with respect to the strain tensor: $\mathbf{P} = \partial W/\partial \mathbf{F}$; $\boldsymbol{\sigma} = J^{-1}(\partial W/\partial \mathbf{F})\mathbf{F}^{T}$; or e.g. $\mathbf{S} = \partial W/\partial \mathbf{E}$. J denotes so-called volume ration defined as $J = v/V = det(\mathbf{F}) = \sqrt{(det(\mathbf{C}))}$. W is also frequently named strain energy density function (density per unit reference volume).

I.2.2 Constitutive model and parameters

Although the biomechanics of large arteries has been extensively studied worldwide, scientific papers reporting the constitutive parameters obtained from pressurisation tests with human abdominal aorta are rare. Labrosse and co-workers have recently published data suitable for a purpose of computational simulation (Labrosse et al. 2013). They conducted inflation tests (with simultaneous free axial extension), determined constitutive parameters and discussed the results with reference to transmural stress distribution (residual strain/stress). Within our study, we adopted the constitutive model, material parameters and reference geometries (thickness, radius, opening angle) presented by them (Labrosse et al. 2013).

The constitutive model is based on the Fung–type exponential strain energy density function W (1) which in the literature is referred to as Guccione's model (Guccione et al.

[11] In the component notation, stress tensors are written as P_{iK}, σ_{ik}, and S_{IK}. Following transformation rules hold: $\mathbf{P} = J\boldsymbol{\sigma}\mathbf{F}^{-T} = \mathbf{FS}$, and $P_{iK} = J\sigma_{ij}F_{Kj}^{-1} = F_{iJ}S_{JK}$. Here J denotes volume ratio v/V. More details can be found in any standard textbook of continuum mechanics (e.g. in Holzapfel G.A. *Nonlinear Solid Mechanics: A Continuum approach for engineering* published in 2000 by J. Wiley and Sons; or in Bonet J. and Wood R.D. *Nonlinear Continuum Mechanics for Finite Element Analysis* published by Cambridge University Press in 1997; the readers who prefer Czech may found helpful courseware text written by the author Horný L. *Patobiomechanika srdečněcévního systému I. díl* published in 2014 available online via http://users.fs.cvut.cz/~hornyluk/files/Patobiomechanika-srdecnecevniho-systemu-I.pdf).

1991). E_{RR}, $E_{\Theta\Theta}$ and E_{ZZ} respectively are the radial, circumferential and axial components of the Green-Lagrange strain tensor in the cylindrical coordinate system and c_0, c_1, c_2 are the material parameters.

$$W = \frac{c_0}{2}\left(e^{c_1 E_{\Theta\Theta}^2 + c_2\left(E_{ZZ}^2 + E_{RR}^2\right)} - 1\right) \quad (1)$$

The artery wall was considered to be incompressible. Stress–strain relationship is then obtained in the form of (2). Here p is hydrostatic stress resulting from incompressibility constraint, $\mathbf{i}$ denotes second order unit tensor (spatial description), and $\boldsymbol{\sigma}$ is the Cauchy stress tensor.[12]

$$\boldsymbol{\sigma} = \mathbf{F}\frac{\partial W}{\partial \mathbf{E}}\mathbf{F}^T - \mathbf{i}p \quad (2)$$

Material parameters, age (38–77 years) and gender are specified in Table 1.

I.2.3 Axial prestretch λ_{zZ}^{ini}

Axial prestretch of the large arteries cannot be directly measured in the living due to the destructive nature of such an experiment (a segment of an artery has to be excised from a body; see Figure 1). Since Labrosse et al. (2013) did not report specific values of the prestretch, population data was adopted from Horny et al. (2014). Horny et al. (2014) measured the retraction of segments of the human abdominal aorta in 365 regular autopsies. The data sample of 365 measurements is large enough to capture trends and variability in the prestretch occurring in the population. The data has been fitted to a regression equation (3) describing dependence on age (a, b denotes regression parameters and x denotes age [years]).

$$\lambda_{zZ}^{ini} = ax^b \quad (3)$$

In the following simulations, initial axial prestretch λ_{zZ}^{ini} will be prescribed to the value obtained from (3) after the substitution of specific age (Table 1). Since no measurement is free from uncertainty and population data is used, the simulations will also employ the upper and lower limit of the prediction interval of the prestretch. Specifically, a 95%-confidence interval for a prediction given by the regression model. This approach will enable us to

[12] When the material is incompressible, its volume is preserved during a deformation. It implies J = 1. Components of a deformation tensor describing a change of the volume are zero. In such a case, however, hydrostatic part of the stress tensor cannot contribute to W because work conjugate deformation is zero. In such a situation the Lagrange method of undetermined multiplier (here denoted p) is adopted. Specific value of p is subsequently obtained in a formulation of a boundary-value problem from force boundary condition.

evaluate the expected behaviour of abdominal aorta (expected behaviour corresponds to estimates based on eq. 3) and its limits implicated by variance in the initial prestretch. They will be denoted *UL* (upper limit) and *LL* (lower limit) and are based on the *classical linear regression model* and its logarithmic transformation (4). Here y denotes initial prestretch, x denotes age, x_i denotes i-th observed age, S_e is residual standard deviation and t is a quantile of *Student-t* distribution for m degrees of freedom at significance α. The significance level 0.05 is used within all the study. We note that assumptions of classical linear model have been proven in Horny et al. (2012b).

$$\ln y = \ln a + b \ln x \pm t_{\frac{\alpha}{2}}(m) S_e \sqrt{1 + \frac{1}{n} + \frac{\left(\ln x - Mean(\ln x_i)\right)^2}{\sum_{i=1}^{n}\left(\ln x_i - Mean(\ln x_i)\right)^2}} \tag{4}$$

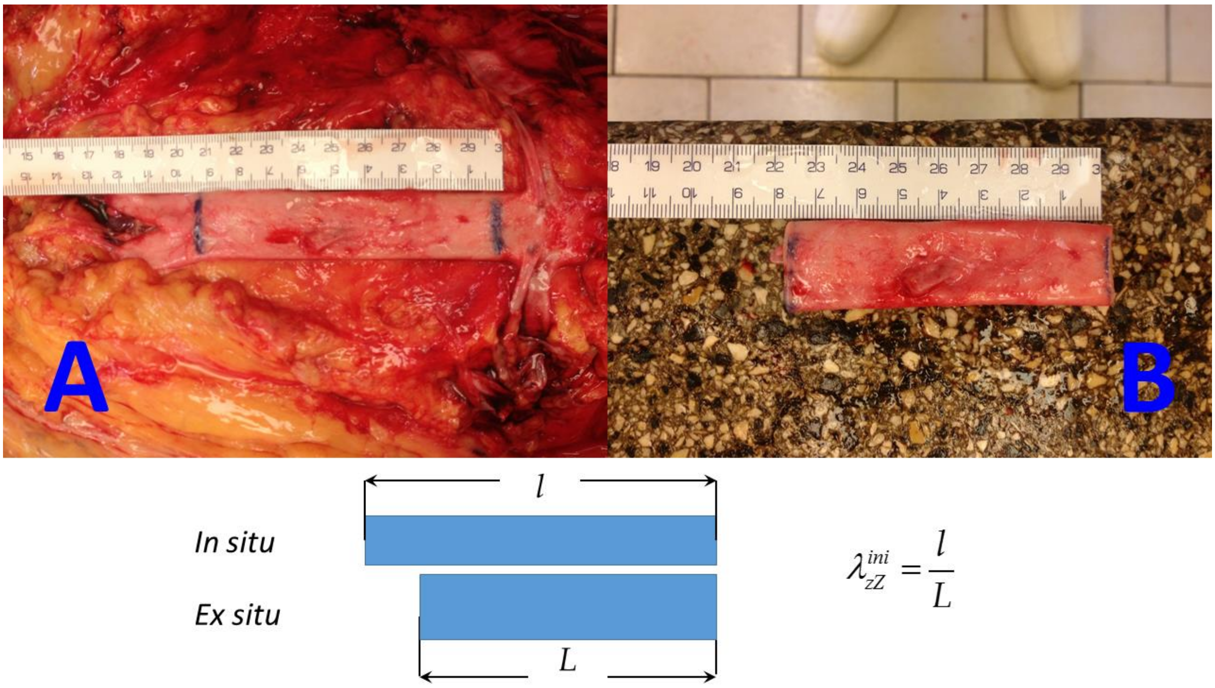

Figure 1. Human abdominal aorta. A – *in situ* infrarenal aorta at the time of autopsy measurement of the prestretch. B – *ex situ* infrarenal aorta at the time of autopsy measurement of the prestretch. Archive of the author.

I.2.4 Computational model for inflation-extension response

Herein we will focus on the quasi-static problem because it is the most frequently used in constitutive model determination. The artery wall will be considered as a one-layered, incompressible, nonlinear, anisotropic, and closed tube which is initially prestrained to its *in* *situ* length and is free at its outer deformed radius r_o and distended by internal pressure P at inner radius r_i. With regard to the thickness of the artery wall, both thin-walled and thick-walled approaches were employed. This is done for two basic reasons. First, the thin-walled model, which operates with mean wall stresses acting at middle radius r_m, may be regarded as more suitable when results of the simulation are compared with *in vivo* data obtained by ultrasound methods because there may be a problem in identifying the outer radius of the wall, in contrast to media-adventitia interface (this interface could be used as an estimate of r_m). On the other hand, the thin-walled model (in contrast to thick-walled) cannot capture residual strain/stress which may significantly change the true stress/strain state of the material.

Thin-walled model. In the thin-walled approximation, the equilibrium equations are written in the form of (5) with kinematic equations (6).

$$\sigma_{rr} = -\frac{P}{2} \qquad \sigma_{\theta\theta} = \frac{r_m P}{h} \qquad \sigma_{zz} = \frac{F_{red}}{2\pi r_m h} + \frac{r_m P}{2h} \tag{5}$$

$$h = \lambda_{rR} H \qquad r_m = \lambda_{\theta\Theta} R_m \qquad z = \lambda_{zZ} Z \tag{6}$$

In (5) σ_{rr}, $\sigma_{\theta\theta}$, and σ_{zz} respectively denote mean radial, circumferential and axial Cauchy stress at middle radius $r_m = (r_i + r_o)/2$, and h is the thickness in the deformed state. Middle reference radius is denoted R_m ($R_m = R_i + H/2$), reference inner radius R_i, and H denotes reference thickness (see Table 1 for specific values). From (6) the deformation gradient can be written as $\mathbf{F} = \mathrm{diag}[\lambda_{rR}, \lambda_{\theta\Theta}, \lambda_{zZ}]$.

F_{red} in (5c) is external axial force necessary to obtain the *in situ* length corresponding to λ_{zZ}^{ini} measured during autopsy. In *ex vivo* experiments, it is frequently generated with a hanging mass connected to a specimen (vertical configuration of the inflation–extension test). The denotation F_{red} was chosen with respect to nomenclature used in Holzapfel et al. (2000), Holzapfel and Ogden (2010a), and Ogden and Saccomandi (2007). This force is developed during the growth period and the literature suggests that elastin fibres are responsible for bearing this load (Carta et al. 2009; Humphrey et al. 2009).

The key problem is that we in fact do not know how large *in vivo* F_{red} is. We only have evidence that arteries retract upon excision. Statistics of λ_{zZ}^{ini} are thus obtained, since measured during autopsy, at $P = 0$. This motivated us to employ F_{red} as a constant during the pressurisation. Throughout the pressurisation, the mechanical response of the artery has to satisfy equilibrium equations (5) and simultaneously mechanical state of the material has to conform to the constitutive equations (2). Combining (2) and (5) and interchanging variables in W to the deformation gradient, the system (7) is obtained.

$$\lambda_{rR}\frac{\partial W}{\partial\lambda_{rR}}-p=-\frac{P}{2}\qquad\lambda_{\theta\Theta}\frac{\partial W}{\partial\lambda_{\theta\Theta}}-p=\frac{r_m P}{h}\qquad\lambda_{zZ}\frac{\partial W}{\partial\lambda_{zZ}}-p=\frac{F_{red}}{2\pi r_m h}+\frac{r_m P}{2h}\qquad(7)$$

Please, remind that in the chosen approach, λ_{zZ}^{ini} is the constant used to compute F_{red} and may not necessarily correspond to λ_{zZ} which can change during pressurisation (according to the system 7). This approach respects the fact the *in vivo* axial stretch has been proven to be slightly different from the prestretch measured in autopsy (Humphrey et al. 2009).

The system (7) describes the inflation–extension of the initially prestrained artery and was solved in the following steps:

1. Specific donor is chosen from Table 1 → R_i, H, c_0, c_1, c_2, and age.

2. From (3) expected λ_{zZ}^{ini} is estimated.

3. Derivatives at left-hand side in (7) are conducted. Subsequently p is eliminated from (7b) and (7c) using (7a). In the remaining system, (7b) and (7c), λ_{rR} is substituted with $1/(\lambda_{\theta\Theta}\cdot\lambda_{zZ})$ because for incompressible material $det\mathbf{F} = 1$ holds.

4. Prestretching force F_{red} corresponding to λ_{zZ}^{ini} is computed from (7b) and (7c) at P = 0 (both equations (7b) and (7c) are necessary because one also has to determine $\lambda_{\theta\Theta}^{ini}$ corresponding to prestretched but unpressurised tube).

5. The system (7b) and (7c) is now numerically solved for unknown $\lambda_{\theta\Theta}$ and λ_{zZ} (with F_{red} substituted from step **4**) at P = 1, 2, .., 20 kPa.

6. When $\lambda_{\theta\Theta}$ and λ_{zZ} are determined, σ_{rr}, $\sigma_{\theta\theta}$, and σ_{zz} can be calculated substituting the results into (5).

7. Instead of (3) the equation (4) is used to compute $\lambda_{zZ,UL}^{ini}$ ($\lambda_{zZ,LL}^{ini}$) and steps **3.** – **6.** are repeated to obtain results for upper limit (lower limit) of initially prestretched arteries.

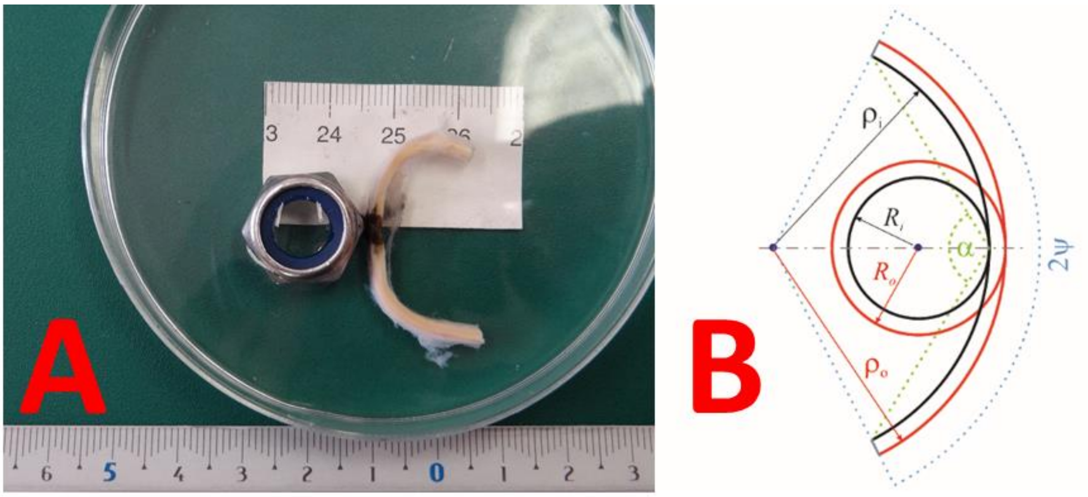

Figure 2. Opened ring of abdominal aorta. A – Real aortic ring after the radial cut. B – Assumed kinematics (opened stress-free configuration and closed but not pressurised). The photo is from author's archive.

Thick-walled model. Arteries are residually stressed in their unloaded configuration (Rachev and Greenwald 2003; Valenta et al. 2002). The basic approach incorporating this fact into the computational model is to consider the opened up configuration as the reference one. When the unloaded ring of an artery is cut radially, it springs to an opened configuration which is (in the first approximation) considered to be stress-free and the geometry is modelled as a circular sector with inner radius ρ_i, outer radius ρ_o and sector angle 2ψ. The so-called opening angle (inscribed angle in the sector), frequently used to characterise residual strain, is then given as $\pi - \psi$. Figure 2 depicts the situation.

Equilibrium equations, with substituted constitutive model, describing the response of the closed thick-walled tube to internal pressure and prestretching force can be written in the form of (8). They are adopted from Labrosse et al. (2013). A detailed derivation of (8) is only rarely found in the literature. One example is the paper of Matsumoto and Hayashi (1996). Since the derivation could be considered somewhat lengthy, it is moved to the Appendix A.[13]

$$P = \int_{r_i}^{r_o} \lambda_{\theta\Theta} \frac{\partial \hat{W}}{\partial \lambda_{\theta\Theta}} \frac{dr}{r} \qquad F_{red} = \pi \int_{r_i}^{r_o} \left(2\lambda_{zZ} \frac{\partial \hat{W}}{\partial \lambda_{zZ}} - \lambda_{\theta\Theta} \frac{\partial \hat{W}}{\partial \lambda_{\theta\Theta}} \right) r dr \tag{8}$$

Here $\hat{W}$ is the strain energy density (1) with variables changed to the components of **F** and λ_{rR} substituted by $\lambda_{rR} = 1/(\lambda_{\theta\Theta} \lambda_{zZ})$; $W = W(\lambda_{rR},\lambda_{\theta\Theta},\lambda_{zZ}) = \hat{W}(1/(\lambda_{\theta\Theta}\lambda_{zZ}),\lambda_{\theta\Theta},\lambda_{zZ})$. Circumferential stretch $\lambda_{\theta\Theta}$ is considered to be a function of the deformed radius r ($r_i \le r \le r_o$)

[13] Detailed derivation is also available in Czech version online in the Biomechanics II courseware created by the author via the link http://users.fs.cvut.cz/~hornyluk/files/Biomechanika-II.pdf (see p. 31 – 38).

and is expressed with respect to the radius in opened configuration ρ ($\rho_i \leq \rho \leq \rho_o$), $\lambda_{\theta\Theta} = \pi r/(\psi\rho)$.[14] Axial stretch λ_{zZ} is considered to be uniform along the length and thickness of the tube (λ_{zZ} = constant). The equations (8) presume that boundary conditions $\sigma_{rr}(r_o) = 0$ and $\sigma_{rr}(r_i) = -P$ are applied. The system (8) was used to simulate the inflation-extension response of aortas in the following way:

1. Specific donor is chosen from Table 1 → R_i, H, c_0, c_1, c_2, opening angle and age.

2. From (3) expected λ_{zZ}^{ini} is estimated.

3. Integrands in (8) are expressed as functions of r and λ_{zZ}. $r_o = r_o(r_i)$ is used in upper bounds of integrals (from incompressibility condition).

4. Prestretching force F_{red} corresponding to λ_{zZ}^{ini} is computed from the system (8) at P = 0 (both equations (8a) and (8b) are necessary because one also has to determine r_i^{ini} corresponding to residually stressed and axially prestretched but unpressurised tube).

5. The system (8) is now numerically solved for unknown r_i and λ_{zZ} (with F_{red} substituted from step **4**) at P = 1, 2, .., 20 kPa.

6. When r_i and λ_{zZ} are found, $\sigma_{rr}(r)$, $\sigma_{\theta\theta}(r)$, and $\sigma_{zz}(r)$ can be calculated from equations (9) considering that $\lambda_{\theta\Theta} = \pi r/(\psi\rho)$.

$$\sigma_{rr} = -\int_r^{r_o} \lambda_{\theta\Theta} \frac{\partial \hat{W}}{\partial \lambda_{\theta\Theta}} \frac{dx}{x} \qquad \sigma_{\theta\theta} = \lambda_{\theta\Theta} \frac{\partial \hat{W}}{\partial \lambda_{\theta\Theta}} + \sigma_{rr} \qquad \sigma_{zz} = \lambda_{zZ} \frac{\partial \hat{W}}{\partial \lambda_{zZ}} + \sigma_{rr} \tag{9}$$

A detailed derivation of (9) is available in Appendix A. It is important to emphasize that in (9a) the right-hand expression is a function of the lower bound r.

6. Instead of (3), the equation (4) is used to compute $\lambda_{zZ,UL}^{ini}$ ($\lambda_{zZ,LL}^{ini}$) and steps **4.** – **5.** are repeated to obtain results for upper limit (lower limit) of initially stretched arteries.

Using the procedures described above, $\lambda_{\theta\Theta}(P)$ and $\lambda_{zZ}(P)$ in the thin-walled, and $\lambda_{\theta\Theta}(r,P)$ and $\lambda_{zZ}(P)$ in the thick-walled approach were determined for all involved donors numerically in Maple 16. The results were used to compute variations in the stretches during the pressure cycle $\varepsilon_{iI} = \lambda_{iI}(P_{SYS}) - \lambda_{iI}(P_{DIA})$ for $iI = \theta\Theta$ and zZ. In what follows circumferential stretch

[14] Notice that the expression for $\lambda_{\theta\Theta}$ still represents a ratio between deformed length, circumference (πr), and reference length ($\psi\rho$). Physical sense is still the same, and when residual strain is not considered, the ratio changes to r/R as in the thin-walled tube; equation (6b).

variation $\varepsilon_{\theta\Theta}$ will also be referred to as *distensibility*.[15] The results were also used to create P–$\lambda_{\theta\Theta}$ and P–λ_{zZ} dependences, and to quantify changes of the axial stress in the course of the pressurisation. Changes of the axial stress were quantified as relative increments between diastole and systole $[\sigma_{zz}(P_{SYS}) - \sigma_{zz}(P_{DIA})]/\sigma_{zz}(P_{DIA})$.

In what follows, the results of the thick-walled model and thin-walled model will not be distinguished by special symbols for quantities in hand but they always will be distinguished by the radius at which they were obtained. This indicates that the results computed at r_i and r_o are always given by the thick-walled model with incorporated residual strain and the results computed with the thin-walled model are always related to r_m.

I.2.5 Stiffness (Elasticity tensor)

Chen et al. (2008) have suggested incorporating the assumption of the constant ratio between circumferential and longitudinal elastic modulus of the artery wall during the pressure cycle to overcome the impossibility of measuring axial stress in the constitutive parameter identification procedure conducted with living subjects. To evaluate this hypothesis, components of the elasticity tensor C (tensor of elastic module) in the material description have been computed.[16]

C is defined as the derivative (10) of the second Piola–Kirchhoff stress tensor $\mathbf{S}$ with respect to the Green–Lagrange strain tensor $\mathbf{E}$, Holzapfel (2000) ch. 6.6.

$$\mathsf{C} = \frac{\partial \mathbf{S}}{\partial \mathbf{E}} \tag{10}$$

The Second Piola–Kirchhoff stress tensor $\mathbf{S}$ measures the stress state of a body using material description. One can say that $\mathbf{S}$ is defined with respect to the material (undeformed) configuration. This is in contrast to the Cauchy stress tensor $\boldsymbol{\sigma}$ which measures the stress state of a body in the deformed configuration (spatial description). Both stress tensors can be mutually transformed using (11) because the deformation gradient $\mathbf{F}$ creates a map from an undeformed to a deformed configuration. The equation (11) involves the inverse of $\mathbf{F}$ since transformation proceeds in the opposite direction – from deformed to undeformed configuration.

$$\mathbf{S} = J\,\mathbf{F}^{-1}\,\boldsymbol{\sigma}\,\mathbf{F}^{-T} \tag{11}$$

---

[15] Bearing in minds our main objective, the effect of axial prestretch on biomechanics of abdominal aorta, it has to be noted that $\varepsilon_{iI} = \varepsilon_{iI}\,(P_{SYS}, P_{DIA},\lambda_{zZ}^{ini}) = \lambda_{iI}(P_{SYS},\lambda_{zZ}^{ini}) - \lambda_{iI}(P_{DIA},\lambda_{zZ}^{ini})$ in fact.

[16] Note that Palatino Linotype is used as a font for Latin symbols of quantities in this study. To distinguish between right Cauchy-Green strain (second order) tensor $\mathbf{C}$ and the tensor of elasticity (fourth order), Futura Bk Bt is used for the elasticity tensor C.

J in (11) denotes the ratio between volume of a body in the deformed and undeformed configuration and, in our specific case, for the incompressible material J = 1. Since in our study only diagonal components of second order tensors are involved, the equation (11) reduces to $S_{KK} = \lambda_{kK}^{-2}\sigma_{kk}$.

Thin-walled model. $\mathsf{C}_{\Theta\Theta\Theta\Theta}$ and C_{ZZZZ} were computed from (10) with the substituted material counterpart of (2) which can be written in the form of (12).

$$\mathbf{S} = \frac{\partial W}{\partial \mathbf{E}} - p\left(2\mathbf{E}+\mathbf{I}\right)^{-1} \tag{12}$$

Specific expression for p is obtained from the radial component of the equation (12). Considering (11), $S_{RR} = \lambda_{rR}^{-2}\sigma_{rr}$ holds and p can be written as $p = (2E_{RR} + 1)\cdot\partial W/\partial E_{RR} - \sigma_{rr}$. In the case of the thin-walled model, $-P/2$ is substituted into the radial Cauchy stress σ_{rr}.

Thick-walled model. In the thick-walled model, the situation is somewhat more complicated. We will use equations (9b) and (9c) with substituted (9a). They will be transformed into the components of **S**. This results in (13) and (14).

$$S_{\Theta\Theta} = \frac{\partial \hat{W}}{\partial E_{\Theta\Theta}} - \left(2E_{\Theta\Theta}+1\right)^{-1}\int_r^{r_o}\left(2E_{\Theta\Theta}+1\right)\frac{\partial \hat{W}}{\partial E_{\Theta\Theta}}\frac{dx}{x} \tag{13}$$

$$S_{ZZ} = \frac{\partial \hat{W}}{\partial E_{ZZ}} - \left(2E_{ZZ}+1\right)^{-1}\int_r^{r_o}\left(2E_{\Theta\Theta}+1\right)\frac{\partial \hat{W}}{\partial E_{\Theta\Theta}}\frac{dx}{x} \tag{14}$$

Using the product rule for differentiation, equations (13) and (14) give (15) and (16), respectively.

$$\begin{aligned}\mathsf{C}_{\Theta\Theta\Theta\Theta} = \frac{\partial S_{\Theta\Theta}}{\partial E_{\Theta\Theta}} = \frac{\partial^2 \hat{W}}{\partial E_{\Theta\Theta}^2} &+ 2\left(2E_{\Theta\Theta}+1\right)^{-2}\int_r^{r_o}\left(2E_{\Theta\Theta}+1\right)\frac{\partial \hat{W}}{\partial E_{\Theta\Theta}}\frac{dx}{x} \\ &-\left(2E_{\Theta\Theta}+1\right)^{-1}\frac{\partial}{\partial E_{\Theta\Theta}}\int_r^{r_o}\left(2E_{\Theta\Theta}+1\right)\frac{\partial \hat{W}}{\partial E_{\Theta\Theta}}\frac{dx}{x}\end{aligned} \tag{15}$$

$$\begin{aligned}\mathsf{C}_{ZZZZ} = \frac{\partial S_{ZZ}}{\partial E_{ZZ}} = \frac{\partial^2 \hat{W}}{\partial E_{ZZ}^2} &+ 2\left(2E_{ZZ}+1\right)^{-2}\int_r^{r_o}\left(2E_{\Theta\Theta}+1\right)\frac{\partial \hat{W}}{\partial E_{\Theta\Theta}}\frac{dx}{x} \\ &-\left(2E_{ZZ}+1\right)^{-1}\frac{\partial}{\partial E_{ZZ}}\int_r^{r_o}\left(2E_{\Theta\Theta}+1\right)\frac{\partial \hat{W}}{\partial E_{\Theta\Theta}}\frac{dx}{x}\end{aligned} \tag{16}$$

To compute derivatives of the integrals in (15) and (16), the chain rule in the form $\partial(\text{-})/\partial E_{KK} = [\partial(\text{-})/\partial r]\cdot[\partial r/\partial E_{KK}]$ (K = Θ and Z) is adopted. Since the differentiation is conducted with respect to r and r simultaneously is a variable integration bound (the integrals are understood as the functions of the lower bound), the procedure leads to equations (17) and (18). Note that $d(\int_r^{ro} f(x)dx)/dr = -f(r)$.

$$C_{\Theta\Theta\Theta\Theta} = \frac{\partial S_{\Theta\Theta}}{\partial E_{\Theta\Theta}} = \frac{\partial^2 \hat{W}}{\partial E_{\Theta\Theta}^2} + 2\left(2E_{\Theta\Theta}+1\right)^{-2} \int_r^{r_o} \left(2E_{\Theta\Theta}+1\right) \frac{\partial \hat{W}}{\partial E_{\Theta\Theta}} \frac{dx}{x} + \frac{\partial \hat{W}}{\partial E_{\Theta\Theta}} \frac{1}{r} \frac{\partial r}{\partial E_{\Theta\Theta}} \tag{17}$$

$$C_{ZZZZ} = \frac{\partial S_{ZZ}}{\partial E_{ZZ}} = \frac{\partial^2 \hat{W}}{\partial E_{ZZ}^2} + 2\left(2E_{ZZ}+1\right)^{-2} \int_r^{r_o} \left(2E_{\Theta\Theta}+1\right) \frac{\partial \hat{W}}{\partial E_{\Theta\Theta}} \frac{dx}{x} + \frac{2E_{\Theta\Theta}+1}{2E_{ZZ}+1} \frac{\partial \hat{W}}{\partial E_{\Theta\Theta}} \frac{1}{r} \frac{\partial r}{\partial E_{ZZ}} \tag{18}$$

What remains to be clarified are derivatives $\partial r/\partial E_{\Theta\Theta}$ and $\partial r/\partial E_{ZZ}$. The expression $r = r(E_{\Theta\Theta},E_{ZZ})$ can be obtained considering a volume preservation during the deformation: $\pi l(r_o^2 - r^2) = \psi L(\rho_o^2 - \rho^2)$. This relation equals the volume of elongated (to length l) and pressurized tube limited by outer deformed radius r_o and variable radius r to the volume of the stress-free (opened up) cylindrical sector (of the length L) limited by outer radius ρ_o and variable radius ρ. Considering $\lambda_{zZ} = l/L$, one obtains (19) substituting ρ from above mentioned volume preservation into $\lambda_{\theta\Theta} = \pi r/(\psi\rho)$.

$$\lambda_{\theta\Theta} = \frac{\pi r}{\psi\sqrt{\rho_o^2 - \frac{\pi}{\psi}\lambda_{zZ}\left(r_o^2 - r^2\right)}} \tag{19}$$

After some algebra, the expression (20), which relates r to $\lambda_{\theta\Theta}$ and λ_{zZ}, is obtained from (19).

$$r = \sqrt{\frac{\lambda_{\theta\Theta}^2 \psi\left(\psi\rho_o^2 - \pi r_o^2 \lambda_{zZ}\right)}{\pi\left(1 - \lambda_{\theta\Theta}^2 \psi \lambda_{zZ}\right)}} \tag{20}$$

One can arrive to the final expression $r = r(E_{\Theta\Theta},E_{ZZ})$ substituting stretches with Green–Lagrange strain components, $\lambda_{\theta\Theta} = (2E_{\Theta\Theta} + 1)^{½}$ and $\lambda_{zZ} = (2E_{ZZ} + 1)^{½}$. Finally, the stiffness ratio $C_{\Theta\Theta\Theta\Theta}/C_{ZZZZ}$ and its relative increment between diastole and systole (normalised with respect to diastole) can be computed.

I.2.6 Blood pressure in ageing

It is well known that the character of pressure pulses in human arteries changes with age (Greenwald 2007; O'Rourke and Hashimoto 2007). With regard to this fact, we adopted numerical values of the diastolic and systolic pressure from recent epidemiological study conducted by Wilkins et al. (2010). They evaluated results of *Canadian Health Measures Survey* 2007 – 2009. Specific values used in our study are listed in Table 2. They were obtained as linear interpolation (with respect to variable age) of the data found in Figure 1 in Wilkins et al. (2010). The data in the original source is gender specific and represents the average in the population. That is, the averaged value is obtained considering healthy, successfully treated, unsuccessfully treated and untreated hypertensive/hypotensive population in the given ageing period.

I.2.7 Correlation

The linear correlation coefficient R was computed for all treated quantities to obtain a basic estimate of their dependence on age. It is supplemented with the test of the hypothesis $R = 0$ (against alternative $R \neq 0$) based on the statistics $T = R[(n - 2)/(1 - R^2)]^{1/2}$ which was evaluated by p–value (here n is the number of observations). Results were considered to be statistically significant at the level 0.05 within this study.

I.3. Results

In the present simulation, the objective is to show how the mechanical response of human abdominal aorta changes because of both changed constitutive parameters and decreased longitudinal prestretch. Details of involved donors are listed in Table 1 (geometry and material parameters) and in Table 2 (estimated prestretch and diastolic and systolic pressure).

I.3.1 Initial axial prestretch

Data describing initial axial prestretch was collected during autopsies as described in Horny et al. (2014). The regression equation (3) was fitted to the resulting sample with parameters a = 2.4016 [1/year]; b = -0.1957 [-]. Regression curve and data are depicted in Figure 3. Limits for interval of 95%-confidence of a prediction (an interval into which a future observation will fall with a probability equal to 0.95) are also depicted. Within the text, these limits are denoted $\lambda_{zZ,UL}^{ini}$ (upper) and $\lambda_{zZ,LL}^{ini}$ (lower). Linear correlation coefficient for $ln(\lambda_{zZ}^{ini})$–$ln(Age)$ R = -0.903 (p–value < 0.001) confirmed a strong correlation between age and axial prestretch. Specific values for λ_{zZ}^{ini}, $\lambda_{zZ,UL}^{ini}$, and $\lambda_{zZ,LL}^{ini}$ used in the simulations are listed in Table 2.

The prediction interval for λ_{zZ}^{ini} based on (4) gives the lower limit smaller than 1 for age > 61 (Figure 3). This is the consequence of the used methodology (*expectation* ± *uncertainty* given as a function of a variance). Nevertheless, Horny et al. (2014) did not report any abdominal aorta with λ_{zZ}^{ini} < 1 (i.e. precompressed artery). Considering this fact in what follows, we have decided to substitute the exact results of the equation (4) with $\lambda_{zZ,LL}^{ini}$ = 1 for donors with age higher than 61.

I.3.2 Inflation-extension response

Prescribed referential geometry, initial prestretch and constitutive parameters (Table 1 and 2) enabled the systems (7) and (8) to be solved with respect to $\lambda_{\theta\Theta}$ and λ_{zZ} for defined internal pressure P. Two representatives of P–$\lambda_{\theta\Theta}$ and P–λ_{zZ} are shown in Figure 4 (M38) and Figure 5 (F65). For the sake of comparison, the results of the thick-walled model with incorporated residual strain as well as the results of the thin-walled model are depicted. Changes in the inflation characteristic induced by the prestretch are demonstrated for λ_{zZ}^{ini} = 1.0, 1.1, 1.2, 1.3, 1.4 with P = 0–20 kPa.

The higher the axial prestretch, the lower the initial circumferential stretch is. It is clearly evident that axial deformation at physiological pressures (10 – 16 kPa) depends on initial prestretch; a property of the so-called *inversion point* is exhibited. The inversion point is the value of axial prestretch in the P–λ_{zZ} diagram which, in an idealised case, divides the diagram into inflation–extension and inflation–shortening behaviour (Ogden and Saccomandi 2007; Schulze-Bauer et al. 2003). Considering P–$\lambda_{\theta\Theta}$, an increased axial prestretch induces a left-side shift as expected. However, it also makes an inflexion point on P–$\lambda_{\theta\Theta}$ more discernible and decreases the steepness of the curve at physiological pressures.

The effect of the initial axial prestretch modelled by (3) and (4) is shown in detail in Figure 6 for M61 (computed with thin-walled model). The upper panel shows the P–λ_{zZ} curve and lower panel P–$\lambda_{\theta\Theta}$. Expected behaviour (λ_{zZ}^{ini} corresponding just to the regression equation (3)) is depicted with a blue solid curve laying in between curves computed with $\lambda_{zZ,LL}^{ini}$ (black dots) and $\lambda_{zZ,UL}^{ini}$ (red dashes) which are based on (4). It is clearly noticeable that aorta M61 exhibits higher variation of the circumferential stretch in pressure cycle $P \in [10\text{kPa};16\text{kPa}]$ for higher axial prestretch $\lambda_{zZ,UL}^{ini}$ than for smaller $\lambda_{zZ,LL}^{ini}$.

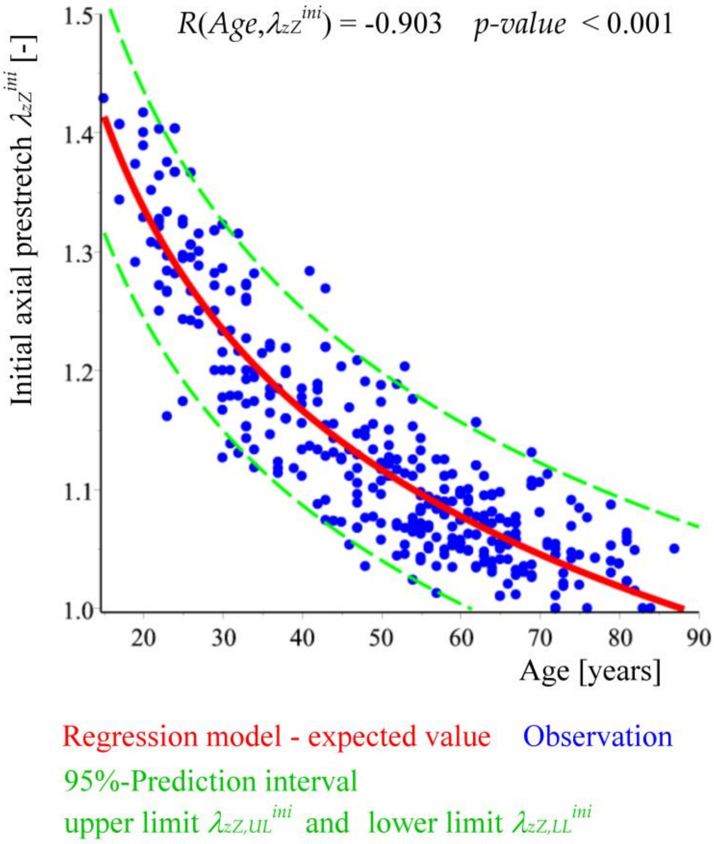

Figure 3. Dependence of initial axial prestretch (found in autopsy) on age. Regression model for expected value λ_{zZ}^{ini} – thick red curve; upper limit $\lambda_{zZ,UL}^{ini}$ and lower limit $\lambda_{zZ,LL}^{ini}$ of 95%-prediction interval – green dashed curves; observations – blue points. Estimated parameters for regression equation (3) are a = 2.4016 [1/year]; b = -0.1957 [-].The data was adopted from Horny et al. (2013a). Since the lower limit of the prediction interval approaches 1 at the age of 61 years (no axial prestretch) and governed by (4) follows with values smaller than 1 (i.e. axial precompresion), it was decided to prescribe $\lambda_{zZ,LL}^{ini}$ = l for age > 61 years. This was motivated by two facts: (1) Horny et al. (2013a) did not report any precompressed artery in their sample, (2) it is not clear whether the constitutive equations used in this study are suitable to describe precompressed arteries.

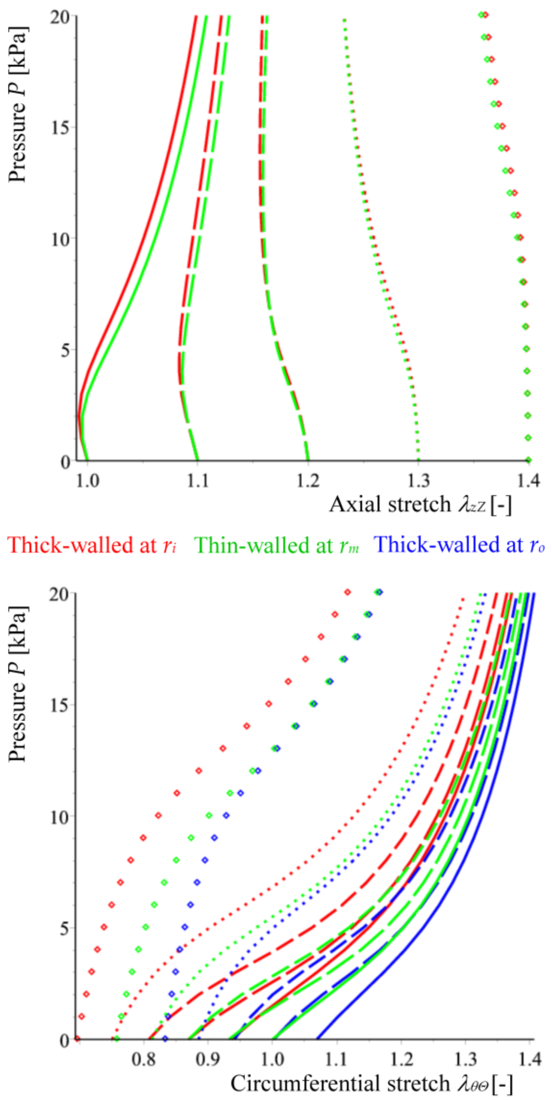

Figure 4. Inflation-extension behaviour of a 38 year old male donor (M38). The upper panel shows P–λ_{zZ} and lower panel P–$\lambda_{\theta\Theta}$. Predictions for thick-walled (residual strain incorporated) model for $\lambda_{\theta\Theta}$ are computed at r_i (red) and r_o (blue) and results based on the thin-walled model are computed at middle radius r_m (green). However, λ_{zZ} is constant at all radii hence upper panel, P–λ_{zZ}, includes only two colours. Each triplet (P–$\lambda_{\theta\Theta}$) or doublet (P–λ_{zZ}) of curves corresponds to specific initial axial stretch $\lambda_{zZ}^{ini} = 1$ (continuous curve), 1.1 (long dashed), 1.2 (dashed), 1.3 (dotted), and 1.4 (diamonds). The easiest way to understand the panels is to consider that in P–λ_{zZ} axial prestretch increases from the left to the right, in contrast to P–$\lambda_{\theta\Theta}$ where axial prestretch increases from the right to the left. This figure manifests two basic points: (a) the axial behaviour of the tube for $P \in [10\text{kPa}, 16\text{kPa}]$ changes from axial extension (low initial axial prestretch) to axial shortening (high initial axial prestretch); and (b) the higher initial axial stretch gives P–$\lambda_{\theta\Theta}$ curves with elevated position of the inflection point (elevated on P–axis). Notice that while P–λ_{zZ} curves show only small differences between computational models (thick/thin), P–$\lambda_{\theta\Theta}$ curves show that at high pressures and high axial prestretches $\lambda_{\theta\Theta}(r_o)$ and $\lambda_{\theta\Theta}(r_m)$ mutually converge more rapidly than $\lambda_{\theta\Theta}(r_i)$ and $\lambda_{\theta\Theta}(r_m)$.

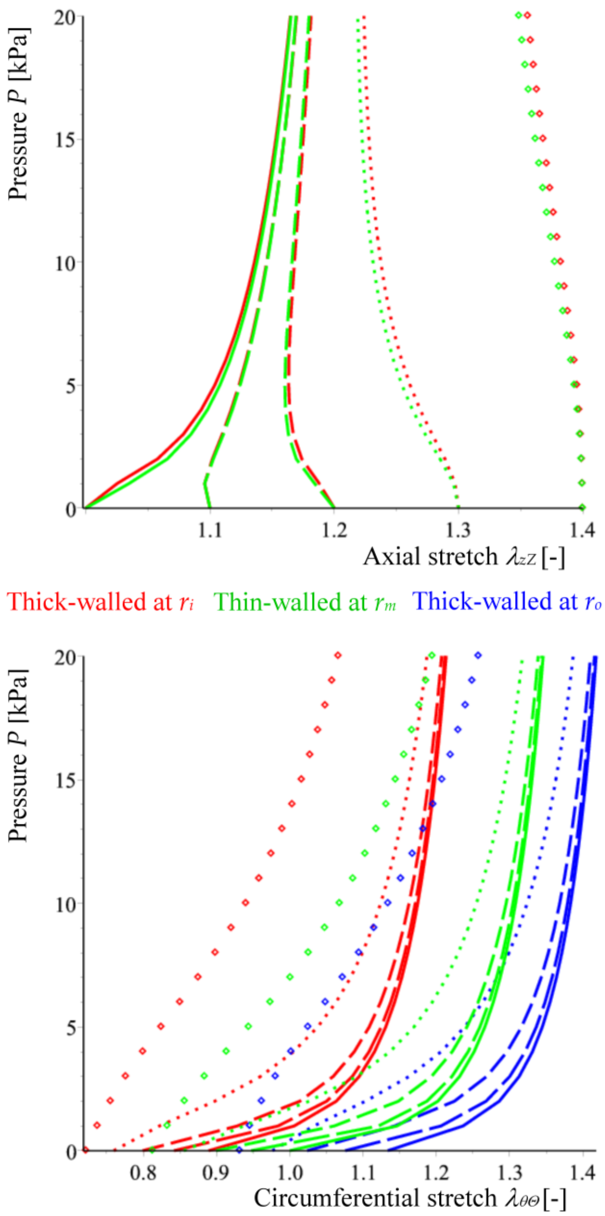

Figure 5. Inflation-extension behaviour of a 65 year old female donor (F65). The panels are arranged in the same way as in Figure 2. The graphs show two differences when compared with M38 in Figure 2. First, P–λ_{zZ} curve for $\lambda_{zZ}^{ini} = 1$ does not exhibit initial shortening. It begins with axial extension. Second, the inflection point does not appear on P–$\lambda_{\theta\Theta}$ curve for $\lambda_{zZ}^{ini} = 1$. However, curves for higher axial prestretch do show the inflection. Note that the existence of an inflection point makes P–$\lambda_{\theta\Theta}$ curve S-shaped and results in higher circumferential distensibility $\varepsilon_{\theta\Theta} = \lambda_{\theta\Theta}(16\text{kPa}) - \lambda_{\theta\Theta}(10\text{kPa})$ (in contrast to J-shaped curve without an inflection).

Table 1. Age, gender, geometry and constitutive parameters of involved donors; adopted from Labrosse et al. (2013).

ID†	F49	F50	F63	F65	M38	M42	M57	M60	M61a	M61b	M66	M67a	M67b	M70a	M70b	M71	M77
Opening angle [°]	252	323	96	248	117	125	322	156	270	335	253	118	174	208	201	118	135
R_i [mm]	5.9	6.7	5.4	6.2	5.3	6.5	7.5	6.3	7.7	7.3	7.2	8	7.9	7.1	7.4	10	7
H [mm]	1.51	1.14	0.96	1.21	1.22	1.56	1.28	1.69	1.22	1.62	1.78	1.58	1.26	1.23	1.64	1.72	1.5
c_0 [kPa]	8.4	8.4	23	1.6	14.7	41.8	0.8	7.6	2.4	2.3	9.4	3.5	2.2	14	1.8	17	1.2
c_1 [-]	5.09	15.21	4.07	9.26	3.04	1.54	6.74	2.96	37.53	6.82	7.81	24.47	56.69	16.09	18.62	13	41.08
c_2 [-]	8.18	9.67	7.2	11.77	7.38	1.44	12.44	10.23	34.01	19.16	12.5	27.9	41.66	7.38	35.99	11.85	49.51

† *ID* indicates sex (female/male) and age [years] of donors.

Table 2. Initial axial prestretches for donors involved in the simulation estimated with regression model (3) and its prediction intervals (4). The table is ordered in the same way as Table 1. Estimated parameters in (3) a = 2.4016 [1/years]; b = -0.1957 [-]; and in (4) $t_{0.95/2}(363)\cdot S_e$ = 0.0707; $Mean(\mathbf{ln}x_i)$ = 3.8414; and $\Sigma(\mathbf{ln}x_i - Mean(\mathbf{ln}x_i))^2$ = 0.0184.

ID†	F49	F50	F63	F65	M38	M42	M57	M60	M61a	M61b	M66	M67a	M67b	M70a	M70b	M71	M77
λ_{zZ}^{ini} [-]	1.121	1.117	1.067	1.061	1.179	1.156	1.089	1.078	1.074	1.074	1.055	1.055	1.055	1.046	1.046	1.043	1.026
$\lambda_{zZ,UL}^{ini}$ [-]	1.204	1.199	1.146	1.139	1.265	1.240	1.168	1.157	1.153	1.153	1.132	1.132	1.132	1.123	1.123	1.119	1.102
$\lambda_{zZ,LL}^{ini}$ [-]	1.045	1.041	0.995*	0.988*	1.098	1.077	1.014	1.004	1	1	0.983*	0.983*	0.983*	0.974*	0.974*	0.971*	0.956*
$\lambda_{zZ}(P_{SYS})$# [-]	1.141	1.158	1.107	1.159	1.149	1.358	1.170	1.088	1.067	1.067	1.079	1.060	1.063	1.154	1.037	1.082	1.040
$\lambda_{zZ}(P_{DIA})$# [-]	1.127	1.146	1.087	1.142	1.145	1.307	1.154	1.072	1.066	1.057	1.067	1.055	1.059	1.129	1.032	1.068	1.035
P_{DIA}§ [kPa]	9.7	9.7	9.8	9.8	10.1	10.3	10.4	10.3	10.3	10.3	10.1	10	10	9.9	9.9	9.8	9.5
P_{SYS}§ [kPa]	15.1	15.2	16.8	17	15.3	15.4	16.1	16.2	16.2	16.2	16.4	16.5	16.5	16.6	16.6	16.6	16.8

† *ID* indicates sex (female/male) and age [years] of donors. *$\lambda_{zZ,LL}^{ini}$ < 1 suggests that arteries may be axially precompressed instead of prestretched. However, Horny et al. (2013b) did not report precompressed arteries in their data sample. Considering also that this values ($\lambda_{zZ,LL}^{ini}$ < 1) occur due to the statistical methodology (± deviation from expected value), $\lambda_{zZ,LL}^{ini}$ = 1 was prescribed rather than the initial precompression. #λ_{zZ} at P_{SYS} and P_{DIA} computed for expected value of λ_{zZ}^{ini} in the thin-walled model. §Gender specific mean values for Canadian population based on Wilkins et al. (2010).

I.3.3 Circumferential and longitudinal stretch variation

Figure 6 demonstrates how stretch variation ε_{I} (iI = $\theta\Theta$ and zZ) is defined. Vertical lines in the figure intersect the horizontal axis at end-points of the segments corresponding to $\varepsilon_{I} = \lambda_{iI}(P_{SYS}) - \lambda_{iI}(P_{DIA})$). The stretch variations ε_{I} predicted by the thick-walled model (residual strains incorporated) at r_i using expected value of the prestretch λ_{zZ}^{ini} are depicted in Figure 7 (blue solid circles in the left upper panel). A marked decrease in $\varepsilon_{\theta\Theta}$ is even significantly correlated with age (R = -0.572, p–value = 0.02). Longitudinal systolic-diastolic stretch variation also decreases with age, but statistical significance was not attained (Figure 7, right upper panel). However, the most important fact is that the results of the simulation show that one should expect a non-zero difference in axial stretch between systolic and diastolic pressure. The range of ε_{zZ} is approx. 0.005 – 0.025 for expected values of λ_{zZ}^{ini}. This can be interpreted as 0.5% – 2.5% of some reference length.

To evaluate how this result could be affected by uncertainty of the axial prestretch, $\lambda_{zZ,LL}^{ini}$ and $\lambda_{zZ,UL}^{ini}$ were used to compute ε_{I} (iI = $\theta\Theta$ and zZ). Results based on the thick-walled tube model (residual strain incorporated) for both axial and circumferential direction are also presented in Figure 7. Here red open squares correspond to the upper limit (higher prestretch) and black open circles to the lower limit. Regressions lines were omitted to keep the figure clear although the results of the correlation analysis were similar to those obtained for the expected value of the prestretch. Specifically, none of the initial axial prestretch ($\lambda_{zZ,LL}^{ini}$ and $\lambda_{zZ,UL}^{ini}$) gave significant correlation between age and ε_{zZ}, and all $\varepsilon_{\theta\Theta}$ were significantly negatively correlated with age.

Much more interesting than the numerical characterisation of the correlation with age is the position of the points. In particular, we would like to point out the difference in positions for circumferential and axial behaviour. Axial response, as can be expected, shows higher stretch variation when lower prestretch limit is used (black open circles). This is in contrast to circumferential response, where higher $\varepsilon_{\theta\Theta}$ is attained when the higher initial axial stretch is used (red open squares). **This suggests, to the best of author's knowledge, up to now a not yet published hypothesis that the axial prestretch not only minimises longitudinal motion of the artery upon pressure cycle, but also endows the artery with higher circumferential distensibility (in comparison with less prestretched artery characterised with the same material parameters).** It is also worth noting that some of the highly prestretched aortas show diastolo-systolic shortening (ε_{zZ} negative) in contrast to the weakly prestretched.

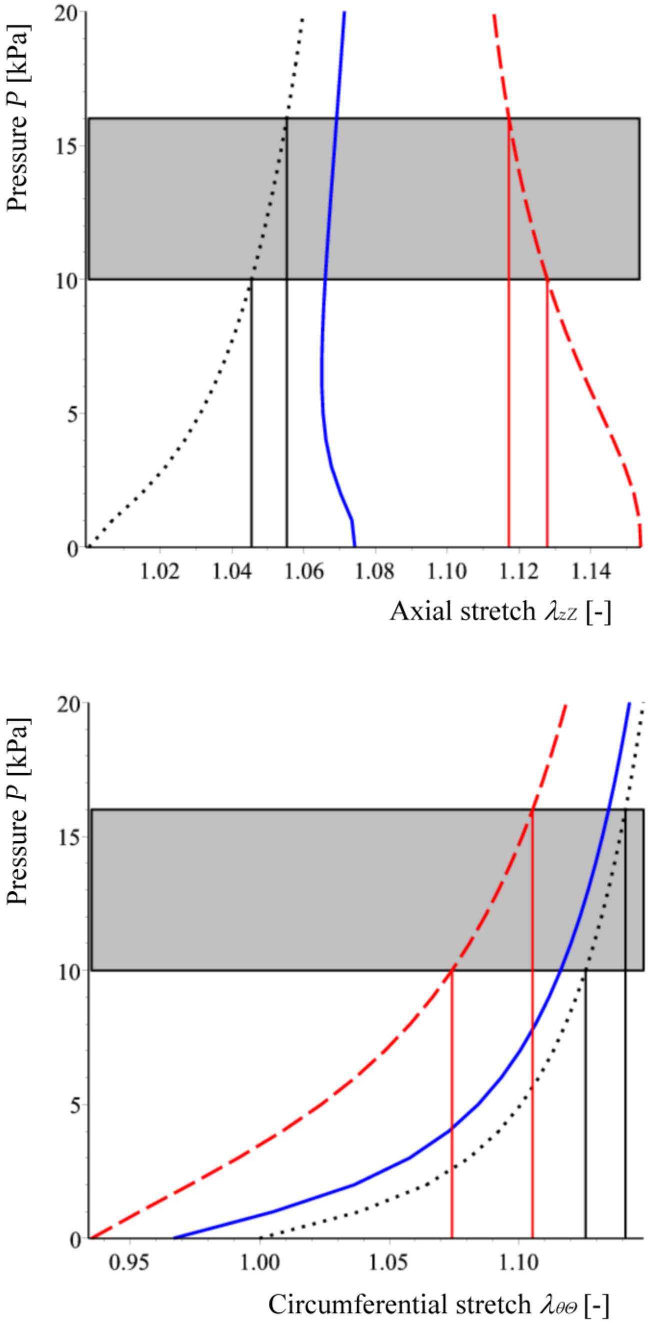

Figure 6. Inflation-extension response of a 61 year old male donor (M61a) – detail. The results of the simulation based on thin-walled approximation. The blue solid curve was computed with expected value λ_{zZ}^{ini} = 1.074; red dashed curve was computed with $\lambda_{zZ,UL}^{ini}$ = 1.153; and black dotted curve was computed with $\lambda_{zZ,LL}^{ini}$ = 1. Shaded rectangle emphasises the region of physiological pressures. Vertical lines aid to identify stretch variation $\varepsilon_{iI} = \lambda_{iI}(16\text{kPa}) - \lambda_{iI}(10\text{kPa})$ ($iI = \theta\Theta$ and zZ).

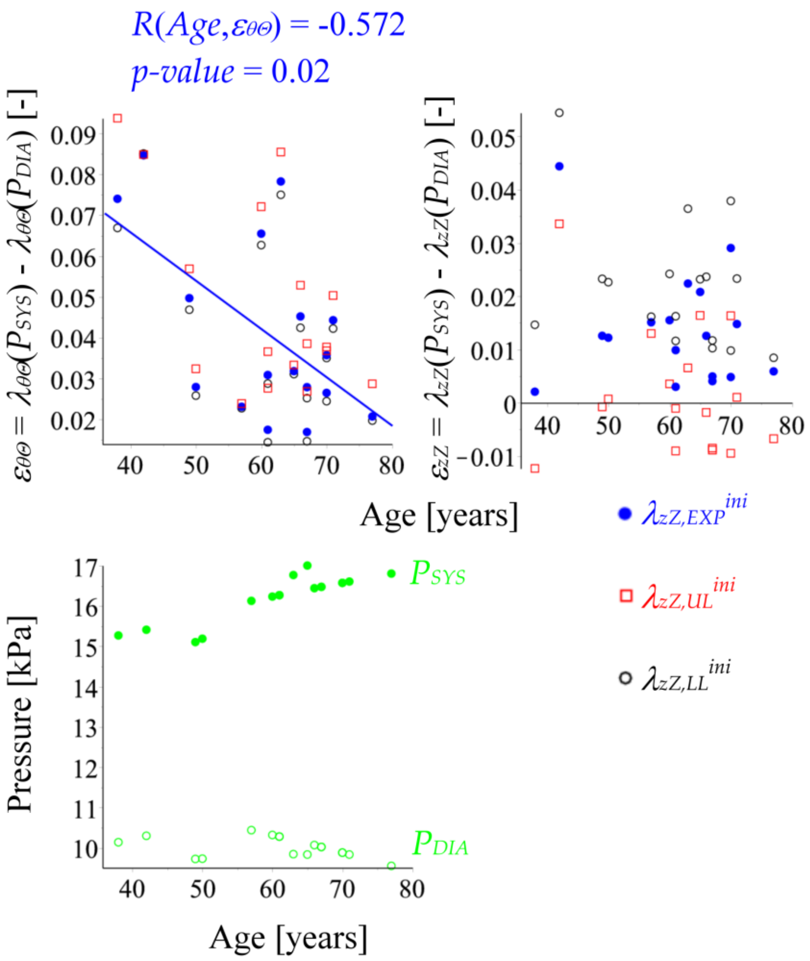

Figure 7. Diastolic-systolic stretch variations. The upper panels show variation of circumferential and axial stretch at r_i and lower panel shows specific values of diastolic (P_{DIA}) and systolic (P_{SYS}) pressure applied in the computations. Due to nonlinear large strain stiffening, ε_{zZ} decreases with increased axial prestretch, which is in contrast to circumferential behaviour ($\varepsilon_{\theta\Theta}$ attained higher values for highly axially prestretched aortas).

I.3.4 F_{red}

The computed reduced axial force F_{red}, which generates the initial axial prestretch, is depicted in Figure 8. It is compared with values obtained for the human abdominal aorta in *ex vivo* elongation tests (at P = 0) in Horny et al. (2013). The figure shows the results of the simulations with expected values as well as lower and upper limit of λ_{zZ}^{ini} computed with the thin-walled model. Expected values of the initial axial stretch demonstrates that prestretching force is significantly correlated with age (R = -0.514, p–$value$ = 0.04). Note that the lower limit of λ_{zZ}^{ini} was prescribed to be 1 for donors older than 61. In such a case F_{red} = 0.

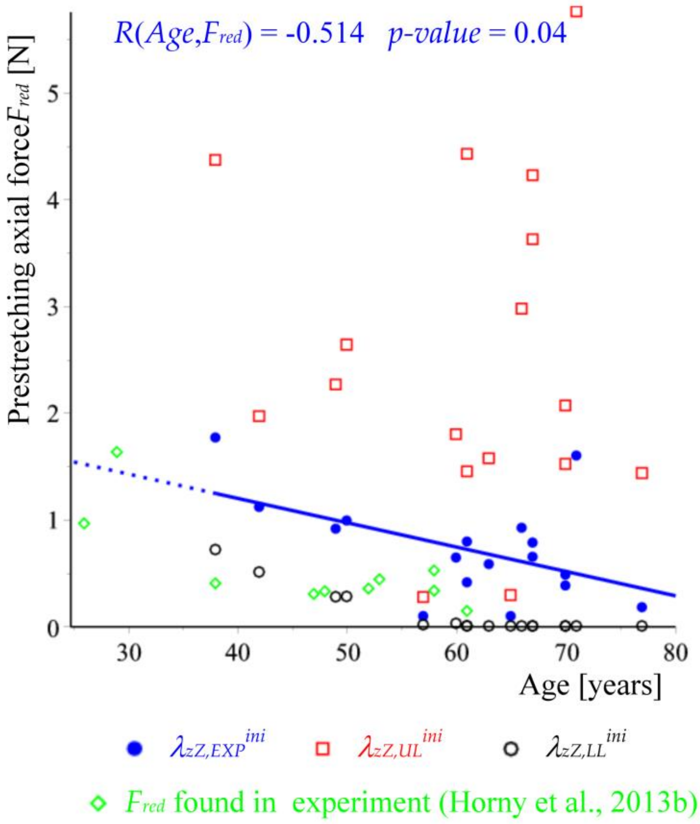

Figure 8. Prestretching axial force. Predictions of F_{red} computed with the thin-walled model are depicted: blue solid circles were obtained with expected values of λ_{zZ}^{ini}; red open squares were obtained with the upper limit; and black open circles were obtained when the lower limit of the initial axial stretch was used. The blue solid line is the linear regression model of the dependence of F_{red} (obtained for expected values of the prestretch) on age: $F_{red} = 2.115 - 0.023 \cdot Age$ for $Age \in [38;77]$ years. Outside of this domain, one should consider the regression model as an extrapolation which is indicated by the dotted line. The results are compared with experiments adopted from Horny et al. (2013). Note that due to the assumption F_{red} computed with $\lambda_{zZ,LL}^{ini}$ for age > 61 years is 0. The regression model (4) predicts $\lambda_{zZ,LL}^{ini} < 1$ for age > 61 years; however, this is a consequence of the used methodology *expectation* ± *uncertainty*. Since very little is known about initially pre-compressed arteries $\lambda_{zZ,LL}^{ini}(Age > 61 \text{ years}) = 1$ was prescribed in our simulation.

I.3.5 Axial stress

Almost constant axial stress during diastolic–systolic pressure variation has at times been mentioned in the literature. The predictions of (9c) for σ_{zz} were used to evaluate this hypothesis in the present data sample. Four representative examples (M38, M57, F50, and M60) of the axial stress considering expected value (solid blue curves), upper (dashed red curves), and lower limit (black dotted curves) of the initial axial stretch are in Figure 9 drawn over circumferential stretch corresponding to P = 0..20 kPa (cf. with Fig. 2 in Dobrin and Doyle 1970). Axial stress was computed employing a thick-walled model (residual strain incorporated) at the inner radius r_i. Systole and diastole are highlighted with green solid circles on the curves. It is obvious that although axial stress indeed increases slowly from the left to the right (as described in Dobrin and Doyle 1970), the diastole and systole are found on the steep part of the curves (diastolic point is always the left-hand one). This is demonstrated with M38, F57, and M60. However, F50 shows that it may not be always true.

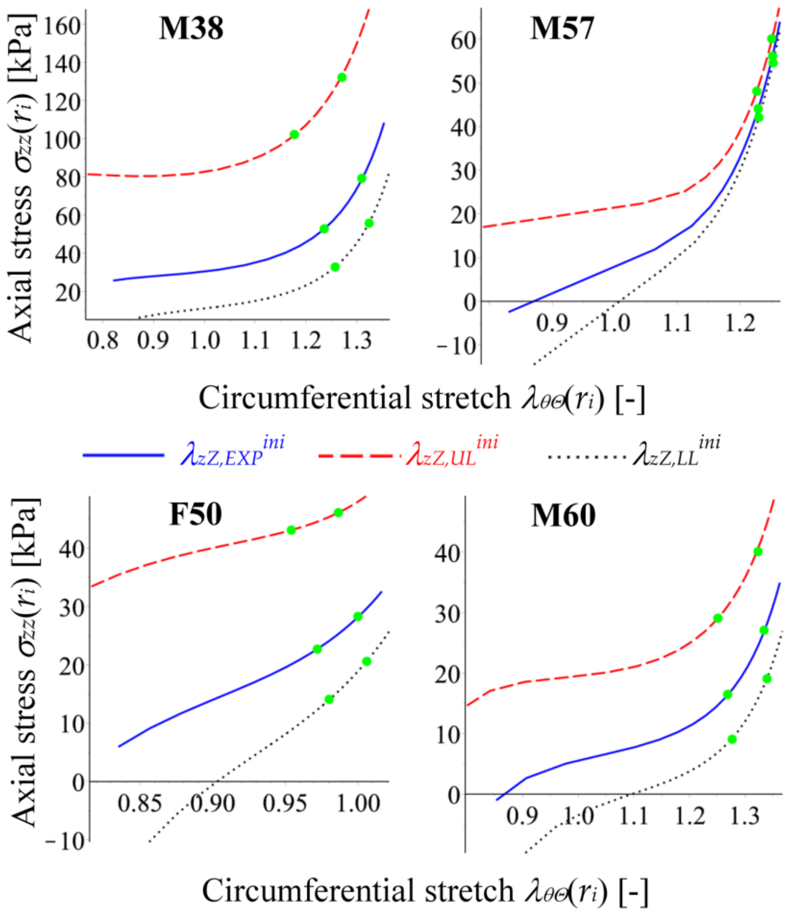

Figure 9. Variation of axial stress $\sigma_{zz}(r_i)$ in the course of the pressurisation. The curves are based on the thick-walled model with incorporated residual strain. Circumferential stretch on horizontal axis starts from values smaller than 1 due to simultaneous effect of the initial axial stretch and residual strain. Predictions obtained with the expected value of λ_{zZ}^{ini} are depicted with blue solid curves; red dashed curves were obtained with $\lambda_{zZ,UL}^{ini}$; and $\lambda_{zZ,LL}^{ini}$ was used to create black dotted curves. Solid circles on the curves highlight the positions of diastolic (the left circle) and systolic (right circle) pressure.

To quantify diastolic-systolic increment in σ_{zz} numerically, Figure 10 depicts the stress increment normalised with respect to the diastole for all involved donors. The upper panel shows increments obtained with the thick-walled model with incorporated residual strain for $\sigma_{zz}(r_i)$ and $\sigma_{zz}(r_o)$, and lower panel was obtained in the thin-walled approximation (mean axial stress at r_m). The symbols are used in the same way as in the previous figures (to distinguish inner and outer radius, small and large symbols are used, respectively). **It is clear from the figure that the lowest changes of the axial stress are obtained using the upper limit of the initial axial stretch. The same is confirmed in the thin-walled model. The lower panel shows that average change of σ_{zz} is in the range 0.2 – 0.5 for highly prestretched aortas whereas weakly prestretched aortas show average change of approx. 0.7.**

Significant correlation between variation of axial stress and age was obtained at r_m and r_o and the lower the initial prestretch, the higher correlation coefficient was obtained (the highest one, $R = 0.790$ *p–value* < 0.001, was at r_o).

I.3.6 Stiffness ratio $C_{\Theta\Theta\Theta\Theta}/C_{ZZZZ}$

The ratio between components of elasticity tensor was computed for all involved individuals. The results are summarised in Figures 11, 12 and 13. To show an order of the magnitude of the components of elasticity tensor, numeric values are compared in Figure 9 for inner, outer, and middle radius of the aortas initially prestrained to the expected axial prestretch and pressurised to P_{DIA} and P_{SYS}. Significant correlation between age and the components of $\mathbf{C}$ were only found in case of $C_{\Theta\Theta\Theta\Theta}$ computed at r_m for P_{SYS} at all prestretches ($R \approx 0.52$ *p–value* ≈ 0.04). All other cases were not significant.

The stiffness ratio $C_{\Theta\Theta\Theta\Theta}/C_{ZZZZ}$ is depicted in Figure 12. All effects are herein summarised – the effect of finite thickness of the wall; effect of the pressure; and the effect of initial prestretch. Two facts are demonstrated by Figure 12. First, the stiffness ratio depends strongly on radial position within the thickness of the artery wall. In average $C_{\Theta\Theta\Theta\Theta}/C_{ZZZZ} < 1$ is at the inner radius (top panels in Figure 12), however $C_{\Theta\Theta\Theta\Theta}/C_{ZZZZ} > 1$ holds at outer radius (bottom panels). Second, with regard to the effect of the prestretch, thin-walled model for r_m and thick-walled model at r_o show that higher prestretch is accompanied with the lower stiffness ratio (and reciprocally lower prestretch with the higher stiffness ratio). However, there are some cases at the inner radius which deviate from this rule. Correlation analysis revealed significant dependence of the stiffness ratio on age only in case of thin-walled model. It was found $R = 0.514$ with *p–value* $= 0.04$ for P_{SYS} and P_{DIA} at expected initial axial stretch.

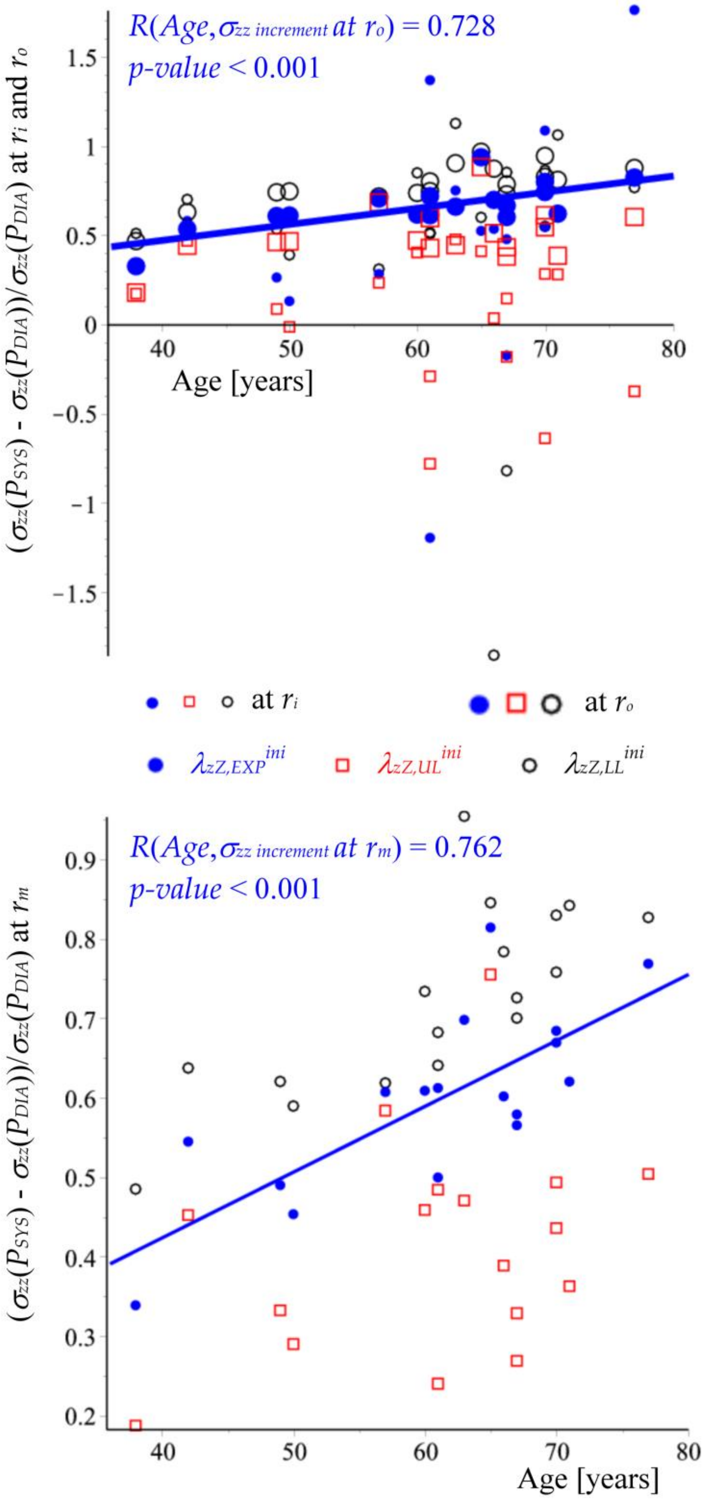

Figure 10. Relative change of the axial stress induced by diastolic–systolic pressure increment. The upper panel shows the results computed with the thick-walled model (residual strain incorporated) at the inner radius (small symbols) and at the outer radius (large symbols). The lower panel shows results obtained by thin-walled approximation. The symbols are used in the same way as in Figure 7 and 8. The figure shows that higher initial axial prestretch is accompanied with smaller changes of the axial stress. Correlation coefficients and regression lines correspond to expected initial prestretch.

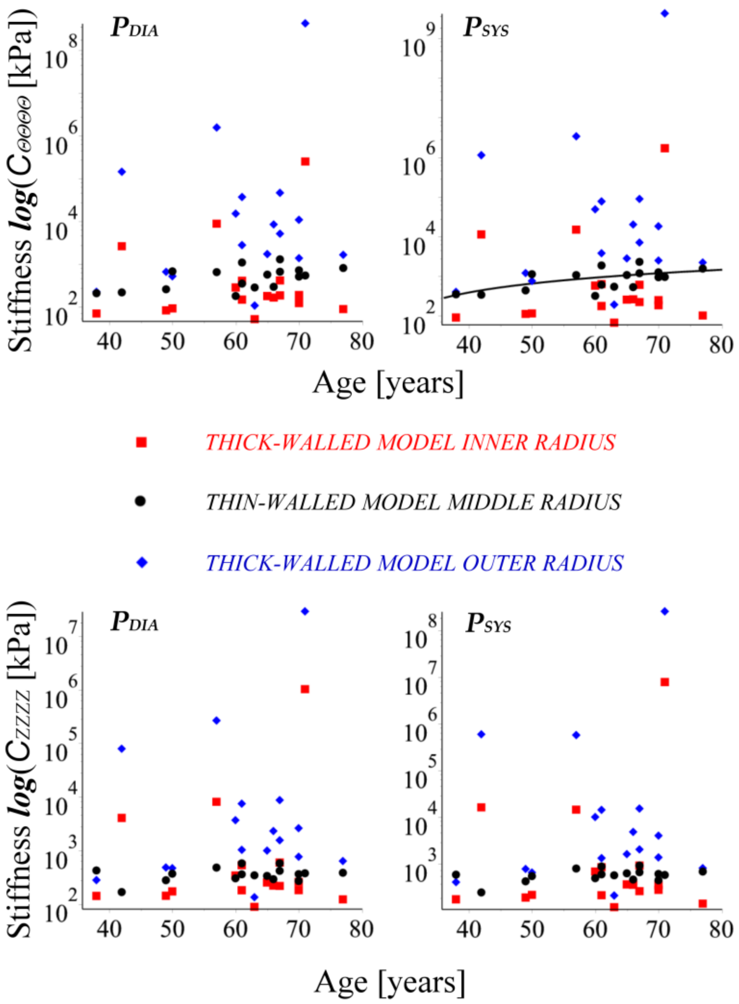

Figure 11. Components of referential elasticity tensor C for expected axial prestretch. Upper panels show the stiffness in circumferential direction ($\mathsf{C}_{\Theta\Theta\Theta\Theta}$) and lower panels in axial direction (C_{ZZZZ}). The symbols indicate the method and position: red solid boxes – at r_i with thick-walled model; black solid circles – at r_m with thin-walled model; and blue solid diamonds – at r_o with thick-walled model. The regression line indicates significant correlation between age and $\mathsf{C}_{\Theta\Theta\Theta\Theta}$ at r_m for P_{SYS} (R = 0.515 *p–value* = 0.04). Note that logarithmic scale is used on vertical axes.

Relative increments of the stiffness ratio induced by diastolic–systolic variation of internal pressure are depicted in Figure 13. The increments are normalised with respect to the ratio at diastolic pressure. In contrast to the stiffness ratio as such, highly prestretched aortas showed higher relative increments of the stiffness ratio from diastole to systole than weakly prestretch aortas. Significant negative correlation with age was found in the case of relative increments computed with the thick-walled model at inner radius (R = -0.600 *p–value* = 0.02 for expected prestretch, and R = -0.539 *p–value* = 0.03 for upper axial prestretch).

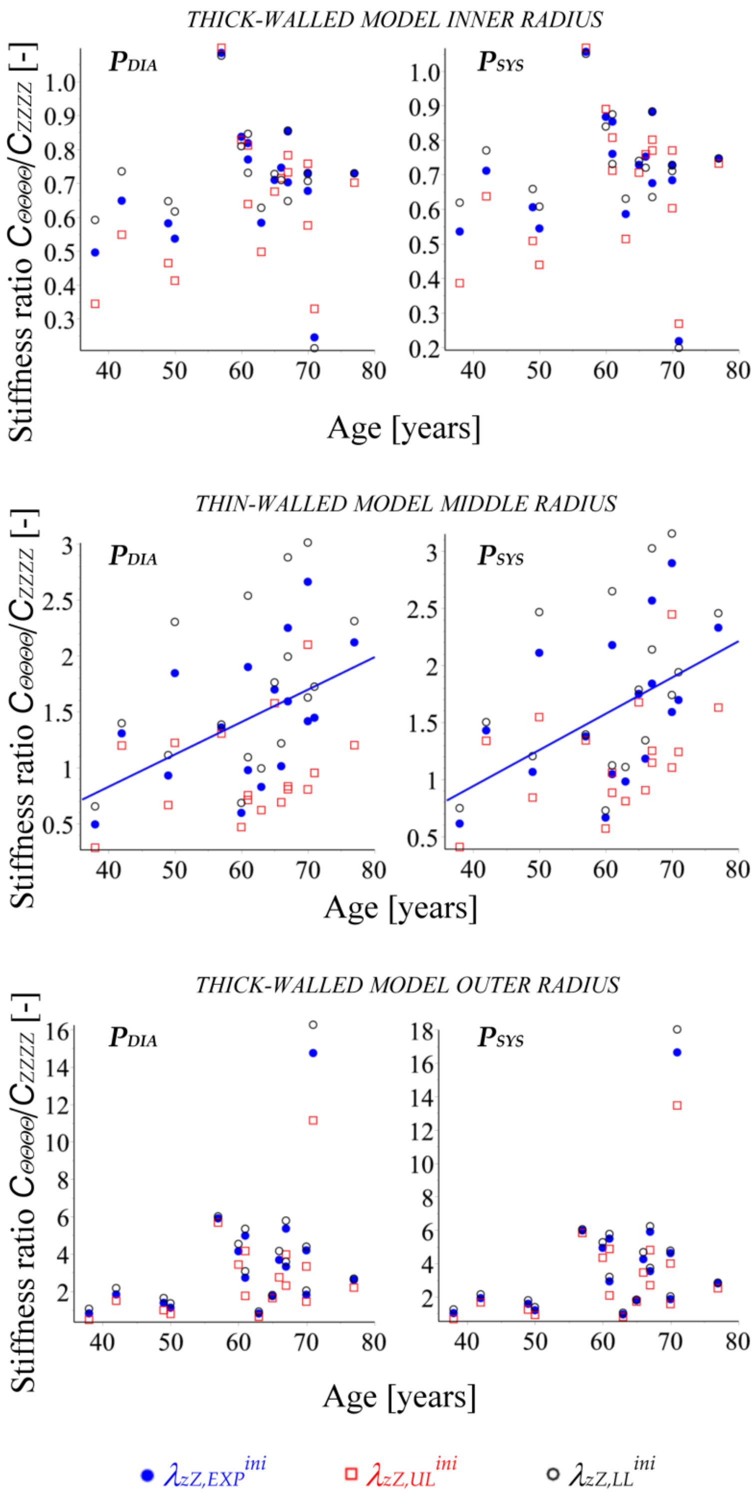

Figure 12 Stiffness ratio. The figure summarises results obtained for stiffness ratio at inner, middle and outer radius of the aortas. Three important things can be derived from the figure: (1) weakly prestretched aortas give higher stiffness ration; (2) the stiffness ratio varies significantly through the thickness of the wall; and (3) aortas may exhibit different stiffness ratios in different ageing periods.

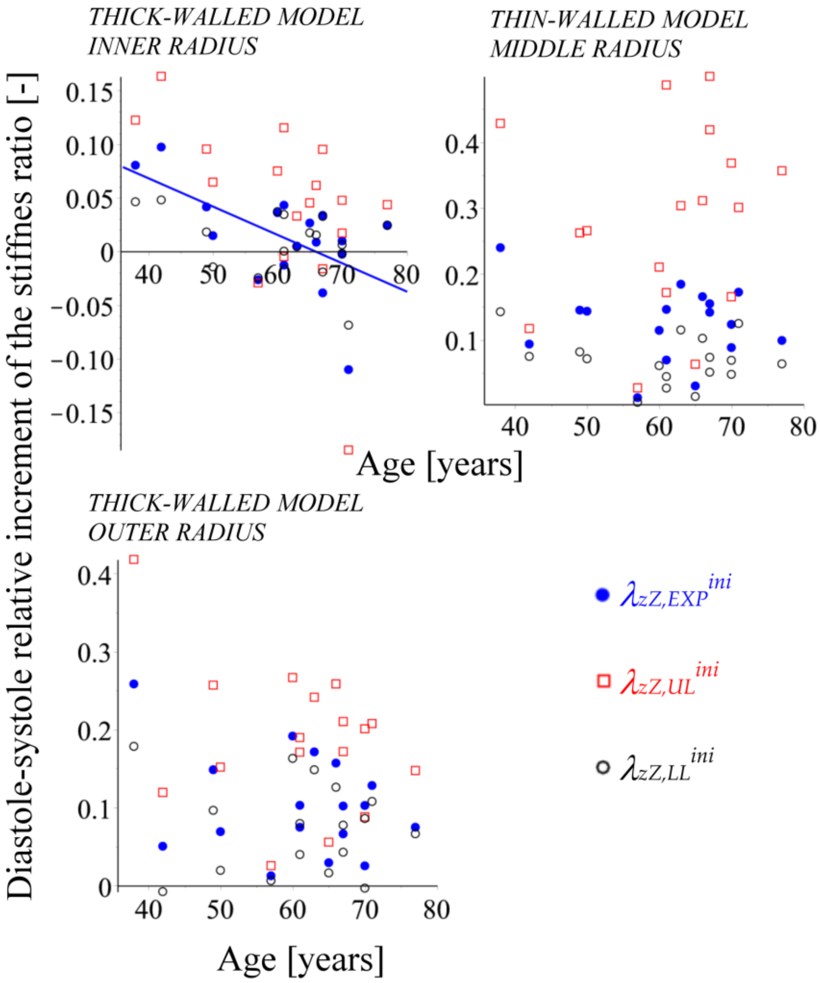

Figure 13. Relative increment of the stiffness ratio. Highly prestretched aortas gave a higher relative increment in the stiffness ratio during pressure cycle.

I.4. Discussion

This study focused on the effect of age-related decrease in the initial longitudinal prestretch of human abdominal aorta on its distensibility, axial stress, and circumferential-to-axial stiffness ratio. Changes induced by the variation of the pressure (systole – diastole) were also evaluated. Since author's bibliographic search did not find a complete description of human abdominal aorta anywhere (i.e. specimens with documented geometry, experimentally determined constitutive parameters and axial prestretch in one study), the characteristics of arteries were adopted from two different papers. Geometry and constitutive description were taken from Labrosse et al. (2013) who conducted experimental *ex vivo* inflation (with free axial extension) of the human abdominal aorta. Statistics of the axial prestretch in the same anatomical location were reported by Horny et al. (2014) who performed autopsy measurement on the sample of 365 human cadavers. Since this approach induces some uncertainty in the true value of the prestretch, all computations were performed with expected prestretch (i.e. prestretch exactly corresponding to the regression equation (3)), and also with upper and lower limit of 95%-confidence interval of a prediction (so-called prediction interval; equation (4)).

Present study modelled the inflation-extension response by considering the aorta to be a prestrained, anisotropic and nonlinear homogenous tube with closed ends by the methods of elastostatics. Two analytical approaches were used. First was the thin-walled model which operates with mean wall stresses acting at middle radius of the tube and its results were considered to be basic estimates of the mechanical response. However, this model cannot capture the effect of residual strain on the stress state of an artery. To this end, the thick-walled model with incorporated residual strain was also used in the situations when transmural distribution of quantities was of interest.

I.4.1 Stretch variation of prestretched artery

The results suggest that, although axial prestretch significantly decreases due to ageing (Figure 3), it can still crucially affect mechanical response. This fact is clearly observable in systolic-diastolic variation of the circumferential stretch $\varepsilon_{\theta\Theta}$. **Circumferential stretch variation was found to decline with age (Figure 7), but the study demonstrated that highly prestretched arteries** ($\lambda_{zZ,UL}^{ini}$) **can be more distended in the circumferential direction by the same internal pressure in comparison with their less prestretched** ($\lambda_{zZ,LL}^{ini}$) **counterparts.** This property was revealed in the thick-walled (at r_i and r_o) and also in the thin-walled (at r_m) model. The results were qualitatively similar, hence, the variation only at the inner radius is presented (Figure 7).

To the best of author's knowledge, preceding studies have not pointed out this fact which might certainly warrant re-examination in the future (experiments are necessary to validate this finding). Results suggest that axial prestretch could play a more important role than merely a way how to endow abdominal aorta with a property of almost constant axial length during the pressure cycle (Dobrin 1978; Dobrin et al. 1990; van Loon et al. 1977). It should be noted there are studies reporting results from which a similar conclusion could be obtained, although they are focused on different anatomical locations. However, their authors did not investigate this property in detail; cf. Figure 5 in Sommer et al. (2010) and Figure 4 in Sommer and Holzapfel (2012) for human carotid artery, and also Figure 4 in Schulze-Bauer et al. (2003) for human iliac artery.

Possible explanation of this interesting fact is that the axial prestretch may align collagen fibres (main load-bearing component of artery wall responsible for arterial anisotropy; Holzapfel et al. 2000) to axial direction and the wall subsequently shows higher stretch variation in the circumferential direction. This hypothesis is in accordance with the stiffness ratio in Figure 12. Here open black circles (weak prestretch prescribed to aortas) most frequently lie above red open squares (high prestretched prescribed). That is to say that the increase in the prestretch leads to the decrease of the circumferential-to-axial stiffness ratio.

Considering "constancy" of the length, Figures 7 suggests that this is "only" an approximation. The simulation indicates axial stretch variation may be expected in the range ε_{zZ} = -0.01 – 0.04, depending on the specific initial axial prestretch. The right panel in Figure 7 shows we should expect higher change in axial stretch during pressure cycle when lower initial axial prestretch is applied (black open circles are the most distant from horizontal axis). On the contrary, the upper limit of initial axial stretch led to ε_{zZ} located closely to the horizontal axis. In some cases, the model predicts a negative value which is the shortening of the artery when pressurised from diastole to systole. However, these results come from simulation, not experiment.

We should avoid over-interpretation of negative/positive ε_{zZ} in specific cases; nevertheless, higher initial prestretch led to ε_{zZ} = -0.01 – 0.02, in contrast to lower prestretch which gave ε_{zZ} = 0.01 – 0.04. Thus, using higher λ_{zZ}^{ini} is in accordance with the property of the relatively constant length of the aorta mentioned in the literature (Dobrin 1978; Dobrin et al. 1990; van Loon et al. 1977). Nevertheless, in the case that age-related changes leading to the loss of the prestretch progress rapidly (i.e. specific λ_{zZ}^{ini} is close to the lower limit of the prediction interval), the simulation suggests we should expect that the property of almost constant length may be lost. **Moreover, considering ε_{zZ} as engineering strain, changes of about 2 – 4% could fall into the range measurable by modern imaging (e.g. ultrasound) methods (Ahlgren et al. 2012; Cinthio et al. 2006; Karatolis et al. 2013; Larsson et al. 2011). Therefore, since the lower prestretch corresponds to higher axial distension in pressure cycle (intra-pressure cycle deformation), it seems to open a new diagnostic**

possibility based on longitudinal strain measurement governed by the hypothesis that high (for instance higher than 2%) intra-cycle axial stretch variation may suggest suboptimal axial prestretch. The word “optimal” is used not only with respect to the implication “minimal change in axial stretch during pressure cycle gives higher circumferential distensibility, which supports a windkessel function”, but also with respect to the hypothesis that no change in axial length implies no energetic demand for axial displacements (Schulze-Bauer et al. 2003) and consequently no dissipation of this energy due to viscoelasticity of the artery wall.

I.4.2 Axial stress and prestretching force

The simulation confirms previous conclusion made by the author and his colleagues (Horny et al. 2013) that prestretching axial force (force induced by λ_{zZ}^{ini}) decreases with age (statistical significance attained). Specific values are slightly higher than in Horny et al. (2013), see Figure 9. The upper limit of the initial axial prestretch in some cases did indeed lead to high force (F_{red} > 3 N).

The simulation also confirmed that the σ_{zz}–$\lambda_{\theta\Theta}$ relationship is initiated with very slow stress increment; c.f. Figure 9 with Figure 2 in Dobrin and Doyle (1970). However, the positions of diastolic and systolic pressure (indicated with green solid circles on the curves in Figure 9) do not correspond with Dobrin and Doyle’s conclusion that axial stress should be almost constant during the pressure cycle. It is more clearly evident in Figure 10 where normalised diastolic-systolic increments of axial stress are depicted. Depending on the specific prestretch, the simulation suggests we should expect a variation of mean axial stress (lower panel) in the order of tens of percentage. The fundamental role of sufficient axial prestretch is again clear.

The substitution of upper-limit values into the calculation led to the smallest increments. This suggests that insufficiently prestretched arteries, because they feel a larger change in axial stress during pressure cycle, may not operate in physiologically optimal conditions and could be vulnerable to a mechano-biological reaction attempting to restore homeostasis because changes in the axial stress/strain state have been identified as quantities initiating a remodelling (Humphrey et al. 2009; Jackson et al. 2002; Lawrence and Gooch 2009). The discrepancy with the observation made by Dobrin and Doyle (1970) may be attributed to the fact that they conducted their experiments with relatively young and healthy laboratory dogs.

An age-related decrease in the prestretch leads to the decrease in the prestretching force and consecutively it leads to decreased initial axial stress. This can be concluded from Figure 9 when $\sigma_{zz}(r_i)$ corresponding to $P = 0$ (starting points of the curves) is considered. When axial prestretch is applied, curves do not begin at $\lambda_{\theta\Theta} = 1$ (decrease in the radius accompanies initial axial extension). Interestingly, some of curves initiate with negative values of axial stress at r_i. This is the effect of the residual strain which, for high opening angles, qualitatively change transmural stress distribution (see Figure 7 in Labrosse et al. 2013). In fact, when residual stress is released in a radial cut of an artery and the arterial ring springs to the open sector, a small axial deformation occurs. The prestretch induced by F_{red} is superimposed on this small axial deformation.

Figure 9 thus documents that the small values of F_{red}, which accompanies small λ_{zZ}^{ini}, with a simultaneous occurrence of high opening angle (see Table 1 for specific values) can result in negative axial stress at r_i in non-pressurised but axially prestretched artery (for the effect of residual strain on closed, non-prestretched and non-pressurised artery see e.g. Figure 2 in the review Rachev and Greenwald 2003; or in Chuong and Fung 1986). This fact, to the best of our knowledge, has also not been previously mentioned in the literature. Nevertheless, we should point out that this configuration (axial prestretch superimposed on residually stressed artery with no luminal pressure) is never attained *in vivo*.

I.4.3 Stiffness ratio

Figures 11, 12 and 13 depict results obtained for components of the elasticity tensor, their circumferential-to-axial ratio, and relative diastolo-systolic increment in the stiffness. In contrast to axial stress, the ratio seems to satisfy more closely the condition of constancy during pressurisation (Figure 13). This suggests that the stiffness ratio could be more suitable for purposes of *in vivo* parameters estimation where some assumption has to be made to overcome the impossibility to directly measure axial force and stress (Chen et al. 2008). Figure 12 (middle panels), however, shows that this ratio may not be constant during ageing. Moreover, the results of thick-walled model show that $\mathrm{C}_{\Theta\Theta\Theta\Theta}/\mathrm{C}_{ZZZZ}$ depends on radial position within the thickness of artery wall (e.g. the stiffness ratio at P_{SYS} and expected λ_{zZ}^{ini} was found to be 0.701 ± 0.182 at r_i, 1.60 ± 0.657 at r_m, and 3.96 ± 3.70 at r_o; mean ± SD).

The results of thick-walled model (residual strain incorporated) suggest that the aortic wall in cardiac cycle is stiffer in axial direction at its inner radius; however, at outer radius it is stiffer in circumferential direction. This is the consequence of non-homogenous strain distribution over the thickness of the artery.

I.4.4 Axial prestretch

Axial prestretch as such and its age-related changes was not the main subject of our study because it has previously been presented elsewhere (Horny et al. 2011, 2012a,b, 2014). Nevertheless, we would like to explicitly emphasise three things. First, our study used the same regression model of λ_{zZ}^{ini}–*age* in the case of both genders because it was previously found that significant differences in the prestretch of abdominal aorta between males and females do not exist (Horny et al. 2012b). In that same paper, the authors proved assumptions of the *classical linear regression model* which is important for construction of the prediction intervals. Finally, according to Horny et al. (2014), we do not expect that the post mortem interval and atherosclerotic changes in abdominal aorta can significantly deviate used estimates of λ_{zZ}^{ini} from their true values (in fact unknown) at time of the death.

I.4.5 Effect blood pressure uncertainty

In the simulation, mean (but age and gender specific) diastolic and systolic pressures adopted from Wilkins et al. (2010) were applied. Used pressures however are only estimates of the true pressures sustained by donors in their life. To eliminate the possible effect of varying quality of medical care in different countries, blood pressures were adopted from very recent survey conducted in the same country (Canada) as the tissue donors came from. For the sake of clarity, we decided to do not complicate it with another quantity considered with uncertainty (blood pressure). This is motivated by two following facts. First, in future it would be better to verify our results in experiments and our article should function as initial motivation. Second, one can, although only roughly, estimate how the results will change with changed P_{DIA} and P_{SYS}. Consider that changes in P_{DIA} and P_{SYS} can be understood as a movement in the vertical direction of the shaded rectangle in Figure 6 (one can also draw such a rectangle into Figure 4 and 5). The figure is created for the range of 0 – 20 kPa. It is clear that the positive effect of the prestretch on the stretch variation in the circumferential direction is restricted by a monotony of $dP/d\lambda_{\theta\Theta}$. This is most clearly seen in Figure 4 (lower panel) when the highest prestretch (red diamonds) is considered. When P_{DIA} decreases less than approx. 5 kPa, the positive effect of the prestretch is lost due to the increasing slope of the curve (reciprocally an increase of P_{SYS} to ≈ 20 kPa has the same effect). This suggests that to reach maxim circumferential stretch variation, it would be optimal for an artery to operate close to the inflection point on P–$\lambda_{\theta\Theta}$. This position, however, depends on specific numerical values of the constitutive parameters.

I.4.6 Limits of the simulation

Presented study has limitations coming from (a) the chosen method, and (b) from the data used. Firstly, it should be pointed out that the elastostatics approach was used. This means that the presented simulations correspond to the so-called inflation-extension experiment (the most frequent way of the experimental constitutive model determination for cylindrical segments of arteries), but true *in vivo* arterial mechanics consists in pressure pulse wave propagation as a result of dynamical fluid-structure interaction. The chosen approach, however, mimics the methods used in *in vivo* parameters estimation procedures presented in recent literature (Åstrand et al. 2011; Masson et al. 2008, 2011; Schulze-Bauer and Holzapfel 2003; Stålhand 2009; Stålhand and Klarbring 2005, Wittek et al. 2013).

It should also be mentioned that recent papers have proven that residual strains in the artery differ with respect to its layered structure. This fact is not captured in the simulation because it is based on the assumption of a homogenous wall (adopted from Labrosse et al. 2013). Layered structure, theoretically, may induce discontinuities and non-smoothness in transmural stress and strain distribution; see e.g. Figure 19 in Holzapfel et al. (2000); Figure 5 in Holzapfel and Ogden (2010b). It might affect results obtained with a thick-model.

II. Analysis of effect of axial prestretch in different computational models

Presented in the version accepted as Horný L., Netušil M. (2015) **How does axial prestretching change the mechanical response of nonlinearly elastic incompressible thin-walled tubes**, DOI: 10.1016/j.ijmecsci.2015.08.014, for publication in *International Journal of Mechanical Sciences*.

Caution: As follows from above mentioned, figures and equations numbering do not continue in the numbers used in the chapter I. It starts again from 1, because the chapter corresponds with new journal article.

Preface to the chapter II (not included in the Int J Mech Sci article)

In Chapter I, it has been found that *elastic arteries*, and here it may be more appropriate to use a term *arterial physiology*, benefit from the axial prestretch because it makes them more distensible in the circumferential direction. This is the main massage delivered by the study and the author considers it to be very interesting especially due to its contra intuitiveness. Once again, tubes made from a material, which is nonlinear and rapidly stiffens at large strains, exhibit higher circumferential deformability when axially prestrained. Now, in Chapter II, physical causes of this fact will be discussed.

Two different analytical models have so far been used in the study. It is the thick-walled computational model, which is able to account for residual strains, and thin-walled model which operates with averaged stresses acting on middle surface of the tube. As was seen in I.3.2 and I.3.1 (Figures 4, 5, and 7 document it), both used models, although they quantitatively differ, give the same qualitative result – axial prestrain enhances circumferential distensibility. Thus an existence of investigated property does not depend substantially on distributions of in-wall stresses through a thickness of a tube. In what follows, for the sake of simplicity, only the thin-walled model will be used. The most important equations creating computational model of the thin-walled tube are repeated herein; (5) equilibrium equations; (6) geometrical equations; and (7) constitutive model substituted into (5). The material is still considered to be incompressible.

$$\sigma_{rr} = -\frac{P}{2} \qquad \sigma_{\theta\theta} = \frac{r_m P}{h} \qquad \sigma_{zz} = \frac{F_{red}}{2\pi r_m h} + \frac{r_m P}{2h} \tag{5}$$

$$h = \lambda_{rR} H \qquad r_m = \lambda_{\theta\Theta} R_m \qquad z = \lambda_{zZ} Z \tag{6}$$

$$\lambda_{rR}\frac{\partial W}{\partial \lambda_{rR}} - p = -\frac{P}{2} \qquad \lambda_{\theta\Theta}\frac{\partial W}{\partial \lambda_{\theta\Theta}} - p = \frac{r_m P}{h} \qquad \lambda_{zZ}\frac{\partial W}{\partial \lambda_{zZ}} - p = \frac{F_{red}}{2\pi r_m h} + \frac{r_m P}{2h} \tag{7}$$

Following considerations are presented in a top-bottom approach. It means that concepts will be step by step simplified to discover a level where the effect of the prestretch on circumferential distensibility will vanish.[10] Particularly, as first, anisotropic large-strain stiffening constitutive model (1) is reduced to isotropic one (classical Fung-Demiray model); as second, large strain stiffening model is reduced to the simplest rational nonlinear material (neo-Hooke); as third, the material response is linearized but reference and deformed configurations are still being recognized (second order linear elasticity); and finally as fourth, total linearization is used (linear material with forces acting in the reference configuration).

[10] Top-bottom approach is preferred because formerly introduced concepts may be used as a starting point instead of lengthy introduction of the linear elasticity of infinitesimal strains.

II.1 INTRODUCTION

An analytical model of a thin-walled tube based on the Laplace law is frequently used in physics and in the engineering sciences to obtain an elementary picture of a mechanical state. In biomechanics, nonlinearly elastic incompressible tubes are used to model arteries, veins, the oesophagus and other tubular organs (Fung 1990, 1997; Humphrey 2002; Taber 2004). The solutions that are obtained are usually considered to be first-order approximations, because the imposed assumptions of the model (the thickness-to-radius ratio, the residual stress and strain, the geometrical non-uniformity etc.; Holzapfel et al., 2000; Holzapfel and Ogden 2010; Horný et al., 2014b) are imperfectly satisfied. The simplicity of the thin-walled tube model might induce the impression that our knowledge of its mechanical response is exhaustive. In this study, however, we will show an example of a phenomenon that has been overlooked until now: the enhanced circumferential distensibility of a pressurized tube due to initial axial prestretching.

Human arteries *in situ* are significantly prestretched in the axial direction (this was probably first reported in the context of biomechanics by Fuchs in 1900, as mentioned by Bergel (1961)). This prestretching is observed during an autopsy as a retraction of the excised arterial segment (Horný et al, 2011, 2012, 2013, 2014a), and the prestretch λ_{zZ}^{ini} is defined as the ratio of the *in situ*-to-*ex situ* length of the segment. *Ex vivo* inflation-extension experiments have shown that axial prestretching is advantageous from the mechanical point of view, because it reduces the extent of the axial stress and strain that is experienced by arteries during the heart cycle (Dobrin and Doyle, 1970). In the optimal case of a young and healthy individual, there is a certain prestretch value at which the artery can be pressurized without a significant change to its length, so it can transmit a pressure pulse wave with negligible axial deformation (Van Loon et al., 1977; Schulze-Bauer et al., 2003; Sommer et al., 2010).

However, recent studies by Horný et al. (2011, 2012, 2013, 2014b) have shown that ageing of the cardiovascular system is, besides general stiffening of elastic arteries, also manifested by a reduction of axial prestretch. Nevertheless, a detailed analysis of the constitutive behaviour of 17 human aortas suggested that aged aortas, although weakly prestretched, still can benefit from the remaining prestretch (Horný et al., 2014b). The decreasing of the prestretch is individual process similarly to (perhaps better to say as a consequence of) the progress of human ageing. A statistical variability reported in Horny et al. (2014b) implies that, for example, a 60-year-old man has the expected axial prestretch λ_{zZ}^{ini} = 1.08 with a 95% confidence interval for a prediction $\lambda_{zZ}^{ini} \in [1.00;1.16]$. An analytical simulation of the inflation-extension response showed that, depending on the initial prestretch, the abdominal aorta of a 60-year-old man sustains the following changes in axial stretch $\lambda_{zZ}(P_{\mathrm{SYSTOLE}}) - \lambda_{zZ}(P_{\mathrm{DIASTOLE}})$ = 0.016, 0.003, and 0.025 for λ_{zZ}^{ini} = 1.08, 1.16, and 1.00, respectively (Horný et al., 2014b). The corresponding normalized changes in the axial Cauchy stress ($\sigma_{zz}(P_{\mathrm{SYSTOLE}}) - \sigma_{zz}(P_{\mathrm{DIASTOLE}}))/\sigma_{zz}(P_{\mathrm{SYSTOLE}})$ were 0.604 for expected prestretch λ_{zZ}^{ini} = 1.08, 0.426 for the upper confidence limit of the prestretch λ_{zZ}^{ini} = 1.16 , and 0.769 for the lower limit λ_{zZ}^{ini} = 1.00. This clearly demonstrates that, although axial prestretch declines (the expected prestretch of the abdominal aorta for a 20-year-old man is 1.34, with a 95% confidence interval for the prediction [1.24;1.43]), remaining prestretch still retains its biomechanical role: to minimize the axial stretch and stress variation.

Horný et al. (2014b) have moreover shown that axial prestretching also has a significant effect on the circumferential stretch variation $\lambda_{\theta\Theta}(P_{\mathrm{SYSTOLE}}) - \lambda_{\theta\Theta}(P_{\mathrm{DIASTOLE}})$ exhibited during pressurization.

Unlike the axial stretch and stress variations, which are minimized by prestretching, circumferential stretch variations were found to be increased by prestretching. For the same example as before of a 60-year-old man, the circumferential stretch variation $\lambda_{\theta\Theta}(P_{\mathrm{SYSTOLE}}) - \lambda_{\theta\Theta}(P_{\mathrm{DIASTOLE}})$, which we will refer to here as distensibility, was computed to be 0.059 for λ_{zZ}^{ini} = 1.08; 0.067 for λ_{zZ}^{ini} = 1.16; and 0.056 for λ_{zZ}^{ini} = 1.00. The study conducted by Horný et al. (2014b) revealed this phenomenon for all 17 investigated aortas. Higher axial prestretching induced inflation responses exhibiting higher circumferential distensibility of the tubes. This implies that the arterial physiology benefits in two ways from prestretching. The first way is from minimization of the axial stress and strain variation during the heart cycle, and the second way is from maximization of the circumferential distensibility during the cycle. Since arteries are conduits for the flowing blood, the higher distensibility of prestretched arteries means that they can accommodate a greater volume of blood at the same pressure than their non-prestretched counterparts. This leads us to regard the effect of axial prestretching as positive. To the best of our knowledge, this is the first time that such a conclusion on the effect on circumferential distensibility described in Horný et al. (2014b) has been presented in the literature.

In the authors' opinion, the positive effect of axial prestretching on circumferential distensibility is rather contra-intuitive at first sight, because we might expect a nonlinearly elastic tube to reach a stiffer state when pretension is applied. In their study, Horný et al. (2014b) hypothesized that anisotropy may be responsible for this phenomenon, because the elastic artery wall is reinforced by helically aligned collagen fibres (Holzapfel et al., 2000; Gasser et al. 2006; Horný et al., 2009, 2010) and Horný et al. (2014b) did indeed use an anisotropic constitutive model. However, they did not compare their results with the mechanical response of isotropic tubes, and anisotropy as a cause of the phenomenon remained only a hypothesis.

An objective of our paper is to show what physical mechanism is responsible for the enhancement the circumferential distensibility of an inflated tube. A bottom-up approach will be used to demonstrate what happens. The model of an incompressible nonlinearly elastic thin-walled tube will be simplified step-by-step from a material with exponential elastic potential at large strains to a linearly elastic material at small strains, and the cause of the enhanced circumferential distensibility will be made clear. We can state in advance that a problem formulated with large displacements but small strains for a linear material (second order linear elasticity) exhibits enhanced circumferential distensibility, and in the elementary linear elasticity of small displacements the model shows no positive effect of axial prestretch.

II.2 Methods

Two different analytical models were used in Horný et al. (2014b). These were the thick-walled computational model, which is capable of accounting for residual strains, and the thin-walled model, which operates with averaged stresses acting on mid-surface of the tube. As is documented in that paper, the two models, although they differ numerically, give the same qualitative result – axial prestrain enhances circumferential distensibility. Since the effect of prestretching is captured by both models, in what follows, for the sake of simplicity and for clear and easy interpretation of the results, only the thin-walled model will be of our interest.

Consider a long thin-walled cylindrical tube with closed ends that, in the reference configuration, has middle radius R, thickness H, and length L. Assume that, during pressurization, the motion of the material particle located originally at (R, Θ, Z), which is sufficiently distant from ends, is described by the equations summarized in (1).

$$r = \lambda_{\theta\Theta} R, \quad h = \lambda_{rR}, \quad z = \lambda_{zZ} Z, \quad \theta = \Theta \tag{1}$$

Here r denotes the deformed middle radius and h denotes thickness. Equations (1) express the fact that the tube inflates and extends (or shortens) uniformly, and that it does not twist. The stretches λ_{kK} (k = r, θ, z; K = R, Θ, Z) are the components of the deformation gradient **F**, $\mathbf{F} = diag[\lambda_{rR},\lambda_{\theta\Theta},\lambda_{zZ}]$. The right Cauchy-Green strain tensor **C** and Green-Lagrange strain tensor **E** can be computed as $\mathbf{C} = \mathbf{F}^T\mathbf{F}$ and $\mathbf{E} = ½(\mathbf{C} - \mathbf{I})$, where **I** is a second-order unit tensor. The material of the tube is considered to be incompressible, so the volume ratio J, $J = det(\mathbf{F})$, gives equation (2) expressing $J = 1$.

$$\lambda_{zZ}\lambda_{rR}\lambda_{\theta\Theta} = 1 \tag{2}$$

The equilibrium equations of a thin-walled tube with closed ends initially prestretched by axial force F_{red} and loaded by internal pressure P can be written in the form (3). Here σ_{rr}, $\sigma_{\theta\theta}$, and σ_{zz} denote the radial, circumferential and axial component, respectively, of the Cauchy stress tensor $\boldsymbol{\sigma}$.

$$\sigma_{rr} = -\frac{P}{2}, \quad \sigma_{\theta\theta} = \frac{Pr}{h}, \quad \sigma_{zz} = \frac{Pr}{2h} + \frac{F_{red}}{2\pi rh} \tag{3}$$

The material of the tube is considered to be hyperelastic, described by the strain energy density function (elastic potential) W defined per unit reference volume. In this case, the constitutive equation relating components of the stress and strain tensor can be written in the form of (4). Here p denotes a Lagrangean multiplier reflecting the hydrostatic stress contribution (not captured in W, due to incompressibility) which has to be determined from the force boundary condition.

$$\sigma_{rr} = \lambda_{rR}\frac{\partial W}{\partial \lambda_{rR}} - p, \quad \sigma_{\theta\theta} = \lambda_{\theta\Theta}\frac{\partial W}{\partial \lambda_{\theta\Theta}} - p, \quad \sigma_{zz} = \lambda_{zZ}\frac{\partial W}{\partial \lambda_{zZ}} - p \tag{5}$$

Equations governing the inflation and extension of the thin-walled tube are obtained after substituting (5) into (3). The system is given explicitly in (6).

$$\lambda_{rR}\frac{\partial W}{\partial \lambda_{rR}} - p = -\frac{P}{2}, \quad \lambda_{\theta\Theta}\frac{\partial W}{\partial \lambda_{\theta\Theta}} - p = \frac{Pr}{2h}, \quad \lambda_{zZ}\frac{\partial W}{\partial \lambda_{zZ}} - p = \frac{Pr}{2h} + \frac{F_{red}}{2\pi rh} \tag{6}$$

For the material behaviour, Horný et al. (2014b) modelled the artery as an anisotropic material described by the Fung-type elastic potential W_{GMW} (7), which was introduced in Guccione et al. (1991). Here c_0 is a stress-like material parameter. c_1 and c_2 are dimensionless parameters which govern the anisotropy of the material. E_{KK} ($K = R$, Θ, Z) are components of the Green-Lagrange strain tensor expressed in the cylindrical coordinate system.

$$W_{GMW} = \frac{c_0}{2}\left(e^{c_1 E_{\Theta\Theta}^2 + c_2\left(E_{ZZ}^2 + E_{RR}^2\right)} - 1\right) \tag{7}$$

In what follows, four different cases will be investigated. They are: (I) an isotropic nonlinearly elastic thin-walled tube described by the strain energy density function exhibiting large strain stiffening studied at finite strains; (II) a neo-Hookean tube at finite strains; (III) a linearized neo-Hookean tube studied at small strains but large displacements (second order linear elasticity); and (IV) a linearized neo-Hookean tube studied at small strains and small displacements (first order linear elasticity).

II.3 Isotropic large strain stiffening model

Since Horný et al. (2014b) documented the positive effect of axial prestretching in an anisotropic material, we will now show whether it is preserved when the problem is reduced to isotropy. The potential (7) belongs to the class of so-called *Fung-type* models (Humphrey 2002). This is a family of elastic potentials based on the exponential function, which has been proved to be very successful in describing the mechanical behaviour of soft tissues (arteries, veins, myocardium, skin, tendons, and ligaments), which generally exhibit large strain stiffening attributed to gradual load-bearing engagement of collagen fibres (Holzapfel et al., 2000; Holzapfel and Ogden, 2010). The first representative of this family was introduced by Y.C. Fung; Fung (1967), and Fung et al. (1979). The simplest isotropic representative of this family is the Fung-Demiray model W_{FD} (8), which was proposed in Demiray (1972).

$$W_{FD} = \frac{\mu}{2\beta}\left(e^{\beta(I_1-3)} - 1\right) \tag{8}$$

Here μ is a stress-like parameter which at infinitesimal strains corresponds to the shear modulus. β is a dimensionless parameter modulating the rate of strain stiffening. I_1 is the first principal invariant of **C** and is expressed in (9). In the cylindrical coordinate system and under the kinematics adopted for an inflated-extended thin-walled tube in (1), equations (6) with substituted (8) and (9) have the form of (10-12).

$$I_1 = \lambda_{rR}^2 + \lambda_{\theta\Theta}^2 + \lambda_{zZ}^2 \tag{9}$$

$$\mu\lambda_{rR}^2 e^{\beta\left(\lambda_{rR}^2+\lambda_{\theta\Theta}^2+\lambda_{zZ}^2-3\right)} - p = -\frac{P}{2} \tag{10}$$

$$\mu\lambda_{\theta\Theta}^2 e^{\beta\left(\lambda_{rR}^2+\lambda_{\theta\Theta}^2+\lambda_{zZ}^2-3\right)} - p = \frac{rP}{h} \tag{11}$$

$$\mu\lambda_{zZ}^2 e^{\beta\left(\lambda_{rR}^2+\lambda_{\theta\Theta}^2+\lambda_{zZ}^2-3\right)} - p = \frac{F_{red}}{2\pi rh} + \frac{rP}{2h} \tag{12}$$

The Lagrangean multiplier p, which accounts for the hydrostatic stress contribution, is determined from (10). This is substituted into (11) and (12). The incompressibility condition (2) and geometric equations (1) are subsequently used to obtain the final form of the governing equations (13-14).

$$\mu e^{\beta\left(\frac{1}{\lambda_{\theta\Theta}^2\lambda_{zZ}^2}+\lambda_{\theta\Theta}^2+\lambda_{zZ}^2-3\right)}\left(\lambda_{\theta\Theta}^2 - \frac{1}{\lambda_{\theta\Theta}^2\lambda_{zZ}^2}\right) + \frac{P}{2} = \lambda_{\theta\Theta}^2\lambda_{zZ}\frac{RP}{H} \tag{13}$$

$$\mu e^{\beta\left(\frac{1}{\lambda_{\theta\Theta}^2\lambda_{zZ}^2}+\lambda_{\theta\Theta}^2+\lambda_{zZ}^2-3\right)}\left(\lambda_{zZ}^2 - \frac{1}{\lambda_{\theta\Theta}^2\lambda_{zZ}^2}\right) + \frac{P}{2} = \lambda_{\theta\Theta}^2\lambda_{zZ}\frac{RP}{H} + \lambda_{zZ}\frac{F_{red}}{2\pi RH} \tag{14}$$

Before we proceed to solve (13-14), the equations will be converted to dimensionless form by (a) dividing by μ, (b) introducing the aspect ratio $\varepsilon = H/R$, and (c) introducing the dimensionless pressure $P_\mu = P/\mu$ and the dimensionless force $F_\mu = F_{red}/(\pi R^2\mu)$. The system that is obtained is given in (15) and (16).

$$e^{\beta\left(\frac{1}{\lambda_{\theta\Theta}^2\lambda_{zZ}^2}+\lambda_{\theta\Theta}^2+\lambda_{zZ}^2-3\right)}\left(\lambda_{\theta\Theta}^2-\frac{1}{\lambda_{\theta\Theta}^2\lambda_{zZ}^2}\right)-\frac{P_\mu}{2}=\frac{P_\mu}{\varepsilon}\lambda_{\theta\Theta}^2\lambda_{zZ} \tag{15}$$

$$e^{\beta\left(\frac{1}{\lambda_{\theta\Theta}^2\lambda_{zZ}^2}+\lambda_{\theta\Theta}^2+\lambda_{zZ}^2-3\right)}\left(\lambda_{zZ}^2-\frac{1}{\lambda_{\theta\Theta}^2\lambda_{zZ}^2}\right)-\frac{P_\mu}{2}=\frac{F_\mu}{2\varepsilon}\lambda_{zZ}+\frac{P_\mu}{\varepsilon}\lambda_{\theta\Theta}^2\lambda_{zZ} \tag{16}$$

It is clear that P_μ and F_μ can easily be resolved from (15-16) as $P_\mu = P_\mu(\lambda_{\theta\Theta},\lambda_{zZ})$ and $F_\mu = F_\mu(\lambda_{\theta\Theta},\lambda_{zZ})$. However, when circumferential distensibility is treated, we are much more interested in $\lambda_{\theta\Theta} = \lambda_{\theta\Theta}(P_\mu,F_\mu)$ and $\lambda_{zZ} = \lambda_{zZ}(P_\mu,F_\mu)$. Since (15-16) is nonlinear in $\lambda_{\theta\Theta}$ and λ_{zZ}, we will continue with a numerical solution. This was conducted in Maple 18, using the *fsolve* command, choosing axial prestretching $\lambda_{zZ}^{ini} \in \{0.1(i-1)+1\}_{i=1}^{n=11}$, computing F_μ and $\lambda_{\theta\Theta}^{ini}$ at $P_\mu = 0$, and finally solving (15-16) at a given F_μ and $\lambda_{\theta\Theta} \in \{0.001(i-1)+\lambda_{\theta\Theta}^{ini}\}_{i=1}^{n=1500}$ for unknown P_μ and λ_{zZ}. In the representative example, $\beta = 1$ was prescribed.

II.4 Neo-Hookean model at finite strains

Strain energy density models (7) and (8) are exponential functions of deformation, and they exhibit rapid large strain stiffening (Kanner and Horgan, 2007; Horgan and Saccomandi, 2003; Horgan, 2015; Ogden and Saccomandi, 2007; Horný et al., 2014c). Depending on specific values of the material parameters, the materials described by these potentials are characterized by progressively increasing stress-strain relationships, which is typical for soft biological tissues. As the second case, rapid strain stiffening will be suppressed, and the procedure will be repeated with the simplest invariant-based nonlinear material model (17). This is the so-called neo-Hooke strain energy density function which, under moderate strains, creates a link between the phenomenological theory and the statistical theory of macromolecular materials (Holzapfel, 2000).

$$W_{nH}=\frac{\mu}{2}\left(I_1-3\right) \tag{17}$$

Here μ is a stress-like material parameter which at infinitesimal strains corresponds to the shear modulus. The mutual relationship between W_{nH} and W_{FD} is given by (18).

$$\lim_{\beta\to 0}\frac{\mu}{2\beta}\left(e^{\beta(I_1-3)}-1\right)=\frac{\mu}{2}\left(I_1-3\right) \tag{18}$$

The constitutive equations obtained by substituting (17) into (5) are listed in (19). It can be observed that the material nonlinearity (strain stiffening) is lacking here, because λ_{kK}^2 ($k = r, \theta, z$; $K = R, \Theta, Z$) represents geometrical nonlinearity.

$$\sigma_{rr} = \mu\lambda_{rR}^2 - p \qquad \sigma_{\theta\theta} = \mu\lambda_{\theta\Theta}^2 - p \qquad \sigma_{zz} = \mu\lambda_{zZ}^2 - p \tag{19}$$

(19) is substituted into the equilibrium equations (3) in (20-22). (20) determines p.

$$\mu\lambda_{rR}^2 - p = -\frac{P}{2} \tag{20}$$

$$\mu\lambda_{\theta\Theta}^2 - p = \frac{rP}{h} \tag{21}$$

$$\mu\lambda_{zz}^2 - p = \frac{F_{red}}{2\pi rh} + \frac{rP}{2h} \tag{22}$$

Substituting p and applying geometrical equations (1), the system (23-24) governing the inflation-extension response of the thin-walled tube is obtained.

$$\mu\left(\lambda_{\theta\Theta}^2 - \frac{1}{\lambda_{\theta\Theta}^2\lambda_{zZ}^2}\right) - \frac{P}{2} = \frac{PR}{H}\lambda_{\theta\Theta}^2\lambda_{zZ} \tag{23}$$

$$\mu\left(\lambda_{zZ}^2 - \frac{1}{\lambda_{\theta\Theta}^2\lambda_{zZ}^2}\right) - \frac{P}{2} = \frac{F_{red}}{2\pi RH}\lambda_{zZ} + \frac{PR}{2H}\lambda_{\theta\Theta}^2\lambda_{zZ} \tag{24}$$

Finally, the aspect ratio $\varepsilon = H/R$, dimensionless pressure $P_\mu = P/\mu$, and dimensionless force $F_\mu = F_{red}/(\pi R^2)/\mu$ are again introduced in (25-26).

$$\lambda_{\theta\Theta}^2 - \frac{1}{\lambda_{\theta\Theta}^2\lambda_{zZ}^2} - \frac{P_\mu}{2} = \frac{P_\mu}{\varepsilon}\lambda_{\theta\Theta}^2\lambda_{zZ} \tag{25}$$

$$\lambda_{zZ}^2 - \frac{1}{\lambda_{\theta\Theta}^2\lambda_{zZ}^2} - \frac{P_\mu}{2} = \frac{F_\mu}{2\varepsilon}\lambda_{zZ} + \frac{P_\mu}{2\varepsilon}\lambda_{\theta\Theta}^2\lambda_{zZ} \tag{26}$$

We observe that equations (25-26) differ from (15-16) only by the absence of the exponential term, which is in accordance with (18). Since (25-26) are again nonlinear with respect to $\lambda_{\theta\Theta}$ and λ_{zZ}, the same approach as in the case of the exponential model will be employed to obtain the extension-inflation behaviour of a neo-Hookean cylindrical tube.

II.5 Second order linear elasticity (small strains but large displacements)

In this section, nonlinear effects will be attenuated by a transition from finite strain theory to linearized elasticity at infinitesimal strains. First, let us reconsider the constitutive equations implied by the neo-Hooke material model (19). Note that the left sides of (23-24) express $\sigma_{\theta\theta}$ and σ_{zz} after p is substituted from the radial equilibrium. Similarly, $\sigma_{\theta\theta}/\mu$ and σ_{zz}/μ are given by the left sides in (25-26). They are repeated in (27-28). It is clear that incompressibility at finite strains is manifested in the constitutive equations by "$- 1/(\lambda_{\theta\Theta}{}^2\lambda_{zZ}{}^2) - P_\mu/2$."

$$\frac{\sigma_{\theta\theta}}{\mu} = \lambda_{\theta\Theta}^2 - \frac{1}{\lambda_{\theta\Theta}^2\lambda_{zZ}^2} - \frac{P_\mu}{2} \tag{27}$$

$$\frac{\sigma_{zz}}{\mu} = \lambda_{zZ}^2 - \frac{1}{\lambda_{\theta\Theta}^2\lambda_{zZ}^2} - \frac{P_\mu}{2} \tag{28}$$

We will now start from (19), which will be linearized. As the first step, the stretches λ_{kK} in (19) are interchanged by components of the Green-Lagrange strain tensor $E_{KK} = ½(\lambda_{kK}{}^2 - 1)$, (29).

$$\sigma_{rr} = \mu\left(2E_{RR} + 1\right) - p, \quad \sigma_{\theta\theta} = \mu\left(2E_{\Theta\Theta} + 1\right) - p, \quad \sigma_{zz} = \mu\left(2E_{ZZ} + 1\right) - p \tag{29}$$

At this point, a description by the infinitesimal (engineering) strain tensor $\boldsymbol{\varepsilon}$ is introduced into (29). Since $\mathbf{E}$ and $\boldsymbol{\varepsilon}$ are approximately equal in the range of infinitesimal theory, we simply interchange E_{KK} and ε_{kk}, obtaining (30) from (29).

$$\sigma_{rr} = \mu\left(2\varepsilon_{rr} + 1\right) - p \qquad \sigma_{\theta\theta} = \mu\left(2\varepsilon_{\theta\theta} + 1\right) - p \qquad \sigma_{zz} = \mu\left(2\varepsilon_{zz} + 1\right) - p \tag{30}$$

It is clear from (30a) that (31) holds.

$$p = \mu\left(2\varepsilon_{rr} + 1\right) + \frac{P}{2} \tag{31}$$

We also need to express geometric equations (1) by means of $\boldsymbol{\varepsilon}$. This is done in system (32).

$$h = \left(1 + \varepsilon_{rr}\right)H \qquad r = \left(1 + \varepsilon_{\theta\theta}\right)R \qquad z = \left(1 + \varepsilon_{zz}\right)Z \tag{32}$$

The incompressibility condition for infinitesimal strains can be written in the form $\varepsilon_{rr} + \varepsilon_{\theta\theta} + \varepsilon_{zz} = 0$. Hence, the radial component of the engineering strain tensor can be substituted by (33).

$$\varepsilon_{rr} = -\varepsilon_{\theta\theta} - \varepsilon_{zz} \tag{33}$$

Substituting (31) into (30b) and (30c), applying (32) and substituting all into the equilibrium equations, system (34-35) is obtained.

$$\mu\left(2\varepsilon_{\theta\theta}+1\right)-\mu\left(1-2\varepsilon_{\theta\theta}-2\varepsilon_{zz}\right)-\frac{P}{2}=\frac{\left(1+\varepsilon_{\theta\theta}\right)RP}{\left(1-\varepsilon_{\theta\theta}-\varepsilon_{zz}\right)H} \tag{34}$$

$$\mu\left(2\varepsilon_{zz}+1\right)-\mu\left(1-2\varepsilon_{\theta\theta}-2\varepsilon_{zz}\right)-\frac{P}{2}=\frac{1}{\left(1+\varepsilon_{\theta\theta}\right)\left(1-\varepsilon_{\theta\theta}-\varepsilon_{zz}\right)}\frac{F_{red}}{2\pi RH}+\frac{\left(1+\varepsilon_{\theta\theta}\right)RP}{2\left(1-\varepsilon_{\theta\theta}-\varepsilon_{zz}\right)H} \tag{35}$$

Equations (34-35) govern the inflation-extension response of a thin-walled incompressible linearly elastic tube in so-called *second order linear elasticity* theory. This means that although the components of the small strain tensor are present in the equations, we still distinguish between the deformed configuration and the reference configuration. Thus equations (34-35) express the equality between the Cauchy stresses computed from the constitutive equations (left sides) and the Cauchy stresses computed from the geometry and the loads (right sides). The situation is similar to the way in which the buckling of a compressed column is treated. To obtain the critical force from a discussion of the boundary conditions, one has to substitute the expression for the bending moment into the equation for the deflection of the beam (Euler-Bernoulli) from the internal reaction forces determined in the deformed configuration. In other words, *small strains with large displacements* are considered here.

Applying the same normalization procedure as in the previous cases, system (34-35) is transformed into dimensionless form (36-37).

$$2\left(2\varepsilon_{\theta\theta}+\varepsilon_{zz}\right)-\frac{P_{\mu}}{2}=\frac{1+\varepsilon_{\theta\theta}}{1-\varepsilon_{\theta\theta}-\varepsilon_{zz}}\frac{P_{\mu}}{\varepsilon} \tag{36}$$

$$2\left(2\varepsilon_{zz}+\varepsilon_{\theta\theta}\right)-\frac{P_{\mu}}{2}=\frac{1}{\left(1+\varepsilon_{\theta\theta}\right)\left(1-\varepsilon_{\theta\theta}-\varepsilon_{zz}\right)}\frac{F_{\mu}}{2\varepsilon}+\frac{1+\varepsilon_{\theta\theta}}{1-\varepsilon_{\theta\theta}-\varepsilon_{zz}}\frac{P_{\mu}}{2\varepsilon} \tag{37}$$

The final equations (36-37) remain nonlinear, because rational expressions occur here. The nonlinearity, however, comes solely from the large displacements (the rational expressions are on the right sides of the equations). The results will again be obtained numerically.

It is interesting to see how the equations are expressed by means of the components the Green-Lagrange strain tensor and finite strain theory. The finite strain counterparts of (36-37) are obtained from (25-26) by transforming λ_{kK} into E_{KK}. They are given in (38) and (39).

$$2E_{\Theta\Theta}+1-\frac{1}{\left(2E_{\Theta\Theta}+1\right)\left(2E_{ZZ}+1\right)}-\frac{P_{\mu}}{2}=\frac{P_{\mu}}{\varepsilon}\left(2E_{\Theta\Theta}+1\right)\sqrt{2E_{ZZ}+1} \tag{38}$$

$$2E_{ZZ}+1-\frac{1}{\left(2E_{\Theta\Theta}+1\right)\left(2E_{ZZ}+1\right)}-\frac{P_\mu}{2}=\frac{F_\mu}{2\varepsilon}\sqrt{2E_{ZZ}+1}+\frac{P_\mu}{2\varepsilon}\left(2E_{\Theta\Theta}+1\right)\sqrt{2E_{ZZ}+1} \quad (39)$$

The left sides of (38-39) give equations for $\sigma_{\theta\theta}/\mu$ and σ_{zz}/μ when p has been eliminated. In (40-42), these equations are rewritten into the form of constitutive equations. Note that incompressibility necessitates loads to enter into the equations. Hence equations (40-42) are not general but they are valid only for the pressurization of a thin-walled tube.

$$\sigma_{rr}=-\frac{P}{2} \quad (40)$$

$$\sigma_{\theta\theta}=\mu\left(2E_{\Theta\Theta}+1\right)-\frac{\mu}{\left(2E_{\Theta\Theta}+1\right)\left(2E_{ZZ}+1\right)}-\frac{P}{2} \quad (41)$$

$$\sigma_{zz}=\mu\left(2E_{ZZ}+1\right)-\frac{\mu}{\left(2E_{\Theta\Theta}+1\right)\left(2E_{ZZ}+1\right)}-\frac{P}{2} \quad (42)$$

It is clear that "$\mu/(2E_{\Theta\Theta}+1)/(2E_{ZZ}+1)-½P$" arises from incompressibility. We can compare (40-42) with (43-45). (43-45) are again constitutive equations obtained from the left sides of (34-35), which are valid for the specific case of a linearly elastic incompressible thin-walled tube with σ_{rr} determined from the external load. It is clear that a correct description using finite strains generates nonlinearity in (41-42) via the incompressibility condition, which is lacking in the description based on the infinitesimal strain tensor (44-45); "$\mu/(2E_{\Theta\Theta}+1)/(2E_{ZZ}+1)$" vs. "$\mu(1-2\varepsilon_{\theta\theta}-2\varepsilon_{zz})$".

$$\sigma_{rr}=-\frac{P}{2} \quad (43)$$

$$\sigma_{\theta\theta}=\mu\left(2\varepsilon_{\theta\theta}+1\right)-\mu\left(1-2\varepsilon_{\theta\theta}-2\varepsilon_{zz}\right)-\frac{P}{2} \quad (44)$$

$$\sigma_{zz}=\mu\left(2\varepsilon_{zz}+1\right)-\mu\left(1-2\varepsilon_{\theta\theta}-2\varepsilon_{zz}\right)-\frac{P}{2} \quad (45)$$

II.6 First order linear elasticity (small strains and displacements)

Total linearization involves (a) introducing the small strain tensor, (b) linearizing the constitutive equations, and (c) taking into consideration small displacements, which justifies substituting the nominal stress tensor (the current force per reference cross-section) into the equilibrium equations. The constitutive equations are the same as in the previous section, given by (30). Equation (31) is again used to determine the contribution of the hydrostatic stress p. Thus the equilibrium equations are given by (34-35), but the right sides are modified according to the assumption of small displacements. The resulting equations are (46-47).

$$2\mu\left(2\varepsilon_{\theta\theta}+\varepsilon_{zz}\right)-\frac{P}{2}=\frac{RP}{H} \tag{46}$$

$$2\mu\left(2\varepsilon_{zz}+\varepsilon_{\theta\theta}\right)-\frac{P}{2}=\frac{F_{red}}{2\pi RH}+\frac{RP}{2H} \tag{47}$$

The dimensionless counterparts of (46-47) are equations (48-49).

$$2\left(2\varepsilon_{\theta\theta}+\varepsilon_{zz}\right)-\frac{P_{\mu}}{2}=\frac{P_{\mu}}{\varepsilon} \tag{48}$$

$$2\left(2\varepsilon_{zz}+\varepsilon_{\theta\theta}\right)-\frac{P_{\mu}}{2}=\frac{F_{\mu}}{2\varepsilon}+\frac{P_{\mu}}{2\varepsilon} \tag{49}$$

The first order linear elasticity gives the linear system of the equations of the problem (48-49), and at this moment the explicit dependence of $\varepsilon_{\theta\theta}$ and ε_{zz} on pressure and force is finally found (50).

$$\varepsilon_{\theta\theta}=\frac{1}{12}\frac{P_{\mu}\left(\varepsilon+3\right)-F_{\mu}}{\varepsilon} \qquad \varepsilon_{zz}=\frac{1}{12}\frac{\varepsilon P_{\mu}+2F_{\mu}}{\varepsilon} \tag{50}$$

Since axial prestrain ε_{zz}^{ini} is applied before the pressurization, i.e. at $P_{\mu}=0$, (50b) gives (51). Computed F_{μ} is constant in the subsequent pressurization. Substituting from (51) into (50a), the explicit dependence of the circumferential strain $\varepsilon_{\theta\theta}$ on the initial axial prestrain ε_{zz}^{ini} is obtained (52).

$$\varepsilon_{zz}^{ini}=\frac{F_{\mu}}{6\varepsilon} \tag{51}$$

$$\varepsilon_{\theta\theta}=\frac{1}{12}\frac{\varepsilon+3}{\varepsilon}P_{\mu}-\frac{1}{2}\varepsilon_{zz}^{ini} \tag{52}$$

Equation (52) implies that the axial prestrain will cause nothing more than a shift of the line that represents the $\varepsilon_{\theta\theta}$–$P_{\mu}$ dependence. However, the slope of the lines is constant during pressurization; from (52), the slope is $(\varepsilon + 3)/(12\varepsilon)$. In contrast to previous cases, the first order linear elasticity immediately shows that in this theory axial prestretching does not affect the character of the pressurization of a thin-walled incompressible tube. It only changes initial conditions of the pressurization.

II.7 NUMERICAL SIMULATIONS, AND A DISCUSSION OF THE RESULTS

The analytical computational models used in deriving the equations governing the inflation-extension of a closed incompressible thin-walled tube revealed that for (I), the exponential elastic potential (nonlinear model with rapid strain stiffening) – equations (15-16), for (II), a neo-Hookean material at finite strains (nonlinear model with moderate material nonlinearity) – equations (25-26), and for (III), a linearized neo-Hookean material considered at small strains but large displacements – equations (36-37), the problem does not lead to systems of equations from which the explicit analytical dependence of the circumferential stretch on the initial axial prestretching can be found. In these cases, numerical simulations were conducted to demonstrate the mechanical behaviour predicted by the models. They were performed in Maple 18, using the *fsolve* command according to the following scheme:

(I) and (II)

(a) $\lambda_{zZ}^{ini} \in \{1 + 0.1(i - 1)\}_{i=1}^{n=11}$

(b) the prestretching axial force F_μ and the initial circumferential stretch $\lambda_{\theta\Theta}^{ini}$ were computed for $P_\mu = 0$ and the chosen prestretch λ_{zZ}^{ini}

(c) P_μ and λ_{zZ} are computed for F_μ determined in (b) and $\lambda_{\theta\Theta} \in \{\lambda_{\theta\Theta}^{ini} + 0.001(i - 1)\}_{i=1}^{m}$ where $m = 1200$;

(III)

(a) $\varepsilon_{zz}^{ini} \in \{0.02(i - 1)\}_{i=1}^{n=11}$

(b) the prestretching axial force F_μ and the initial circumferential strain $\varepsilon_{\theta\theta}^{ini}$ were computed for $P_\mu = 0$ and chosen prestretch ε_{zz}^{ini}

(c) P_μ and ε_{zz} are computed for F_μ determined in (b) and $\varepsilon_{\theta\theta} \in \{\varepsilon_{\theta\theta}^{ini} + 0.001(i - 1)\}_{i=1}^{m}$ where $m = 1200$.

A thickness-to-radius ratio of $\varepsilon = 0.1$ was applied in all the simulations. Parameter β, modulating the rate of stiffening in (8), was prescribed to be $\beta = 1$.

RESULTS FOR THE ISOTROPIC LARGE STRAIN STIFFENING MODEL

Figure 14 depicts the results of the simulation of the inflation-extension behaviour of an incompressible thin-walled tube with isotropic exponential elastic potential (8). Panels A and B show the initial conditions of the inflation, i.e. the dependence of the prestretching force F_μ and the initial circumferential compression $\lambda_{\theta\Theta}^{ini}$ on the applied axial prestretch. The colours used to distinguish the individual prestretches are same in all figures and are chosen from HTML colour specification (in ascending order, they are: Black, Maroon, Red, DarkOrange, Gold, Yellow, GreenYellow, Cyan, DodgerBlue, Fuchsia, and DeepPink).

The inflation-extension responses predicted by the system of equations (15-16) are depicted in C and D of Figure 14. It is clear that the circumferential distensibility, understood as $\lambda_{\theta\Theta}(P_2) - \lambda_{\theta\Theta}(P_1)$ for some fixed λ_{zZ}^{ini} (where $P_1 < P_2$), depends strongly on the chosen axial prestretch λ_{zZ}^{ini}. Consider e.g. the deep pink ($\lambda_{zZ}^{ini} = 2$) and black ($\lambda_{zZ}^{ini} = 1$) curves in panel C. It is clear that if $P_{\mu 2} = 1$ and $P_{\mu 1} = 0.5$, a greater stretch difference $\lambda_{\theta\Theta}(P_{\mu 2}) - \lambda_{\theta\Theta}(P_{\mu 1})$ is obtained for greater prestretch.

This property is better documented in panels E and F. In E, the contours of the constant pressure $P_\mu = k$, where $k \in \{0.1(i-1)\}_{i=1}^{n=11}$, are added to the graph showing the inflation-extension responses as traces in the $\lambda_{\theta\Theta}$–λ_{zZ} plane. Choosing again $\lambda_{zZ}^{ini} = 1$ and 2 (black and deep pink solid curves), and for example $P_{\mu 2} = 0.2$ and $P_{\mu 1} = 0.1$ (red and maroon dashed curves), one can see that higher circumferential distensibility $\lambda_{\theta\Theta}(P_{\mu 2}) - \lambda_{\theta\Theta}(P_{\mu 1})$ is obtained for $\lambda_{zZ}^{ini} = 1$ (black solid). This demonstrates that the circumferential distensibility of the tube, $\lambda_{\theta\Theta}(P_{\mu 2}) - \lambda_{\theta\Theta}(P_{\mu 1})$ (where $P_{\mu 1} < P_{\mu 2}$), is not monotonic with respect to the applied λ_{zZ}^{ini} in the model based on (8).

Panel F displays this for pressures $P_{\mu 2} = P_\mu$ and $P_{\mu 1} = 0$. In other words, panel F shows the difference between the circumferential stretch achieved at some pressure P_μ and the initial circumferential stretch that is ordinarily attained at $P_\mu = 0$. It can be concluded that weakly prestretched tubes show mechanical responses with high circumferential distensibility at low pressures (consider e.g. the maroon ~ $\lambda_{zZ}^{ini} = 1.1$, red ~ $\lambda_{zZ}^{ini} = 1.2$, and dark orange ~ $\lambda_{zZ}^{ini} = 1.3$ curves) in contrast to highly prestretched tubes. However, at higher pressures, the curves corresponding to higher prestretches exceed the curves obtained for less prestretched tubes (consider e.g. the curves in dodger blue ~ $\lambda_{zZ}^{ini} = 1.8$, fuchsia ~ $\lambda_{zZ}^{ini} = 1.9$, and deep pink ~ $\lambda_{zZ}^{ini} = 2$).

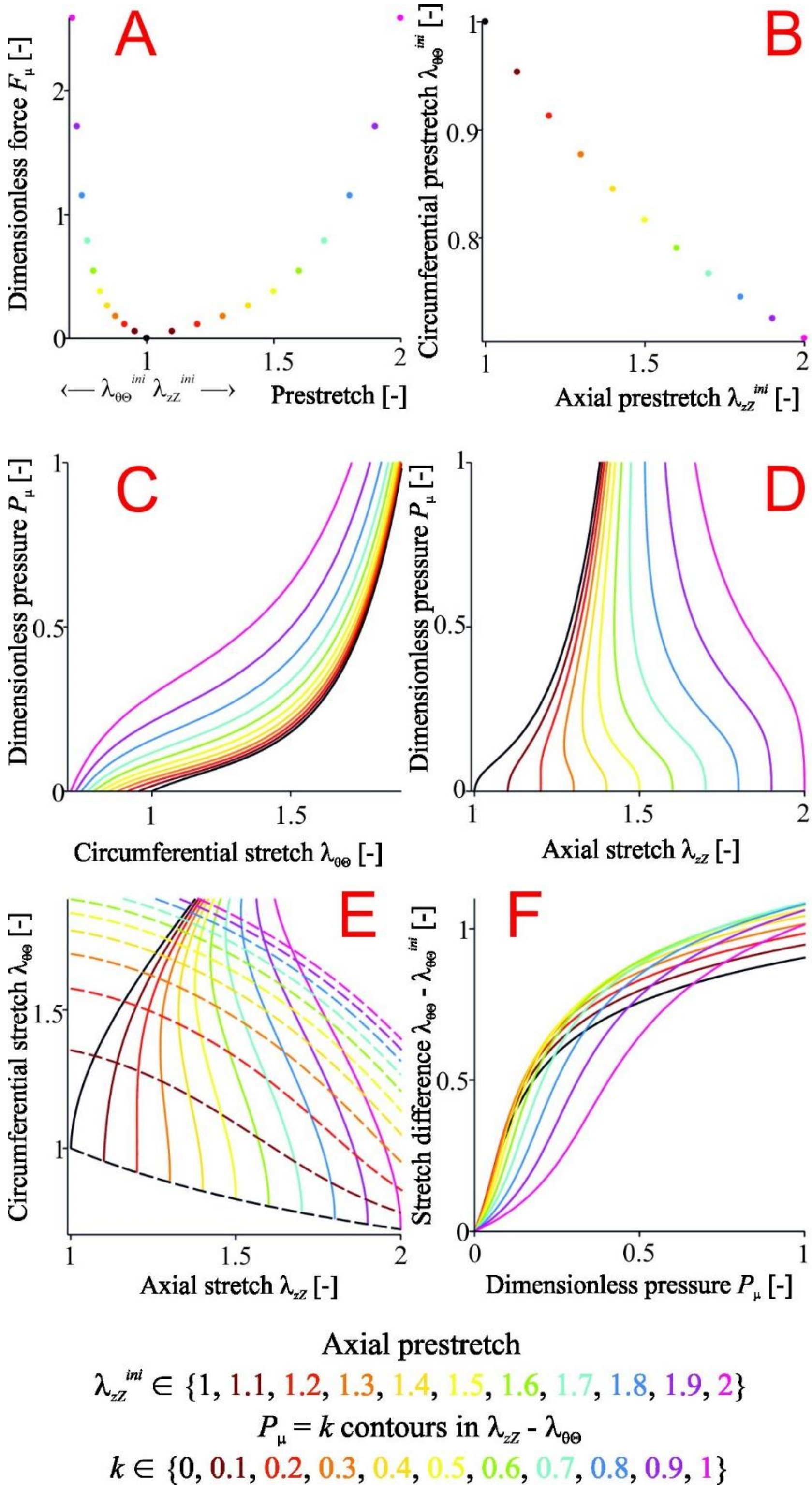

Figure 1. Fung-Demiray inflation-extension response. A – initial prestretch and dimensionless force. B – mutual dependence of initial prestretches (λ_{zZ}^{ini} – $\lambda_{\theta\Theta}^{ini}$). C and D – dimensionless pressure vs. stretch. E – traces of the inflation-extension responses in the phase space of the deformation (solid curves) and contour curves for dimensionless pressure $P_\mu = k$ (dashed curves). F – stretch difference $\lambda_{\theta\Theta} - \lambda_{\theta\Theta}^{ini}$ achieved by loading a tube with pressure P_μ.

This implies that $\lambda_{\theta\Theta} - \lambda_{\theta\Theta}^{ini}$ is not monotonous in its first derivatives with respect to P_{μ} for a given λ_{zZ}^{ini}. A consequence of this is the existence of inflection points where tangents to $\lambda_{\theta\Theta} - \lambda_{\theta\Theta}^{ini}$ will have extremal slopes (see Figure 14 F). Such a property, theoretically, allows tubes to be programmed to operate in an optimal working range (to optimize either the pressure difference for a given distensibility or the distensibility at some chosen pressure difference). We will not go into further details here. We have already found what we had been looking for: the positive effect of the axial prestretch is not restricted to anisotropy, as had been hypothesized in Horný et al. (2014b).

RESULTS FOR A NEO-HOOKEAN TUBE AT FINITE STRAINS

Figure 2 depicts the mechanical responses obtained for an incompressible neo-Hookean thin-walled tube at finite strains. The responses are governed by equations (25-26), and numerical simulation is again the only way to make a theoretical investigation of the effect of the prestretch. Figure 2 is fashioned in a similar way as Figure 1. Panels A and B show the initial conditions for inflation, C and D show the dimensionless pressure and the achieved stretches, and E and F again document the circumferential distensibility as such.

In comparison with Figure 1, there is one substantial difference, which is indicated by the dotted parts of the curves. The dotted curves correspond to a loss of deformation stability. This phenomenon is well known to anyone who has ever inflated a party balloon (Chater and Hutchinson 1984; Gent 2005; Kanner and Horgan 2007; Gonçalves et al., 2008; Rodriguez and Merodio, 2011; Mao et al., 2014; Horný et al., 2015). The inflation instability is exhibited as a non-monotonic dependence of the inflation pressure on the circumferential stretch. At the point where stability is lost, increments in circumferential stretch are accompanied by decrements in applied pressure. This is exactly what happens with a party balloon - after some initial loading its response becomes unstable.

Since the onset of loss of stability is accompanied by buckling, which in the case of a cylindrical tube may appear as a bulge propagated in the axial direction, or as bending (resembling the deflection of a beam), or a bulge propagated in the radial direction, the assumptions contained in the geometrical equations (1) are violated in the subsequent inflation. In the absence of serious post-buckling analysis, results related to the post-buckling behaviour therefore have to be considered uncertain. However, this is beyond the scope of our present study. We will limit ourselves to the stable elastic response, which is indicated by the solid parts of the curves.

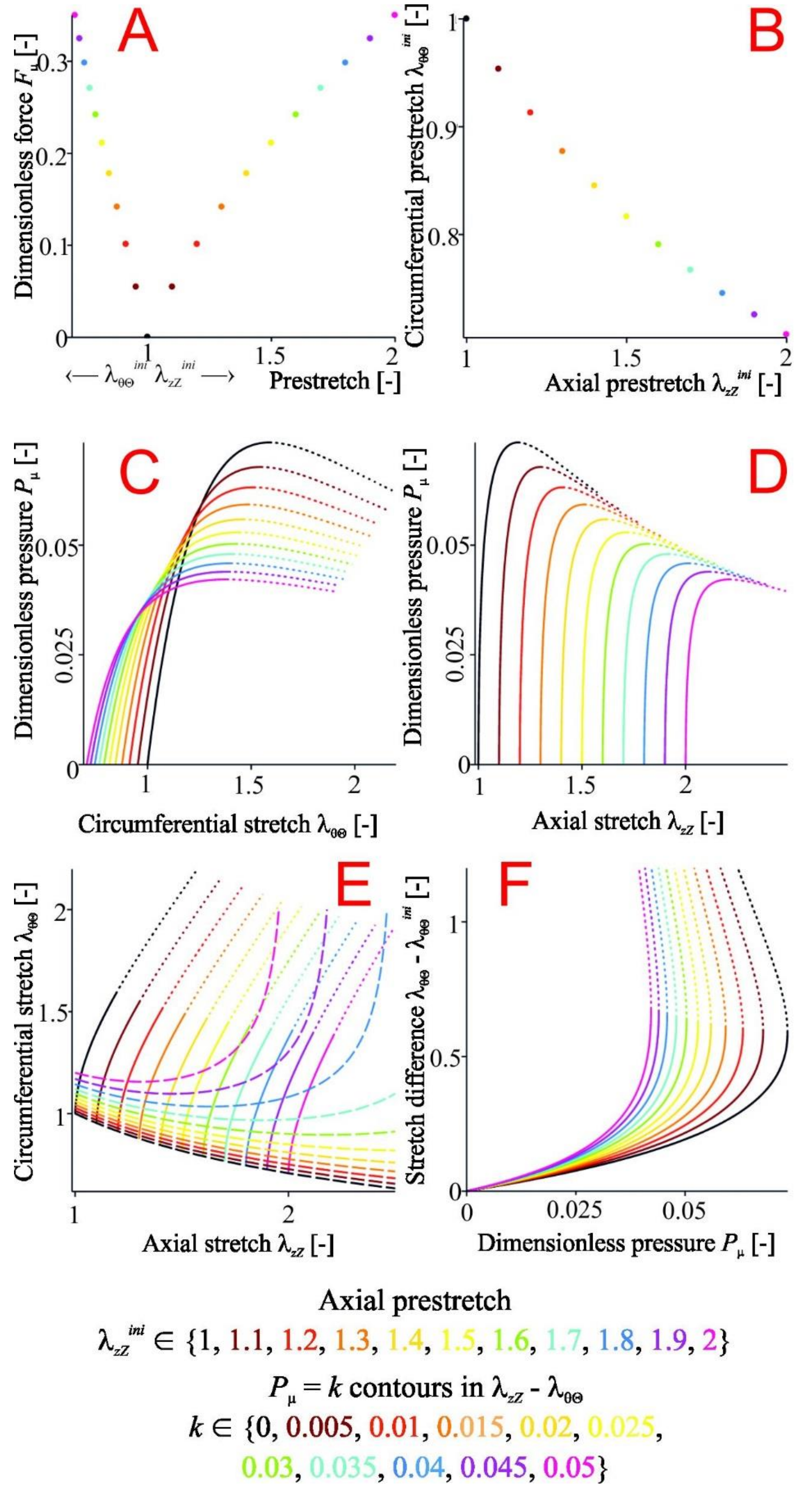

Figure 2. Neo-Hookean inflation-extension response. A – initial prestretches and dimensionless force. B – mutual dependence of the initial prestretches ($\lambda_{zZ}^{ini} - \lambda_{\theta\Theta}^{ini}$). C and D – dimensionless pressure vs. stretch. E – traces of the inflation-extension responses in the phase space of the deformation (solid curves) and contour curves for dimensionless pressure $P_\mu = k$ (dashed curves). F – stretch difference $\lambda_{\theta\Theta} - \lambda_{\theta\Theta}^{ini}$ achieved by loading a tube with pressure P_μ. Dotted curves indicate a loss of deformation stability.

Panel C in Figure 2 shows that the applied axial prestretch (a) decreases the maximum pressure achievable in the deformation, and (b) also makes the tube more distensible in the circumferential direction. This is clear, when one considers the slopes of the tangents made to the pressure–stretch curves at any fixed pressure (Panel C). In other words, the pressure–circumferential stretch dependences in panel C form concave curves (under elastically stable deformations).

The same conclusion is obtained for panels E and F. Especially F, which, similarly to Figure 1, shows the difference between the circumferential stretch achieved by some pressure P_{μ} and the initial circumferential stretch obtained at $P_{\mu} = 0$, clearly demonstrates that the higher the axial prestretch, the higher the circumferential distensibility at a given pressure.

Unlike for the strain-stiffening model (8), there is no violation of monotony. Considering equation (18), we see that both models have topredict the same mechanical behaviour whe $\beta \to 0$. Thisis also clear when the governing equations (15-16) and (25-26) are compared. Now we see that the existence of the non-monotonic effect of the axial prestretch (increased vs. decreased circumferential distensibility) in the Fung-Demiray model (8) is a consequence of the presence of material parameter β. β contributes to the system by one additional degree of freedom, and allows a switch between the positive effect (enhancing the distensibility) and the negative effect (suppressing the distensibility) of prestretching that is exhibited by a tube while it is being inflated.

SECOND ORDER LINEAR ELASTICITY

Figure 3 shows the results obtained for a linearized neo-Hookean material with the deformation described using the engineering strain tensor (36-37). It is depicted with solid curves and filled circles. The panels are again arranged in the same way as in Figures 1 and 2. However, for the sake of easy comparison, the results predicted using the finite strain neo-Hooke model are also displayed here; equations (38-39). They are indicated by dotted curves and empty circles. For the finite strain model, the results depicted in the figure were transformed from the original Green-Lagrange deformations to engineering strains according to the equation $\varepsilon_{kk} = \sqrt{(1 + 2E_{KK})} - 1$, where $k = \theta, z$, and $K = \Theta, Z$. Thus the two models are displayed in the same quantities, which helps when comparing them, because the nonlinear effects are immediately clear when the results are displayed over coordinate axes scaled in infinitesimal strains.

The same axial prestrain sequences were applied in the linearized model (III) and in the in the finite strain model (II); $\{\varepsilon_{zz}{}^{ini}{}_{j}\}_{j=1}{}^{11} = \{0.02(j - 1)\}_{j=1}{}^{11}$. On the basis of the conclusion obtained using the totally linearized model (IV, equations 50-52), we know that in this case the system of governing equations gives linear pressure–deformation relationships. Hence, if the solid curves in Figure 3 deflect from (imaginary) straight lines, this is the effect of large displacements sustained by linear material. When the dotted curves are deflected from the solid curves, this is the effect of the incompressibility formulated in the finite strain description; compare equations (36-37) and (38-39).

The nonlinearity of the P_μ–$\varepsilon_{\theta\theta}$ relationship is clear from Figure 3 (panel C), and occurs in both models. In contrast with panel C, where both finite strain neo-Hooke and also linearized neo-Hooke with infinitesimal strains but large displacements show clear nonlinearity, P_μ–ε_{zz} relationships for the linearized model with the small strains but large displacements (solid curves) presented in panel D exhibit only limited deviations from straightness. Moreover, nonlinearity occurs where there are strains say $0.1 < \varepsilon_{zz}$. In this region, the results obtained with $\boldsymbol{\varepsilon}$ used in the description have to be considered as estimates of reality, rather than as facts. However, the finite strain model displayed over the axis scaled in ε_{zz} clearly deflects from straightness.

It is hard to draw conclusions about the circumferential distensibility on the basis of panel C of Figure 3. The effect of the prestretch is less clearly visible than in Figures 1 and 2. The stretch variation $|\varepsilon_{\theta\theta} - \varepsilon_{\theta\theta}^{ini}|$ is therefore depicted separately in Figure 4. In panel A, we observe that the curves are convex. This indicates that distensibility increases with increasing pressure. The effect of the prestretch is positive; that is the greater the prestretch, the greater the distensibility. This is found by comparing the mutual positions of the curves (panel B). However, in the range of linear elasticity, this effect is almost negligible.

3.4 First order linear elasticity

Total linearization (small strains and displacements) is the only case where conclusions can be drawn immediately on the basis of the equations (50-52). There is no effect of the axial prestrain on the mechanical response of an incompressible linearly elastic thin-walled tube apart from the shift of the linear P_μ–$\varepsilon_{\theta\theta}$ relationship. There is no enhancement or suppression of circumferential distensibility, as is documented in Figure 5.

However, from a different point of view, insensitivity of the circumferential distensibility in the first order linear elasticity to the axial prestrain elucidates a source of the phenomenon under discussion here. The difference between first order and second order linear elasticity consists in the form of the right side in the equilibrium equations (48-49) vs. (36-37); i.e. in the nominal stress tensor (current force per reference cross-section, 48-49) vs. the Cauchy stress tensor (current force per deformed cross-section, 36-37). In other words, the reason for the enhanced distensibility in the second order linear theory lies in the large displacements. However, the comparison in Figure 3 shows that a finite strain formulation of the incompressibility moves the effect of the prestretch from a rather abstract mathematical phenomenon to a fact measurable by engineering methods.

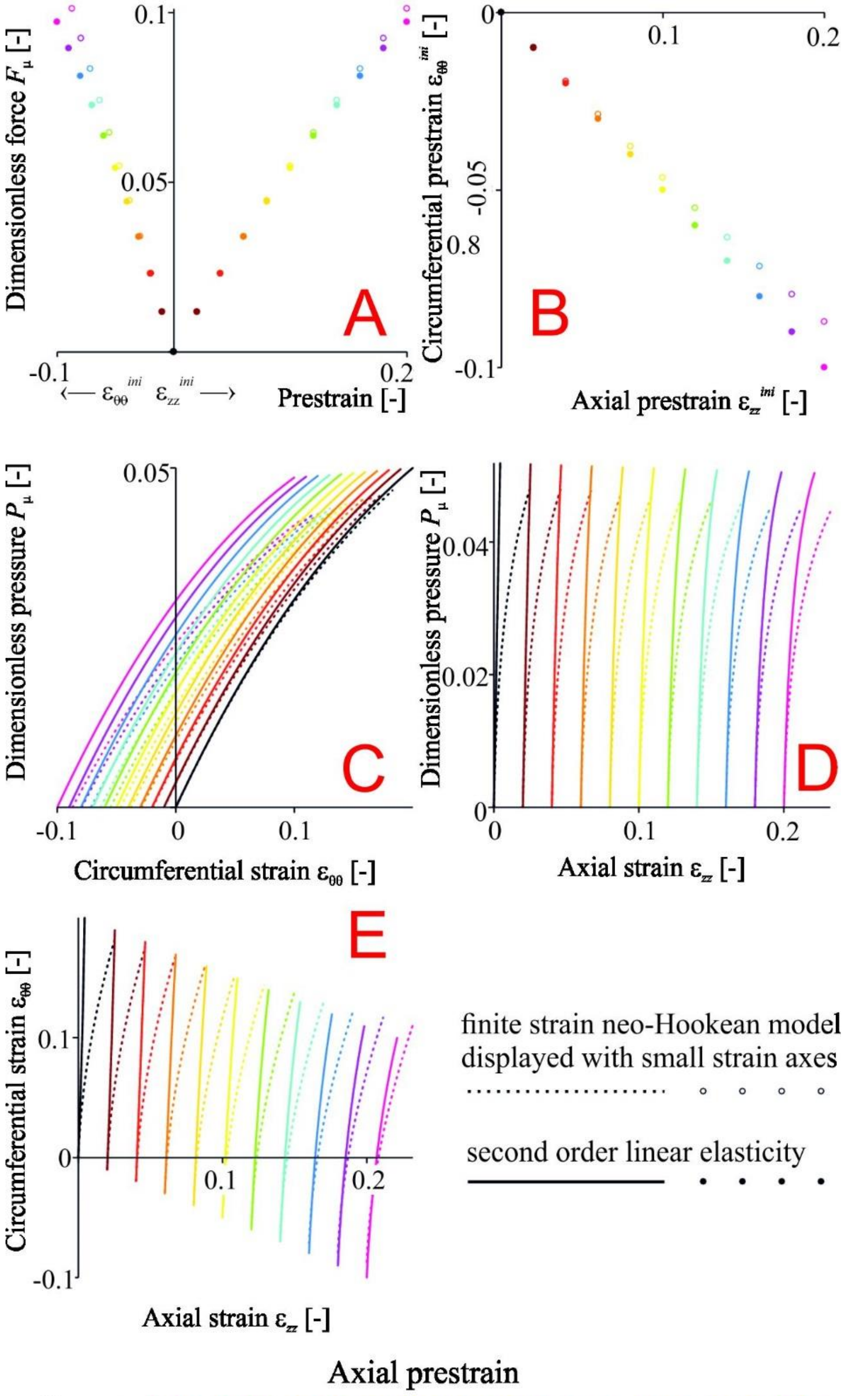

Figure 3. The neo-Hookean and linearized inflation-extension response at small strains but large displacements. A – prestrains and dimensionless force. B – mutual dependence of initial prestrains. C and D – dimensionless pressure vs. infinitesimal strain. E – traces of inflation-extension responses. The solid circles and continuous curves correspond to second order linear theory. The dotted curves and empty circles correspond to nonlinear theory applied to a neo-Hookean material, but the results are displayed over infinitesimal strain coordinates according to $\varepsilon_{kk} = \sqrt{(1 + 2E_{KK})} - 1$.

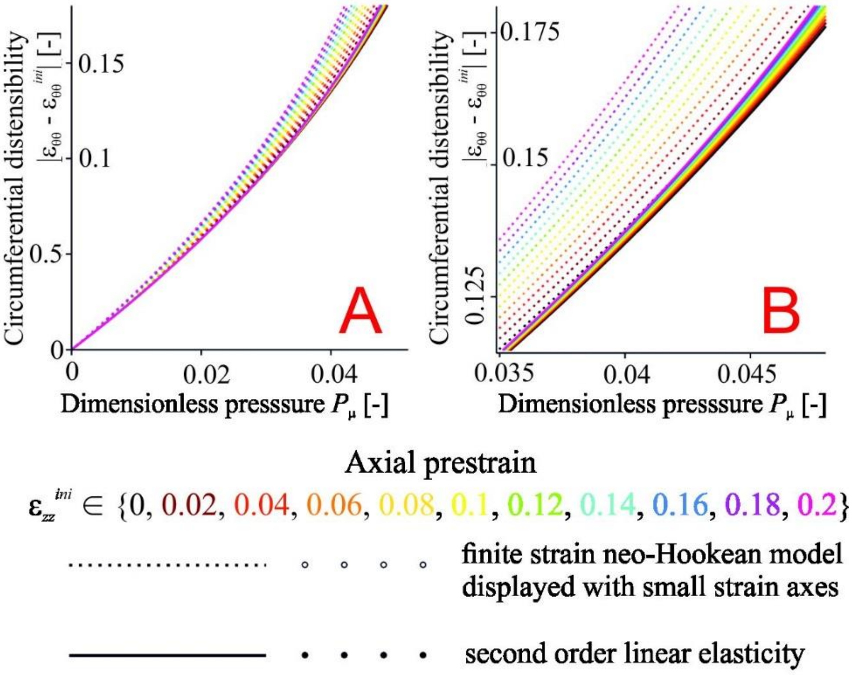

Figure 4. Circumferential distensibility of the Neo-Hookean model and the linearized model in the inflation-extension response at small strains but large displacements. A – overall dependences. B – detail.

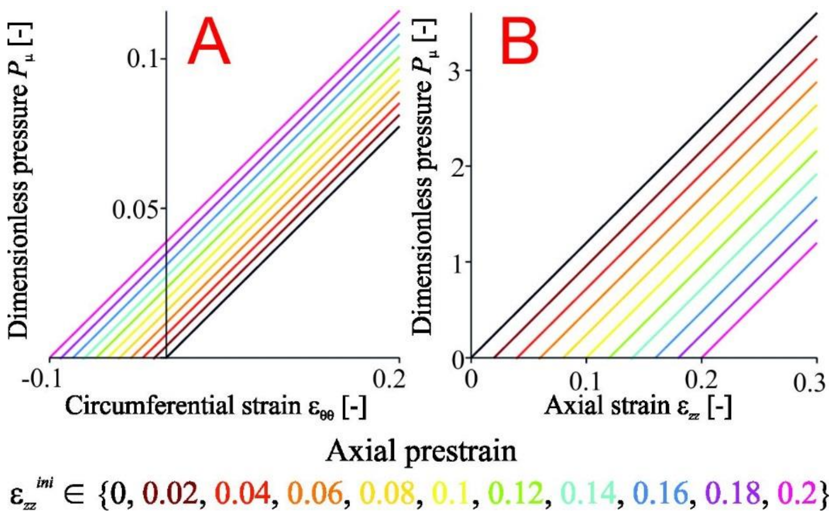

Figure 5. Inflation-extension responses in the first order linear elasticity. A – circumferential responses. B – longitudinal responses.

II.8 Conclusion to the chapter II

The study published by Horný et al. (2014b) showed that nonlinear incompressible anisotropic thin-walled tubes exhibit higher circumferential distensibility when they are axially prestretched than non-prestretched tubes with the same constitutive properties and geometry. From a physiological point of view, this effect is positive because aortas, which were investigated in Horný et al. (2014b), serve as conduits for flowing blood. Thus the greater the distension that they are capable of achieving at some pressure, the larger is the volume of the blood that they can accommodate. Horný et al. (2014b) hypothesized that this effect, which had not been described previously in the literature, could be a consequence of arterial anisotropy.

In the present study, we have tried to show the true physical cause of the increased distensibility of axially prestretched tubes. The approach that has been adopted is based on a mutual comparison of four computational models. To be more specific, our study has investigated the mechanical response of a thin-walled incompressible tube (I) with a material based on the exponential strain energy density function, (II) with a neo-Hooke material, (III) with a linearly elastic material sustaining small strains but large displacements, and (IV) a tube with a totally linearized material. All the material models were isotropic.

The simulations showed that the positive effect of axial prestretching is not a property exclusively related to anisotropy, because the results obtained in (I) showed that axially prestretched tubes can distend more than non-prestretched tubes. The Fung-Demiray constitutive model used in case (I) is a direct isotropic restriction of the model used by Horný et al. (2014b).

It has been proved that nonlinear effects are crucial for the positive role of axial prestretching in pressurization. Nonlinear constitutive models depending on more than one parameter (exemplified here by the Fung-Demiray model in I) can exhibit both enhancement and suppression of the circumferential distensibility of the tube, due to prestretching. This implies that the effect of prestretching in two or more parametrical nonlinear constitutive models can be positive (higher circumferential distensibility) or negative (lower distensibility relative to the response of a non-prestretched tube), and the specific result depends on the constitutive model and the pressure that is applied. By contrast, the one-parameter nonlinear model (II, neo-Hooke) showed only increased distensibility when axial prestretching had been applied.

A reduction of the computational model to second order linear elasticity (III, small strains but large displacements) led to mechanical responses that exhibited only a slight effect of prestretching in comparison with previous nonlinear models. However, from the purely mathematical point of view, the positive effect of prestretching on circumferential distensibility is still present. In case (III), highly prestretched tubes showed higher distensibility than weakly prestretched tubes.

Finally, total linearization (IV) proved that the significant effect is present only to the point at which the deformed configuration and the reference configuration are considered to be different. In other words, first order linear elasticity (IV), which does not distinguish between the two configurations when the stresses are computed from the loads applied to a structure, showed no other effect of prestretching apart from a change in the initial conditions of the pressurization. Neither enhancement nor suppression of the circumferential distensibility was found.

To the best of our knowledge, this is the first study that has made a systematic evaluation of the effect of prestretching on the mechanical response of pressurized nonlinear tubes. However, this does not mean that there have been no previous papers documenting our results. As is shown in Horný et al. (2014b), there have been studies documenting experimentally that arteries pressurized ex vivo exhibit higher circumferential distensibility when they are axially prestretched (cf. Figure 4 in Schulze-Bauer et al., 2003; Figure 5 in Sommer et al., 2010; Figure 4 in Sommer and Holzapfel 2012; Figure 6 in Avril et al., 2013). However, a detailed discussion of this phenomenon was not an objective of these papers. Details of the physiological and mechanobiological role of prestretching can be found in Humphrey et al. (2009) and Cardamone et al. (2009).

Finally it should be noted explicitly that first order linear theory is a limit of all nonlinear theories. Hence, irrespective of the formalism (nonlinear theory, a linear material for finite strains, a linear material under large displacements but small strains), if the displacements and strains are sufficiently small, the results obtained with first order linear elasticity will also hold for other formalisms. In other words, one when chooses some small positive epsilon as the error between linear and nonlinear predictions, there will always be some delta bordering a subset in the space of deformations where the errors between linear and nonlinear theory will be smaller than the chosen epsilon. In engineering practice, epsilon depends on the sensitivity and the confidence of our experimental methods.

Conclusion

Biomechanics. The above presented calculations have shown that, although ageing led to significantly decreased longitudinal prestretch, the biomechanical response of the human abdominal aorta was changed significantly depending on used initial axial stretch within the computation. Particularly, substituting the upper limit of the confidence of prediction for the axial prestretch gave mechanical responses which can be characterised by (a) lower variation in axial length, and (b) higher circumferential distensibility, in contrast to the responses obtained for arteries with low initial axial prestretch.

The simulation also showed a significant effect of the axial prestretch on the variation of mean axial stress during the pressure cycle. Again, highly prestretched aortas showed low variation of axial stress and contrary weakly prestretched arteries exhibited high intra-cycle stress variation. This result should attract more scientific attention in future because axial stress exceeding physiological values may be a trigger of adaptation processes which could result in abnormal thickening, or an aneurysm or tortuosity formation.

Finally, the obtained biomechanical results are in accordance with the hypothesis that the circumferential-to-axial stiffness ratio is the quantity relatively constant within this cycle. This can be used in *in vivo* constitutive model determination procedures which needs some physical constraints replacing axial equilibrium equation because true values of F_{red} are unavailable *in vivo*.

General solid mechanics of deformable bodies. The positive effect of the prestretch found in arteries led the author to attempt to explain it or, better to say, to find a source of this phenomenon. In the second section of the thesis, an effect of anisotropy, effect of nonlinear constitutive model (material nonlinearity), effect of finite strains (geometrical nonlinearity), and large displacements with infinitesimal strain formulation, were discussed in top–bottom approach.

Since isotropic models were used in the second section, we can conclude that the positive effect of the axial prestretch is not a property exclusively related to anisotropy which is exhibited by arteries. It has been proved that nonlinear effects are crucial for positive role of the axial prestretch in a pressurization of an incompressible tube. Nonlinear constitutive models depending on more than one parameter (herein exemplified by Fung-Demiray model) can exhibit both enhancing as well as suppressing of the circumferential distensibility of the tube by the prestretch. Contrastingly one-parameter neo-Hookean model showed only increased distensibility when axial prestretch had been applied.

A reduction of the computational model to the second order linear elasticity (small strains but large displacements) led to mechanical responses which exhibited only slight effect of the prestretch in comparison with previous nonlinear models. But from purely mathematical point of view, the positive effect of the prestretch on the circumferential distensibility is still present. And finally, the total linearization proved that the positive effect is present only to a point where deformed and reference configuration is considered to be different. In other words, first order linear elasticity, which does not distinguish between both of the configurations when stresses are computed from loads applied to a structure, showed no other effect of the prestretch than a change of initial conditions of the pressurization. This result was obtained despite the fact that incompressibility was still considered.

Finally it should be mentioned explicitly that first order linear theory is a limit of all nonlinear theories.[11] Hence, independently of a formalism, (nonlinear theory, linear material at finite strains, linear material under large displacements but small strains) if displacements and strains are sufficiently small, the results obtained with first order linear elasticity will hold also for other formalisms. In other words, one when chooses some small positive epsilon as an error between linear and nonlinear predictions, there will always be some delta bordering a subset in the space of deformations where errors between linear and nonlinear theory will be smaller than the chosen epsilon. In an engineering practice, the epsilon depends on a sensitivity and confidence of our experimental methods.

[11] Otherwise one could not consider the nonlinear theory as a meaningful concept.

References I

Ahlgren TR, Cinthio M, Persson HW, Lindström K (2012). Different patterns of longitudinal displacement of the common carotid artery wall in healthy humans are stable over a four-month period. Ultrasound Med Biol 38:916-925. doi: 10.1016/j.ultrasmedbio.2012.02.005

Åstrand H, Stålhand J, Karlsson J, Karlsson M, Sonesson B, Länne T (2011) In vivo estimation of the contribution of elastin and collagen to the mechanical properties in the human abdominal aorta: Effect of age and sex. J Appl Physiol 110:176-187. doi: 10.1152/japplphysiol.00579.2010

Chater, E., & Hutchinson, J. W. (1984). On the propagation of bulges and buckles. J Appl Mech - Trans ASME 51(2):269-277.

Carta L, Wagenseil, JE, Knutsen RH, Mariko B, Faury G, Davis EC, et al. (2009) Discrete contributions of elastic fiber components to arterial development and mechanical compliance. Arterioscler Thromb Vasc Biol 29:2083-2089. doi: 10.1161/ATVBAHA.109.193227

Chen K, Fata B, Einstein DR (2008) Characterization of the highly nonlinear and anisotropic vascular tissues from experimental inflation data: A validation study toward the use of clinical data for in-vivo modeling and analysis. Ann Biomed Eng 36:1668-1680. doi: 10.1007/s10439-008-9541-9

Chuong CJ, Fung YC (1986) On residual stresses in arteries. J Biomech Eng 108:189-92.

Cinthio M, Ahlgren ÅR, Bergkvist J, Jansson T, Persson HW, Lindström K (2006). Longitudinal movements and resulting shear strain of the arterial wall. Am J Physiol Heart Circ Physiol 291:H394-H402. doi: 10.1152/ajpheart.00988.2005

Demiray, H. (1972). A note on the elasticity of soft biological tissues. *Journal of Biomechanics, 5*(3), 309-311. doi.: 10.1016/0021-9290(72)90047-4

Dobrin PB (1978) Mechanical properties of arteries. Physiol Rev 58:397-460

Dobrin PB, Doyle JM (1970) Vascular smooth muscle and the anisotropy of dog carotid artery. Circ Res 27:105-119

Dobrin PB, Schwarcz TH, Mrkvicka R (1990) Longitudinal retractive force in pressurized dog and human arteries. J Surg Res 48:116-120. doi: 10.1016/0022-4804(90)90202-D

Gent, A. N. (2005). Elastic instabilities in rubber. Int J Non-Lin Mech, 40(2-3), 165-175. doi: 10.1016/j.ijnonlinmec.2004.05.006

Greenwald SE (2007) Ageing of the conduit arteries. J Pathol 211:157-172. doi: 10.1002/path.2101

Guccione JM, McCulloch AD, Waldman LK (1991) Passive material properties of intact ventricular myocardium determined from a cylindrical model. J Biomech Eng 113:42–55. doi: 10.1115/1.2894084

Han HC, Fung YC (1995) Longitudinal strain of canine and porcine aortas. J Biomech 28:637-641. doi: 10.1016/0021-9290(94)00091-H

Holzapfel GA, Gasser TC, Ogden RW (2000) A new constitutive framework for arterial wall mechanics and a comparative study of material models. J Elast 61:1-48. doi: 10.1023/A:1010835316564

Holzapfel GA (2000) Nonlinear solid mechanics: A continuum approach for engineering. Wiley & Sons, Chichester.

Holzapfel GA, Ogden RW (2010a) Constitutive modelling of arteries. Proc R Soc A 466:1551-1597. doi: 10.1098/rspa.2010.0058

Holzapfel GA, Ogden RW (2010b) Modelling the layer-specific three-dimensional residual stresses in arteries, with an application to the human aorta. J R Soc Interface 7:787-99. doi: 10.1098/rsif.2009.0357

Horny L, Adamek T, Gultova E, Zitny R, Vesely J, Chlup H, Konvickova S (2011) Correlations between age, prestrain, diameter and atherosclerosis in the male abdominal aorta. J Mech Behav Biomed Mater 4:2128-2132. doi: 10.1016/j.jmbbm.2011.07.011

Horny L, Adamek T, Vesely J, Chlup H, Zitny R, Konvickova S (2012a) Age-related distribution of longitudinal pre-strain in abdominal aorta with emphasis on forensic application. Forensic Sci Int 214:18-22. doi: 10.1016/j.forsciint.2011.07.007

Horny L, Adamek T, Chlup H, Zitny R (2012b) Age estimation based on a combined arteriosclerotic index. Int J Leg Med 126:321-326. doi: 10.1007/s00414-011-0653-7

Horny L, Adamek T, Zitny R (2013) Age-related changes in longitudinal prestress in human abdominal aorta. Arch Appl Mech 83:875-888. doi: 10.1007/s00419-012-0723-4

Horny L, Adamek T, Kulvajtova M (2014) Analysis of axial prestretch in abdominal aorta with reference to post mortem interval and degree of atherosclerosis. J Mech Behav Biomed Mater 33:93-98. doi: 10.1016/j.jmbbm.2013.01.033

Humphrey JD (2002) Cardiovascular solid mechanics: Cells, tissues and organs. Springer-Verlag, New York

Humphrey JD, Eberth JF, Dye WW, Gleason RL (2009) Fundamental role of axial stress in compensatory adaptations by arteries. J Biomech 42:1-8. doi: 10.1016/j.jbiomech.2008.11.011

Jackson ZS, Gotlieb AI, Langille BL (2002) Wall tissue remodeling regulates longitudinal tension in arteries. Circ Res 90:918-925. doi: 10.1161/01.RES.0000016481.87703.CC

Kalita P, Schaefer R (2008) Mechanical models of artery walls. Arch Comput Methods Eng 15:1-36. doi: 10.1007/s11831-007-9015-5

Kanner LM, Horgan, CO (2007) Elastic instabilities for strain-stiffening rubber-like spherical and cylindrical thin shells under inflation. Int J Non-Lin Mech 42(2), 204-215. doi: 10.1016/j.ijnonlinmec.2006.10.010

Karatolios K, Wittek A, Nwe TH, Bihari P, Shelke A, Josef D, Schmitz-Rixen T, Geks J, Maisch B, Blase C, Moosdorf R, Vogt S. (2013) Method for aortic wall strain measurement with three-dimensional ultrasound speckle tracking and fitted finite element analysis. Ann Thorac Surg, in press. doi: 10.1016/j.athoracsur.2013.06.037

Labrosse MR, Beller CJ, Mesana T, Veinot JP (2009) Mechanical behavior of human aortas: Experiments, material constants and 3-D finite element modeling including residual stress. J Biomech 42:996-1004. doi: 10.1016/j.jbiomech.2009.02.009

Labrosse MR, Gerson ER, Veinot JP, Beller CJ (2013) Mechanical characterization of human aortas from pressurization testing and a paradigm shift for circumferential residual stress. J Mech Behav Biomed Mater 17:44-55. doi: 10.1016/j.jmbbm.2012.08.004

Langewouters GJ, Wesseling KH, Goedhard WJA (1984) The static elastic properties of 45 human thoracic and 20 abdominal aortas in vitro and the parameters of a new model. J Biomech 17:425-435.

Larsson M, Kremer F, Claus P, Kuznetsova T, Brodin L, D'Hooge J (2011) Ultrasound-based radial and longitudinal strain estimation of the carotid artery: A feasibility study. IEEE Trans Ultrason Ferroelectr Freq Control 58(10), 2244-2251. doi: 10.1109/TUFFC.2011.2074

Lawrence AR, Gooch KJ (2009) Transmural pressure and axial loading interactively regulate arterial remodeling ex vivo. Am J Physiol Heart Circ Physiol 297:H475-H484. doi: 10.1152/ajpheart.00972.2008

Learoyd BM, Taylor MG (1966) Alterations with age in the viscoelastic properties of human arterial walls. Circ Res 18:278-292

Matsumoto T, Hayashi K (1996) Stress and strain distribution in hypertensive and normotensive rat aorta considering residual strain. J Biomech Eng 118:62-71. doi: 10.1115/1.2795947

Masson I, Boutouyrie P, Laurent S, Humphrey JD, Zidi M (2008) Characterization of arterial wall mechanical behavior and stresses from human clinical data. J Biomech 41:2618-27. doi: 10.1016/j.jbiomech.2008.06.022

Masson I, Beaussier H, Boutouyrie P, Laurent S, Humphrey JD, Zidi M (2011) Carotid artery mechanical properties and stresses quantified using in vivo data from normotensive and hypertensive humans. Biomech Model Mechanobiol 10:867-882. doi: 10.1007/s10237-010-0279-6

McEniery CM, Wilkinson IB, Avolio AP (2007) Age, hypertension and arterial function. Clin Exp Pharmacol Physiol 34:665-671. doi: 10.1111/j.1440-1681.2007.04657.x

Rodríguez J, Merodio J (2011) A new derivation of the bifurcation conditions of inflated cylindrical membranes of elastic material under axial loading. application to aneurysm formation. Mech Res Commun 38(3), 203-210. doi: 10.1016/j.mechrescom.2011.02.004

Ogden RW, Saccomandi G (2007) Introducing mesoscopic information into constitutive equations for arterial walls. Biomech Model Mechanobiol 6:333-344. doi: 10.1007/s10237-006-0064-8

O'Rourke MF, Hashimoto J (2007) Mechanical factors in arterial aging: A clinical perspective. J Am Coll Cardiol 50:1-13. doi: 10.1016/j.jacc.2006.12.050

Rachev A, Greenwald SE (2003) Residual strains in conduit arteries. J Biomech 36:661-70. doi: 10.1016/S0021-9290(02)00444-X

Rubinstein M, Colby RH (2003) Polymer physics. Oxford University Press, New York.

Schulze-Bauer CAJ, Holzapfel GA (2003) Determination of constitutive equations for human arteries from clinical data. J Biomech 36:165-169. doi: 10.1016/S0021-9290(02)00367-6

Schulze-Bauer CAJ, Morth C, Holzapfel GA (2003) Passive biaxial mechanical response of aged human iliac arteries. J Biomech Eng 125:395-406. doi: 10.1115/1.1574331

Shadwick RE (1999) Mechanical design in arteries. J Exp Biol 202:3305-3313

Sommer G, nad Holzapfel GA (2012) 3D constitutive modeling of the biaxial mechanical response of intact and layer-dissected human carotid arteries. J Mech Behav Biomed Mater 5:116-128. doi: 10.1016/j.jmbbm.2011.08.013

Sommer G, Regitnig P, Költringer L, Holzapfel GA (2010) Biaxial mechanical properties of intact and layer-disected human carotid arteries at physiological and supraphysiological loadings. Am J Physiol - Heart Circ Physiol 298:898-912. doi: 10.1152/ajpheart.00378.2009

Stålhand J (2009) Determination of human arterial wall parameters from clinical data. Biomech Model Mechanobiol 8:141-148. doi: 10.1007/s10237-008-0124-3

Stålhand J, Klarbring A (2005) Aorta in vivo parameter identification using an axial force constraint. Biomech Model Mechanobiol 3:191-199. doi: 10.1007/s10237-004-0057-4

Treloar LRG (1975) The physics of rubber elasticity. Oxford University Press, New York, 3rd edition 2005.

Valenta J, Vitek K, Cihak R, Konvickova S, Sochor M, Horny L (2002). Age related constitutive laws and stress distribution in human main coronary arteries with reference to residual strain. Bio-Medical Materials and Engineering, 12(2):121-134.

Van Loon P, Klip W, Bradley EL (1977) Length-force and volume-pressure relationships of arteries. Biorheology 14:181-201

Wilkins K, Campbell NR, Joffres MR, McAlister FA, Nichol M, Quach S, Johansen HL, Tremblay MS. (2010) Blood pressure in canadian adults. Health Reports / Statistics Canada, Canadian Centre for Health Information = Rapports Sur La Santé / Statistique Canada, Centre Canadien d'Information Sur La Santé 21:37-46.

Wittek A, Karatolios K, Bihari P, Schmitz-Rixen T, Moosdorf R, Vogt S, Blase C (2013) In vivo determination of elastic properties of the human aorta based on 4D ultrasound data. J Mech Behav Biomed Mater 27:167-183. doi: 10.1016/j.jmbbm.2013.03.014

References II

Avril, S., Badel, P., Gabr, M., Sutton, M. A., Lessner, S. M., 2013. Biomechanics of porcine renal arteries and role of axial stretch. Journal of Biomechanical Engineering, 135(8), art. no. 081007.

Bergel, D.H., 1961. The static elastic properties of the arterial wall. J. Physiol. 156, 445-457.

Cardamone, L., Valentín, A., Eberth, J. F., Humphrey, J. D., 2009. Origin of axial prestretch and residual stress in arteries. Biomechanics and Modeling in Mechanobiology, 8(6), 431-446.

Chater, E., Hutchinson, J.W., 1984. On the propagation of bulges and buckles. J. Appl. Mech. Trans. ASME 51, 269-277.

Demiray, H., 1972. A note on the elasticity of soft biological tissues. J. Biomech. 5, 309-311.

Dobrin, P.B., Doyle, J.M., 1970. Vascular smooth muscle and the anisotropy of dog carotid artery. Circ. Res. 27, 105-119.

Fuchs, R.F., 1900. Zur Physiologie und Wachstumsmechanik des Blutgefass-systems. Arch. Anat. Physiol. 102-154.

Fung, Y.C. 1967. Elasticity of soft tissues in simple elongation. Am. J. Physiol. 213, 1532-1544.

Fung, Y.C., Fronek, K., Patitucci, P., 1979. Pseudoelasticity of arteries and the choice of its mathematical expression. Am. J. Physiol. 237, H620-631.

Fung, Y.C., 1990. Biomechanics: Motion, Flow, Stress, and Growth. Springer-Verlag, New York.

Fung, Y.C., 1997. Biomechanics: Circulation. Springer-Verlag, New York, second edition.

Gasser, T.C., Ogden, R.W., Holzapfel, G.A., 2006. Hyperelastic modelling of arterial layers with distributed collagen fibre orientations. J. R. Soc. Interface 3, 15-35.

Gent, A.N., 2005. Elastic instabilities in rubber. Int. J. Non-Lin. Mech. 40, 165-175.

Gonçalves, P.B., Pamplona, D., Lopes, S.R.X., 2008. Finite deformations of an initially stressed cylindrical shell under internal pressure. Int. J. Mech. Sci. 50, 92-103.

Guccione, J.M., McCulloch, A.D., Waldman, L.K. 1991. Passive material properties of intact ventricular myocardium determined from a cylindrical model. J. Biomech. Eng. 113, 42-55.

Holzapfel, G.A., 2000. Nonlinear solid mechanics: A continuum approach for engineering. John Wiley and Sons, Chichester.

Holzapfel, G.A., Gasser, T.C., Ogden, R.W., 2000. A new constitutive framework for arterial wall mechanics and a comparative study of material models. J. Elast. 61, 1-48.

Holzapfel, G.A., Ogden, R.W., 2010. Constitutive modelling of arteries. Proc. R. Soc. A-Math. Phys. Eng. Sci. 466, 1551-1597.

Horgan, C.O., Saccomandi, G., 2003. A description of arterial wall mechanics using limiting chain extensibility constitutive models. Biomech. Model. Mechanobiol. 1, 251-266.

Horgan, C.O., 2015. The remarkable Gent constitutive model for hyperelastic materials. Int. J. Non-Lin. Mech. 68, 9-16.

Horny, L., Hulan, M., Zitny, R., Chlup, H., Konvickova, S., Adamek, T., 2009. Computer-aided analysis of arterial wall architecture. IFMBE Proceedings, 25(4):1494-1497.

Horny, L., Kronek, J., Chlup, H., Zitny, R., Vesely, J., Hulan, M., 2010. Orientations of collagen fibers in aortic histological section. B. Appl. Mech. 6, 25-29.

Horný, L., Adámek, T., Gultová, E., Žitný, R., Veselý, J., Chlup, H., Konvičková, S., 2011. Correlations between age, prestrain, diameter and atherosclerosis in the male abdominal aorta. J. Mechan. Behav. Biomed. Mater. 4, 2128-2132.

Horny, L., Adamek, T., Vesely, J., Chlup, H., Zitny, R., Konvickova, S., 2012. Age-related distribution of longitudinal pre-strain in abdominal aorta with emphasis on forensic application. Forensic Science International, 214(1-3), 18-22.

Horny, L., Adamek, T., Chlup, H., Zitny, R., 2012. Age estimation based on a combined arteriosclerotic index. International Journal of Legal Medicine, 126(2), 321-326.

Horný, L., Adámek, T., Žitný, R., 2013. Age-related changes in longitudinal prestress in human abdominal aorta. Arch. Appl. Mech. 83, 875-888.

Horny, L., Adamek, T., Kulvajtova, M., 2014a. Analysis of axial prestretch in the abdominal aorta with reference to post mortem interval and degree of atherosclerosis. J. Mechan. Behav. Biomed. Mater. 33, 93-98.

Horný, L., Netušil, M., Voňavková, T., 2014b. Axial prestretch and circumferential distensibility in biomechanics of abdominal aorta. Biomech. Model. Mechanobiol. 13, 783-799.

Horný, L., Netušil, M., Daniel, M., 2014c. Limiting extensibility constitutive model with distributed fibre orientations and ageing of abdominal aorta. J. Mechan. Behav. Biomed. Mater. 38, 39-51.

Horný, L., Netušil, M., Horák, Z., 2015. Limit point instability in pressurization of anisotropic finitely extensible hyperelastic thin-walled tube. Int. J. Non-Lin. Mech., article in press. DOI: 10.1016/j.ijnonlinmec.2015.08.003

Humphrey, J.D., 2002. Cardiovascular Solid Mechanics: Cells, Tissues, and Organs. Springer-Verlag, New York.

Humphrey, J. D., Eberth, J. F., Dye, W. W., Gleason, R. L., 2009. Fundamental role of axial stress in compensatory adaptations by arteries. Journal of Biomechanics, 42(1), 1-8.

Kanner, L.M., Horgan, C.O., 2007. Elastic instabilities for strain-stiffening rubber-like spherical and cylindrical thin shells under inflation. Int. J. Non-Lin. Mech. 42, 204-215.

Mao, G., Li, T., Zou, Z., Qu, S., Shi, M., 2014. Prestretch effect on snap-through instability of short-length tubular elastomeric balloons under inflation. Int. J. Solids Struct. 51, 2109-2115.

Ogden, R.W., Saccomandi, G., 2007. Introducing mesoscopic information into constitutive equations for arterial walls. Biomech. Model. Mechanobiol. 6, 333-344.

Rodríguez J., Merodio, J., 2011. A new derivation of the bifurcation conditions of inflated cylindrical membranes of elastic material under axial loading: application to aneurysm formation. Mech. Res. Commun. 38, 203-210.

Schulze-Bauer, C.A.J., Mörth, C., Holzapfel, G.A., 2003. Passive biaxial mechanical response of aged human iliac arteries. J. Biomech. Eng. 125, 395-406.

Sommer, G., Regitnig, P., Költringer, L., Holzapfel, G.A., 2010. Biaxial mechanical properties of intact and layer-dissected human carotid arteries at physiological and supraphysiological loadings. Am. J. Physiol. - Heart Circ. Physiol. 298, H898-H912.

Sommer, G., Holzapfel, G. A., 2012. 3D constitutive modeling of the biaxial mechanical response of intact and layer-dissected human carotid arteries. Journal of the Mechanical Behavior of Biomedical Materials, 5(1), 116-128.

Taber, L.A., 2004. Nonlinear Theory of Elasticity: Applications in Biomechanics. World Scientific Publishing, New Jersey.

Van Loon, P., Klip, W., Bradley, E.L., 1977. Length-force and volume-pressure relationships of arteries. Biorheology 14, 181-201.

Appendix A

Equilibrium equations for incompressible hyperelastic thick-walled tube and in-wall stresses distribution

Detailed derivation of equilibrium equations (8) used in the analytical simulation will be provided here. It is done for more convenience of readers and also due to the fact that the derivation as such is rarely presented in the literature with all its steps. As the first step, let us repeat them here. Radial equilibrium is expressed in (8a), and (8b) shows the equilibrium of axial force in the closed thick-walled tube.

$$P = \int_{r_i}^{r_o} \lambda_{\theta\Theta} \frac{\partial \hat{W}}{\partial \lambda_{\theta\Theta}} \frac{dr}{r} \tag{8a}$$

$$F_{red} = \pi \int_{r_i}^{r_o} \left(2\lambda_{zZ} \frac{\partial \hat{W}}{\partial \lambda_{zZ}} - \lambda_{\theta\Theta} \frac{\partial \hat{W}}{\partial \lambda_{\theta\Theta}} \right) r dr \tag{8b}$$

The reader immediately recognizes that in fact, the equations (8a) and (8b) are not true equilibrium equations, rather they express a solution of the boundary-value problem (it is clear from the appearance of the loadings P and F_{red}). This terminological distinction here will not be made similarly to many other papers. But the author feels it to be worth noting.

Assumptions. The material of the tube is considered to be hyperelastic described by the strain energy density function W. The material is incompressible. Shear stresses and strains are neglected. Axial strain does not depend on axial coordinate.

Constitutive equation with $\hat{W}$**.** The first step is the derivation of a new form of the constitutive equation where $\hat{W}$ appears instead of W. Remind that the material is incompressible and that there are no shear strains. It implies that strain measures have the form expressed in (21).

$$\mathbf{F} = \begin{pmatrix} \lambda_{rR} & 0 & 0 \\ 0 & \lambda_{\theta\Theta} & 0 \\ 0 & 0 & \lambda_{zZ} \end{pmatrix} \qquad \mathbf{E} = \frac{1}{2}\begin{pmatrix} \lambda_{rR}^2 - 1 & 0 & 0 \\ 0 & \lambda_{\theta\Theta}^2 - 1 & 0 \\ 0 & 0 & \lambda_{zZ}^2 - 1 \end{pmatrix} \tag{21}$$

The incompressibility constraint implies $det(\mathbf{F}) = \lambda_{rR}\lambda_{\theta\Theta}\lambda_{zZ} = 1$ from which $\lambda_{rR} = 1/(\lambda_{\theta\Theta}\lambda_{zZ})$ is clear. $\hat{W}$ is the strain energy W with substituted $\lambda_{rR} = 1/(\lambda_{\theta\Theta}\lambda_{zZ})$, i.e. $\hat{W} = \hat{W}(1/(\lambda_{\theta\Theta}\lambda_{zZ}), \lambda_{\theta\Theta}, \lambda_{zZ})$.

Consider now a unite cube subjected to normal Cauchy stresses σ_{rr}, $\sigma_{\theta\theta}$, and σ_{zz}. Assume the cube deforms to a cuboid (no shear stresses and strains) whose edges have lengths λ_{rR}, $\lambda_{\theta\Theta}$, and λ_{zZ}. Infinitesimal increment in the strain energy W caused by $\lambda_{rR} \rightarrow \lambda_{rR} + d\lambda_{rR}$, $\lambda_{\theta\Theta} \rightarrow \lambda_{\theta\Theta} + d\lambda_{\theta\Theta}$, and $\lambda_{zZ} \rightarrow \lambda_{zZ} + d\lambda_{zZ}$ is expressed in (22).

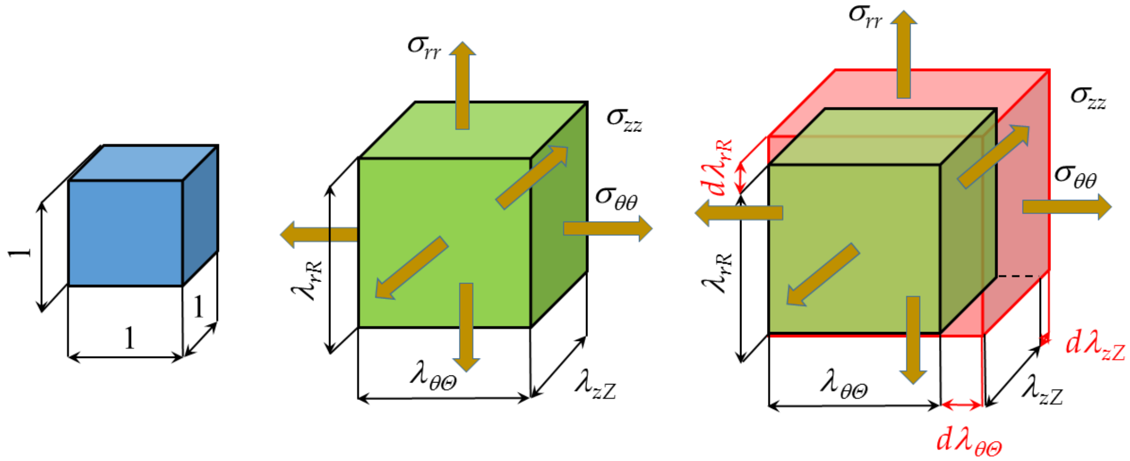

Figure 20. Differential increment dW. Infinitesimal contributions of the order higher than the first are neglected.

$$dW = \lambda_{\theta\Theta}\lambda_{zZ}\sigma_{rr}d\lambda_{rR} + \lambda_{rR}\lambda_{zZ}\sigma_{\theta\theta}d\lambda_{\theta\Theta} + \lambda_{rR}\lambda_{\theta\Theta}\sigma_{zz}d\lambda_{zZ} \tag{22}$$

Now differentiate the incompressibility condition $\lambda_{rR}\lambda_{\theta\Theta}\lambda_{zZ} = 1$ (23).

$$\lambda_{\theta\Theta}\lambda_{zZ}d\lambda_{rR} + \lambda_{rR}\lambda_{zZ}d\lambda_{\theta\Theta} + \lambda_{rR}\lambda_{\theta\Theta}d\lambda_{zZ} = 0 \tag{23}$$

Using (23), dW can be written as (24) where $\lambda_{\theta\Theta}\lambda_{zZ}d\lambda_{rR}$ is eliminated.

$$dW = \lambda_{rR}\lambda_{zZ}\left(\sigma_{\theta\theta} - \sigma_{rr}\right)d\lambda_{\theta\Theta} + \lambda_{rR}\lambda_{\theta\Theta}\left(\sigma_{zz} - \sigma_{rr}\right)d\lambda_{zZ} \tag{24}$$

Considering $\hat{W}$ which is a function of two independent variables, the increment in the strain energy can also be written as (2).

$$d\hat{W} = \frac{\partial\hat{W}}{\partial\lambda_{\theta\Theta}}d\lambda_{\theta\Theta} + \frac{\partial\hat{W}}{\partial\lambda_{zZ}}d\lambda_{zZ} \tag{25}$$

Since both W and $\hat{W}$ express the same energy state of a material, we can write (26) which makes equal components of (25) and (24).

$$\lambda_{rR}\lambda_{zZ}\left(\sigma_{\theta\theta} - \sigma_{rr}\right)d\lambda_{\theta\Theta} = \frac{\partial\hat{W}}{\partial\lambda_{\theta\Theta}}d\lambda_{\theta\Theta} \qquad \lambda_{rR}\lambda_{\theta\Theta}\left(\sigma_{zz} - \sigma_{rr}\right)d\lambda_{zZ} = \frac{\partial\hat{W}}{\partial\lambda_{zZ}}d\lambda_{zZ} \tag{26}$$

From it (27) immediately follows.

$$\lambda_{rR}\lambda_{zZ}\left(\sigma_{\theta\theta}-\sigma_{rr}\right)=\frac{\partial\hat{W}}{\partial\lambda_{\theta\Theta}}\qquad \lambda_{rR}\lambda_{\theta\Theta}\left(\sigma_{zz}-\sigma_{rr}\right)=\frac{\partial\hat{W}}{\partial\lambda_{zZ}} \tag{28}$$

The final form of the new constitutive equations (28) is obtained after the substitution form incompressibility constraint.

$$\sigma_{\theta\theta}-\sigma_{rr}=\lambda_{\theta\Theta}\frac{\partial\hat{W}}{\partial\lambda_{\theta\Theta}}\qquad \sigma_{zz}-\sigma_{rr}=\lambda_{zZ}\frac{\partial\hat{W}}{\partial\lambda_{zZ}} \tag{28}$$

We now see that (28) are equations used to compute a stress distribution through thickness of the wall in (9b) and (9c).

Radial equilibrium (8a). After preceding preliminary computation, we can approach to (8a) as such. The first step consists in the derivation of true radial equilibrium equation. It is done by the well-known approach which is usually explained in the second course of the theory of elasticity and strength of materials in engineering schools around entire the world.[12] Consider internal element of a tube as depicted in Figure 21.

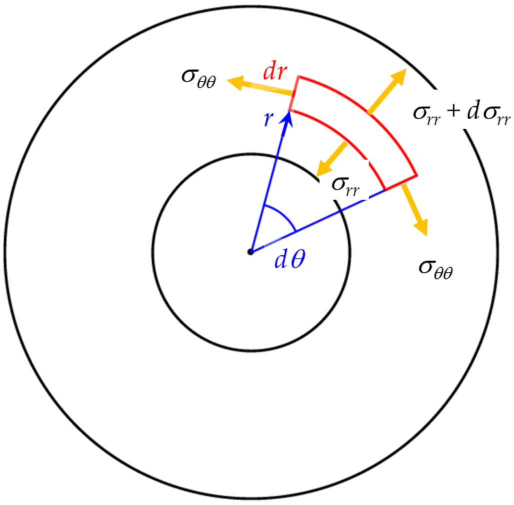

Figure 21. Internal element of deformed thick-walled circular tube.

[12] The second course of the theory of elasticity and strength of materials is here meant in the sense of the famous Timoshenko's books: Timoshenko S. (1930) *Strength of Materials, Part I, Elementary Theory and Problems*. D. Van Nostrand Company, Princeton; and Timoshenko S. (1930) *Strength of Materials, Part II, Advanced Theory and Problems*. D. Van Nostrand Company, Princeton.

Components contributing to the radial net force are summed in (29).

$$\left(\sigma_{rr}+d\sigma_{rr}\right)\left(r+dr\right)d\theta dz-\sigma_{rr}rd\theta dz-2\sigma_{\theta\theta}sin\left(\frac{d\theta}{2}\right)drdz=0 \tag{29}$$

After some algebra, considering infinitesimal approximation $sin(dx) \approx dx$, and neglecting higher order term, one approaches to ordinary differential equation (30), which will be subsequently used in the form (31) expressing differential increment of the radial stress as a function of r.

$$\frac{d\sigma_{rr}}{dr}+\frac{\sigma_{rr}-\sigma_{\theta\theta}}{r}=0 \tag{30}$$

$$d\sigma_{rr}=\frac{\sigma_{\theta\theta}-\sigma_{rr}}{r}dr \tag{31}$$

Now (31) is integrated from r_i to r_o and simultaneously boundary conditions, $\sigma_{rr}(r_i) = -P$ and $\sigma_{rr}(r_o) = 0$, are applied.

$$\int_{\sigma_{rr}(r_i)}^{\sigma_{rr}(r_o)} d\sigma_{rr}=\sigma_{rr}\left(r_o\right)-\sigma_{rr}\left(r_i\right)=0+P=P \tag{32}$$

On the other hand, we also can write (33).

$$\int_{\sigma_{rr}(r_i)}^{\sigma_{rr}(r_o)} d\sigma_{rr}=\int_{r_i}^{r_o}\frac{\sigma_{\theta\theta}-\sigma_{rr}}{r}dr \tag{33}$$

Substituting from the new form of constitutive equation (28a) into (33) and comparing it with (32), the final form is obtained, (8a).

$$P=\int_{r_i}^{r_o}\lambda_{\theta\Theta}\frac{\partial\hat{W}}{\partial\lambda_{\theta\Theta}}\frac{1}{r}dr \tag{8a}$$

Note that a key assumption was the constant axial stretch along entire length of the tube, otherwise the problem will result in a formulation with two independent variables (r and z). Note also that final expression has to be transformed from $\lambda_{\theta\Theta}$ to r by $\lambda_{\theta\Theta}(r) = \pi r/(\psi\rho)$ before an integration.[13]

[13] Here ρ denotes referential variable radius defined in the opened-up (stress-free) configuration as was established in Section 2.3. When stress-free configuration coincides with unpressurized cylinder (no residual strain), then $\rho = R$ and $\psi = \pi$, and $\lambda_{\theta\Theta} = r/R$ follows from it.

Prior approaching the axial equilibrium, the equation (9a), which is closely related with the preceding, will be derived. Consider again (31). But now as a function of lower bound r. Integrals (34) and (35) have to equal. It implies that (9a) must have the form of (36).

$$\int_{\sigma_{rr}(r)}^{\sigma_{rr}(r_o)} d\sigma_{rr} = \sigma_{rr}(r_o) - \sigma_{rr}(r) = 0 - \sigma_{rr}(r) \tag{34}$$

$$\int_{\sigma_{rr}(r)}^{\sigma_{rr}(r_o)} d\sigma_{rr} = \int_{r}^{r_o} \frac{\sigma_{\theta\theta} - \sigma_{rr}}{r} dr = \int_{r}^{r_o} \lambda_{\theta\Theta} \frac{\partial \hat{W}}{\partial \lambda_{\theta\Theta}} \frac{1}{r} dr \tag{35}$$

$$\sigma_{rr}(r) = -\int_{r}^{r_o} \lambda_{\theta\Theta} \frac{\partial \hat{W}}{\partial \lambda_{\theta\Theta}} \frac{1}{x} dx \tag{36}$$

Axial equilibrium (8b). The situation is depicted in Figure 22. Prestretching force F_{red}, which is constant during loading, has to be in equilibrium with the force generated by pressure P acting on sufficiently distant end of a tube and resulting stress σ_{zz}. It implies that we can write (37).

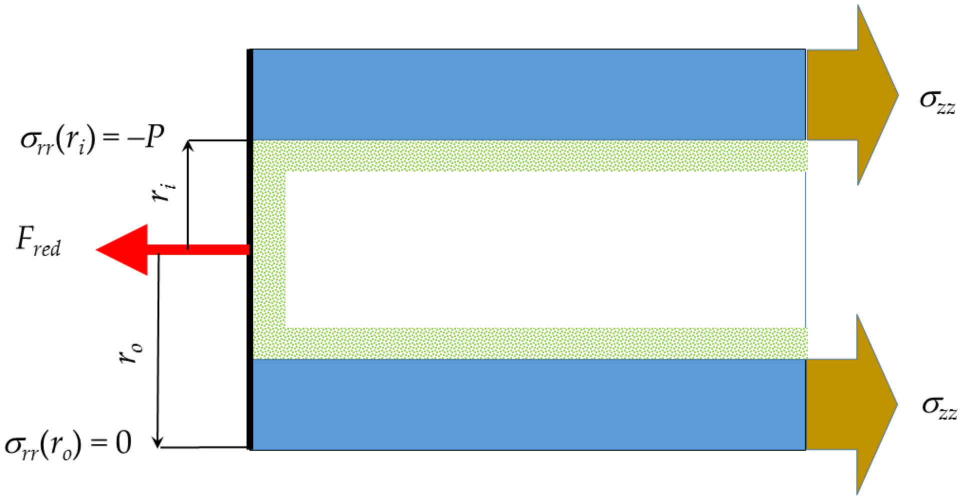

Figure 22. Axial equilibrium.

$$F_{red} = -\pi r_i^2 P + 2\pi \int_{r_i}^{r_o} \sigma_{zz} r dr \tag{37}$$

This (37) is our beginning, and (8b), which is form more convenience repeated, is desired result.

$$F_{red} = \pi \int_{r_i}^{r_o} \left(2\lambda_{zZ} \frac{\partial \hat{W}}{\partial \lambda_{zZ}} - \lambda_{\theta\Theta} \frac{\partial \hat{W}}{\partial \lambda_{\theta\Theta}} \right) rdr \tag{8b}$$

As the first step, substitute from (28b) (constitutive equation with $\hat{W}$) to (37).

$$F_{red} = -\pi r_i^2 P + 2\pi \int_{r_i}^{r_o} \left(\sigma_{rr} + \lambda_{zZ} \frac{\partial \hat{W}}{\partial \lambda_{zZ}} \right) rdr \tag{38}$$

Integral term in (38) is separated to two integrals. Subsequently "2" standing in front of the first integral is used to write "2r" which is finally substituted by a differentiation $d(r^2)/dr$.

$$\begin{aligned} F_{red} &= -\pi r_i^2 P + 2\pi \int_{r_i}^{r_o} \left(\sigma_{rr} + \lambda_{zZ} \frac{\partial \hat{W}}{\partial \lambda_{zZ}} \right) rdr = -\pi r_i^2 P + 2\pi \int_{r_i}^{r_o} \sigma_{rr} rdr + 2\pi \int_{r_i}^{r_o} \lambda_{zZ} \frac{\partial \hat{W}}{\partial \lambda_{zZ}} rdr = \\ &= -\pi r_i^2 P + \pi \int_{r_i}^{r_o} \sigma_{rr} 2rdr + 2\pi \int_{r_i}^{r_o} \lambda_{zZ} \frac{\partial \hat{W}}{\partial \lambda_{zZ}} rdr = \\ &= -\pi r_i^2 P + \pi \int_{r_i}^{r_o} \sigma_{rr} \frac{dr^2}{dr} dr + 2\pi \int_{r_i}^{r_o} \lambda_{zZ} \frac{\partial \hat{W}}{\partial \lambda_{zZ}} rdr \end{aligned} \tag{39}$$

Now consider that the term arising from internal pressure acting on ends can be written as (40); boundary conditions $\sigma_{rr}(r_i) = -P$ and $\sigma_{rr}(r_o) = 0$ are applied.

$$-\pi r_i^2 P = \pi r_i^2 \sigma_{rr}\left(r_i\right) - \pi r_o^2 \sigma_{rr}\left(r_o\right) = -\pi \left[r^2 \sigma_{rr}\left(r\right) \right]_{r_i}^{r_o} \tag{40}$$

Substituting (40) in to the last step of (39) gives (41).

$$\begin{aligned} F_{red} &= -\pi r_i^2 P + \pi \int_{r_i}^{r_o} \sigma_{rr} \frac{dr^2}{dr} dr + 2\pi \int_{r_i}^{r_o} \lambda_{zZ} \frac{\partial \hat{W}}{\partial \lambda_{zZ}} rdr = \\ &= -\pi \left[r^2 \sigma_{rr}\left(r\right) \right]_{r_i}^{r_o} + \pi \int_{r_i}^{r_o} \sigma_{rr} \frac{dr^2}{dr} dr + 2\pi \int_{r_i}^{r_o} \lambda_{zZ} \frac{\partial \hat{W}}{\partial \lambda_{zZ}} rdr \end{aligned} \tag{41}$$

Now, an integration by parts can be applied to the first and second term in (41c). It is written as (42).

$$\pi \left[r^2 \sigma_{rr}\left(r\right) \right]_{r_i}^{r_o} = \pi \int_{r_i}^{r_o} \sigma_{rr} \frac{dr^2}{dr} dr + \pi \int_{r_i}^{r_o} \frac{d\sigma_{rr}}{dr} r^2 dr \tag{42}$$

(42) can be rearranged to (43) which is then substituted into (41) giving (44).

$$-\pi \int_{r_i}^{r_o} \frac{d\sigma_{rr}}{dr} r^2 dr = -\pi \left[r^2 \sigma_{rr}\left(r\right) \right]_{r_i}^{r_o} + \pi \int_{r_i}^{r_o} \sigma_{rr} \frac{dr^2}{dr} dr \tag{43}$$

$$F_{red} = -\pi \int_{r_i}^{r_o} \frac{d\sigma_{rr}}{dr} r^2 dr + 2\pi \int_{r_i}^{r_o} \lambda_{zZ} \frac{\partial \hat{W}}{\partial \lambda_{zZ}} r dr \tag{44}$$

Now substitute the term $d\sigma_{rr}/dr$ in (44) from radial equilibrium equation (30).

$$F_{red} = -\pi \int_{r_i}^{r_o} \frac{\sigma_{\theta\theta} - \sigma_{rr}}{r} r^2 dr + 2\pi \int_{r_i}^{r_o} \lambda_{zZ} \frac{\partial \hat{W}}{\partial \lambda_{zZ}} r dr = -\pi \int_{r_i}^{r_o} \left(\sigma_{\theta\theta} - \sigma_{rr} \right) r dr + 2\pi \int_{r_i}^{r_o} \lambda_{zZ} \frac{\partial \hat{W}}{\partial \lambda_{zZ}} r dr \tag{45}$$

The final step consists in replacing the bracket term in the first integral in (45c) by the expression from the new constitutive equation (28a). We are approaching to (46c) which equals to desired expression (8b).

$$F_{red} = -\pi \int_{r_i}^{r_o} \lambda_{\theta\Theta} \frac{\partial \hat{W}}{\partial \lambda_{\theta\Theta}} r dr + 2\pi \int_{r_i}^{r_o} \lambda_{zZ} \frac{\partial \hat{W}}{\partial \lambda_{zZ}} r dr = \pi \int_{r_i}^{r_o} \left(2\lambda_{zZ} \frac{\partial \hat{W}}{\partial \lambda_{zZ}} - \lambda_{\theta\Theta} \frac{\partial \hat{W}}{\partial \lambda_{\theta\Theta}} \right) r dr \tag{46}$$

Appendices B and C are not included in the www version of the thesis.

Brief biography of the author

Lukáš Horný

Curriculum Vitae

Nationality:	Czech
Location:	Czech Republic
Contact:	lukas.horny@fs.cvut.cz
Web:	http://www.fs.cvut.cz/~hornyluk/home.html
Date of birth:	1977/07/11

Current position	since 2007 Research Associate
Department	Faculty of Mechanical Engineering
Institution	Czech Technical University in Prague (CTU)
Previous Positions:	2006 – 2007 Teacher of mathematics at secondary school SSPE Eltodo (school of industrial electro-technics) 2000 – 2005 Research assistant at Faculty of Mechanical Engineering (CTU)
Education	2012 Ph.D. in Biomechanics, Faculty of Mechanical Engineering (CTU), 2012 – 2009 2000 MSc. in Mathematics and Technical Mechanics, collaborative education program of Brno University of Technology (Faculty of Mechanical Engineering) and Masaryk University in Brno (Faculty of Sciences), 1995 - 2000
Expertise	Nonlinear continuum mechanics of solids and its applications in biomechanics of cardiovascular system; constitutive modeling; arterial and venous physiology and pathology; biomechanics of arterial aging; experimental methods
Personal keywords	*constitutive modeling; stress; strain; hyperelasticity; histology; histomorphometry; aging; atherosclerosis; arteriosclerosis; collagen; elastin; uniaxial and biaxial tensile test; inflation-extension test; stent; FEM; dissection; aneurysm; pulse wave velocity; remodeling; adaptation; residual stress; graft; tissue engineering; digital image correlation; damage; stress softening; viscoelasticity*
Activities	Member of the European Society of Biomechanics Member of the Czech Society of Biomechanics Member of the Union of Czech Mathematicians and Physicists
Awards:	*Professor Jaroslav Valenta and Professor Radomír Čihák Award* from Czech Foundation of Human Biomechanics 2012 for young investigators

Profiles

SCOPUS ID 22947354000
Google Scholar: http://scholar.google.cz/citations?user=Zlkwb Q4AAAAJ&hl=cs&oi=sra
ResearchGate: https://www.researchgate.net/profile/Lukas_Horny/

Invited lectures

Horný L. Axial prestretch in aorta and effect on circumferential distensibility. Invited lecture presented in: LOEWE Preventive Biomechanics Research Center, University of Applied Sciences and Goethe-University, Frankfurt am Main. 23 September 2013.

Ad hoc reviewer

Biomechanics and Modeling in Mechanobiology, *Journal of the Mechanical Behavior of Biomedical Materials*, *Experimental Mechanics*, *Mechanics of Materials*, *Journal of Biomechanics*

Technology Agency of the Czech Republic

Ph.D. thesis reviewer, S. Polzer (2012) Stress-strain analysis of aortic aneurysms. Brno Universtiy of Technology, Faculty of Mechanical Engineering.

Research projects involvement (Principal Co-Investigater)

TA04010330 - Development of resorbable collagen-calcium phosphate nanolayer with controlled elution of antibiotics for implants survival rate enhancement

Research projects involvement (team member)

MSM 210000012 - Transdisciplinary Biomedical Engineering Research (1999-2004, MSM)
MSM6840770012 - Transdisciplinary Research in the Field of Biomedical Engineering II (2005-2011, MSM)
GA106/04/1181 - Identification of the vessel wall materials properties (2004-2006, GA0/GA)
GA106/08/0557 - Material properties of veins and their remodelling (2008-2011, GA0/GA)
GAP108/10/1296 - Development and Characterization of Active Hybrid Textiles with Integrated Nanograin NiTi Micro Wires (2010-2012, GA0/GA)
TA01010185 - New materials and coatings for joint replacement bionical design (2011-2014, TA0/TA)
NT13302 - The optimalization of physical characteristics of vascular substitutes for low flow (2012-2015, MZ0/NT)

Member of Organizing committee European Society of Biomechanics Congress 2015

List of selected publications

Leading author of articles in international peer-reviewed journals with impacfactor received from Journal of Citation Reports (IF)

Horny, L., Netusil, M., & Daniel, M. (2014). Limiting extensibility constitutive model with distributed fibre orientations and ageing of abdominal aorta. *J Mechan Behav Biomed Mater*, 38:39-51. **IF 3.048**

Horny, L., Adamek, T., & Kulvajtova, M. (2014). Analysis of axial prestretch in the abdominal aorta with reference to post mortem interval and degree of atherosclerosis. *J Mechan Behav Biomed Mater* 33:93-98. **IF 3.048**

Horny, L., Netusil, M., Vonavkova, T. (2014). Axial prestretch and circumferential distensibility in biomechanics of abdominal aorta. *Biomech Model Mechanobiol* 13(4):783-799. **IF 3.251**

Horny, L., Adamek, T., & Zitny, R. (2013). Age-related changes in longitudinal prestress in human abdominal aorta. *Arch Appl Mech* 83(6), 875-888. **IF 1.438**

Horny, L., Chlup, H., Zitny, R., Vonavkova, T., Vesely, J., & Lanzer, P. (2012). Ex vivo coronary stent implantation evaluated with digital image correlation. *Exp Mech* 52(9), 1555-1558. **IF 1.567**

Horny, L., Adamek, T., Chlup, H., & Zitny, R. (2012). Age estimation based on a combined arteriosclerotic index. *Int J Leg Med* 126(2), 321-326. **IF 2.597**

Horny, L., Adamek, T., Vesely, J., Chlup, H., Zitny, R., & Konvickova, S. (2012). Age-related distribution of longitudinal pre-strain in abdominal aorta with emphasis on forensic application. *Forensic Sci Int* 214(1-3), 18-22. **IF 2.115**

Horny, L., Adamek, T., Gultova, E., Zitny, R., Vesely, J., Chlup, H., & Konvickova, S. (2011). Correlations between age, prestrain, diameter and atherosclerosis in the male abdominal aorta. *J Mechan Behav Biomed Mater* 4(8), 2128-2132. **IF 3.048**

Horny L, Chlup H, Zitny R, Adamek T (2010) Constitutive modeling of coronary artery bypass graft with incorporated torsion. *Metalurgija* 49(2):273-277. **IF 0.755**

Co-author of articles in international peer-reviewed journals with impacfactor received from Journal of Citation Reports (IF)

Gultova, E., **Horny, L.**, Chlup, H., Zitny, R., Adamek, T., & Kulvajtova, M. (2013). Preservation of tangent modulus of pericardial tissue during cold storage. *Comput Method Biomech Biomed Eng* 16(SUPPL 1), 318-319. **IF 1.793**

Gultova, E. **Horny, L.,** Chlup, H., Žitný, R. (2011) A comparison between exponential and limiting fiber extensibility pseudo-elastic model for the Mullins effect in arterial tissue. *Journal of Theoretical and Applied Mechanics*. 49(4):1203-1216. **IF 0.620**

Kronek J, Zitny, **Horny L**, Chlup H, Beran M (2010) Mechanical properties of artery-artery connection based upon transglutaminase cross-linked collagen. *Metalurgija* 49(2):356-360.
IF 0.755

Valenta, J., Vitek, K., Cihak, R., Konvickova, S., Sochor, M., & **Horny, L**. (2002). Age related constitutive laws and stress distribution in human main coronary arteries with reference to residual strain. *Bio-Med Mater Engr* 12(2), 121-13. **IF 0.847**

Articles in national journals

Horny L (2014) Effect of axial prestretch on inflation instability in finitely extensible thin-walled tube. *B Appl Mech*, in press.

Horny L, Vesely J, Chlup H, Janouchova K, Vysanska M. (2012). Single fiber pull-out test of nitinol-silicon-textile composite. *B Appl Mech* (32), 77-80.

Horny L, Kronek J, Chlup H, Zitny R, Vesely J, Hulan M. (2010). Orientations of collagen fibers in aortic histological section. *B Appl Mech* 6(22), 25-29.

Horný L, Gultova E, Chlup H, Kronek J, Veselý J, Žitný R. (2010). Mullins effect in aorta and limiting extensibility evolution. *B Appl Mech* 6(21), 1-5.

Conference proceedings papers indexed in ISI WOK or SCOPUS

Vesely J, **Horny L**, Chlup H, Krajicek M, Zitny R. (2015). The influence of the opening angle on the stress distribution through the saphenous vein wall. IFMBE Proceedings 45:399-402.

Vesely J, **Horny L**, Chlup H, Beran M, Krajicek M, Zitny R. (2014). Mechanical properties of polyvinyl alcohol/collagen hydrogel. In: EAN 2014 - 52nd International Conference on Experimental Stress Analysis, Marianske Lazne; Czech Republic.

Kronek J, **Horny L**, Adamek T, Chlup H, Zitny R. (2014). Site-specific mechanical properties of aortic bifurcation. IFMBE Proceedings 41:939-942.

Veselý J, **Horný L**, Chlup H, Žitný R. (2014). Inflation tests of vena saphena mangna for different loading rates. IFMBE Proceedings 41:1041-1044.

Vesely J, Hadraba D, Chlup H, **Horny L**, Adamek T, Zitny R (2014) Constitutive Modelling and Histology of Vena Saphena. Applied Mechanics and Materials 486:249-254.

Gultova E, **Horny L**, Chlup H, Filova E, Pirk J, Bacakova L, Zitny R (2014) Mechanical Response of the Cross-Linked Pericardial Tissue Applied Mechanics and Materials 486:255-258.

Filova, E., Burdikova, Z., Stankova, L., Hadraba, D., Svindrych, Z., Schornik, et al. (2013) Collagen structures in pericardium and aortic heart valves and their significance for tissue engineering. 4th IEEE E-Health and Bioengineering Conference EHB 2013, Article number 6707382.

Horný, L., Chlup, T., Žitný, R., Gultová, E., Veselý, J. (2011) Longitudinal prestrain in male abdominal aorta from pulse wave velocity viewpoint. Computational Plasticity XI, COMPLAS XI 757-763.

Vesely, J., **Horny, L.**, Chlup, H., Zitny, R.(2011) Collagen orientation and waviness within the vein wall. Computational Plasticity XI, COMPLAS XI 720-728.

Gultova, E., **Horny, L.**, Chlup, H., Zitny, R.(2011) An anisotropic pseudo-elastic model for the Mullins effect in arterial tissue. Computational Plasticity XI, COMPLAS XI 713-719.

Horny, L., Gultova, E., Adamek, T., Zitny, R., Chlup, H. (2011) In situ longitudinal pretension in human aorta. IFMBE Proceedings 37:430-433.

Horny, L., Chlup, H., Vesely, J., Gultova, E., Kronek, J., Zitny, R., Vonavkova, T., Adamek, T., Lanzer, P., Hromadka, D.(2011) In vitro coronary stent implantation: Vessel wall-stent interaction IFMBE Proceedings 37:795-798.

Horny, L., Kronek, J., Chlup, H., Gultova, E., Heller, L., Zitny, R., Vokoun, D. (2011) Inflation-extension test of silicon rubber-nitinol composite tube IFMBE Proceedings 37:1027-1030.

Horny, L., Gultova, E., Chlup, H., Sedlacek, R., Kronek, J., Vesely, J., Zitny, R. (2010) Mullins effect in human aorta described with limiting extensibility evolution IFMBE Proceedings 29:768-771.

Horny, L., Kronek, J., Chlup, H., Zitny, R., Hulan, M. (2010) A distribution of collagen fiber orientations in aortic histological section. IFMBE Proceedings 29:772-775.

Horny, L., Chlup, H., Zitny, R., Konvickova, S., Adamek, T. (2009) Constitutive behavior of coronary artery bypass graft. IFMBE Proceedings 25(4):181-184.

Horny, L., Hulan, M., Zitny, R., Chlup, H., Konvickova, S., Adamek, T. (2009) Computer-aided analysis of arterial wall architecture. IFMBE Proceedings 25(4):1494-1497.

Horny, L., Zitny, R., Chlup, H. (2008) Strain energy function for arterial walls based on limiting fiber extensibility. IFMBE Proceedings 22:1910-1913.